2010

Investigation of the Behavior of Open Cell Aluminum Foam

Patrick J. Veale
University of Massachusetts Amherst, pveale7@gmail.com

INVESTIGATION OF THE BEHAVIOR OF OPEN CELL ALUMINUM FOAM

A Thesis Presented

by

PATRICK J. VEALE

Submitted to the Graduate School of the
University of Massachusetts Amherst in fulfillment
of the requirements for the degree of

MASTER OF SCIENCE IN CIVIL ENGINEERING

May 2010

Civil and Environmental Engineering

INVESTIGATION OF THE BEHAVIOR OF OPEN CELL ALUMINUM FOAM

A Thesis Presented

by

PATRICK J. VEALE

Approved as to style and content by:

_____
Sanjay R. Arwade, Chair

_____
Thomas J. Lardner, Member

_____
Robert N. Palmer, Department Head
Civil and Environmental Engineering

ABSTRACT

INVESTIGATION OF THE BEHAVIOR OF OPEN CELL ALUMINUM FOAM

MAY 2010

PATRICK J. VEALE, B.S., VILLANOVA UNIVERSITY

M.S., UNIVERSITY OF MASSACHUSETTS AMHERST

Directed by: Dr. Sanjay R. Arwade

The study investigates the behavior open cell aluminum foam in scenarios applicable to potential use in structural applications. Foam behavior was examined through mechanical testing, computer modeling and analytic expressions. Existing assumptions about the elastic properties of foam were expanded to include contributions of axial and shear deformations and expressions were rewritten in terms of the axial and bending stiffness ratios of ligaments. Compressive and tensile tests were performed to gain a measure of the elastic properties of foams for different porosities and 6-8% defined relative density, as well as the behavior and failure mechanisms in both loading conditions. Fatigue tests were performed on open cell foam samples to determine the strain to fatigue life relationship for the material at high applied strain amplitudes. Finally, finite element models were created in ADINA for both ordered and random networks. The changes in elastic properties due to relative density, defined by ligament geometry, cell anisotropy and joint connectivity were measured for ordered networks, while irregular, random networks were used to investigate the forces developed within ligaments. Conclusions from this study provide insight on the behavior of open cell foam and promote further research in an effort to determine the viability of structural use of the material.

TABLE OF CONTENTS

LIST OF TABLES

LIST OF FIGURES

LIST OF SYMBOLS

ENGLISH

c	=	Fatigue ductility exponent
E_s	=	Elastic modulus of solid material
E^*	=	Elastic modulus of foam
G	=	Shear modulus
G^*	=	Shear modulus of foam
ℓ	=	Ligament length
m	=	Mass
N_f	=	Fatigue life
I	=	Bending moment of inertia
V	=	Volume

GREEK

β	=	Strain correction factor
γ	=	Shear strain
δ	=	Deformation
ε	=	Strain
ε_a	=	Applied strain amplitude
ε_f'	=	Fatigue ductility coefficient
v	=	Poisson's ratio
v^*	=	Poisson's ratio of foam
ξ	=	Perturbation parameter
ρ^*	=	Density of cellular material
ρ_s	=	Density of solid material from which cell walls are made
ρ^*/ρ_s	=	Relative density
σ	=	Normal stress
τ	=	Shear stress
φ	=	Ligament orientation

CHAPTER 1

INTRODUCTION

Metal foam is a cellular material defined by solid material surrounded by a three-dimensional network of voids. As a lightweight, porous material, metal foam possesses a high strength and stiffness relative to its weight, making it an attractive option for a variety of applications. The properties of metal foams make them desirable materials for use in situations where high strength and stiffness to weight ratios are essential, as well as applications where energy absorption and permeability characteristics are valued. To date, metal foams are mainly being used in aerospace, filter and impact or insulation applications. Foamed materials are also useful due to their favorable sound absorption, fire retardation and heat dissipation properties. Unlike other porous materials that are currently utilized, metal foams are less susceptible to alteration due to environmental surroundings. Cellular metals have not yet experienced widespread use in the structural engineering field, mainly due to their high cost in comparison to other commonly used structural materials. However, the characteristics of foams make them an attractive option for use in structural engineering, especially in energy absorption for structures subject to impact or cyclic loading. This project aims to investigate the basic properties of metal foam, specifically cellular aluminum, that are relevant to structural applications.

The most basic classification of aluminum foams is the degree of interconnection between adjacent cells within the microstructure of the material. Metal foams are defined as either open or closed celled. Open-cell foam is comprised of only cell edges, or ligaments, so that open spaces exist between adjoining cells. Conversely, closed-cell

foams are defined by solid faces so that each cell is closed off from those adjacent to it. The difference in cellular structure of open and closed cell foams is apparent in Figure 1.
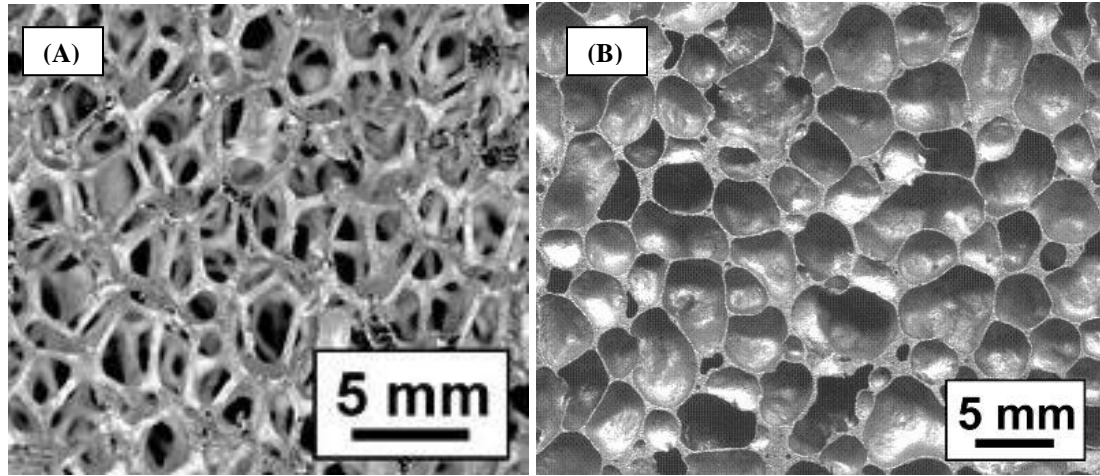
Figure 1: (A) Open-cell (from ERG Duocel) and (B) closed-cell (from Alporas) aluminum foam

Currently, the most prominent numerical property of any cellular solid is its relative density, ρ^*/ρ_s. This is defined as the density of the cellular material (ρ^*) divided by the density of the solid material from which the cell walls are made (ρ_s). Much of the research performed has presented the mechanical properties of foam as a function of the material's relative density. A goal of this project will be to investigate whether relative density is in fact the controlling characteristic in determining the properties of the foam. It is possible for foams with identical relative densities to have differing cellular structure or alternative ligament geometry which could significantly influence the behavior and properties of the material.

Foams can also be classified according to their porosity, or the number of cells (pores) that exist per unit length. Foams with the same relative density but a larger number of pores per inch (henceforth referred to as ppi) will contain ligaments with smaller cross sections as a greater number of pores and thus more ligaments will exist.

This definition of porosity is used by the manufacturer of the foam in lieu of more descriptive definitions (i.e. pores per unit volume), and will be used in this project for simplicity and consistency. The primary focus of this research will be open cell aluminum foam with low relative density, approximately 6 to 10%, and porosities of 10, 20 and 40 ppi. Example specimens of each of these porosities are shown in Figure 2 below.
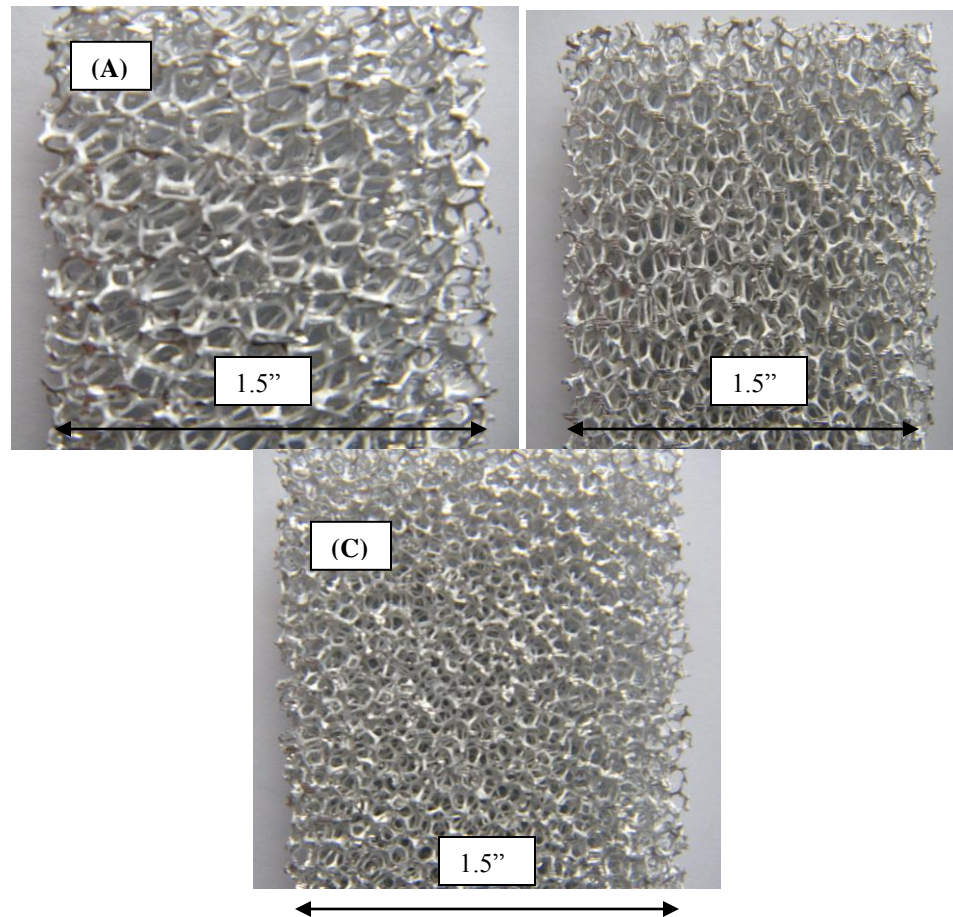
Figure 2: 6-8% density aluminum foam manufactured and provided by ERG Duocel with (A) 10 ppi, (B) 20 ppi, and (C) 40 ppi

To accurately determine the potential applications for metal foam, it is essential that the mechanical properties of the material be known. Presently, analytical expressions exist for the elastic properties based on the properties of the solid material and

deformation mechanics of one unit cell within the network. This project aims to verify that these expressions are accurate in predicting the properties by comparing the results obtained from mechanical testing to values predicted with the existing expressions. Furthermore, these expressions are currently derived based on specific assumptions about the geometry of the network and properties of the ligaments. A portion of this project will seek to loosen these assumptions and rewrite the expressions for the elastic properties in terms of the relative stiffnesses (bending and axial) of the ligaments.

Many of the desired structural uses for metal foams require them to be subjected to fatigue loading. For this reason, it is applicable to investigate the response of foam under cyclic load tests. The understanding of fatigue behavior and failure of foams is essential for the ability to translate their properties for use in applications in which fatigue is an issue, a common consideration in structural capacities. Much of the fatigue research performed on foams to this point has dealt with compression-compression loading despite the fact that many of the proposed structural uses of foam would result in both tension and compression cycles to be experienced. The research on open cell foam subjected to fully reversed cyclic loading is extremely limited and this project will perform tests to develop a basis for open cell fatigue behavior and begin the process of determining a useful definition of fatigue failure for the material.

The effective elastic properties of foam will also be investigated using computational modeling. The finite element program ADINA Version 8.4.4 was used to create models of both regular and random networks featuring geometry consistent with that measured in actual foam samples and in previous studies in which finite element modeling was performed. Simulations were performed to analyze the behavior of regular

and irregular foam networks under applied loading and calculate the properties of the network based on the results. Irregular networks were included to determine the effect of randomness on the system on the microstructure. The effect of randomness on ligament orientation, and further the effect of microstructural irregularity on the forces and stresses developed in the individual ligaments, was specifically examined.

Through mechanical testing and computer modeling, the properties and behavior of open cell foam will be measured and analyzed with great attention paid to the material characteristics that significantly affect them. Results for the elastic properties can be compared with predictions found using existing expressions to determine whether the assumption of relative density as the primary characteristic governing elastic properties is accurate. Furthermore, the understanding of open cell foam fatigue behavior will be enhanced through the testing performed in this project and a strain-life relationship will be developed for the material that could serve as a basis for future exploration of open cell foam fatigue. Finally, simulations on random foam microstructure will highlight the effects of variable ligament orientation and cell isotropy on the stresses developed within the ligaments, governing failure of the material as a whole. With the greater understanding of foam properties and behavior, as well as the parameters that impact them, achieved by this project, steps can be made possible which will ultimately lead towards designing foam material tailored specifically for use in structural engineering applications.

1.1. Project Motivation and Background

The high stiffness to weight ratio possessed by aluminum foam makes it an ideal material for use in a number of different applications, especially structural engineering. In order to

use foams efficiently in any situation it is essential to understand their behavior and properties in scenarios relevant to potential uses. The level of accountability that exists in structural engineering projects and catastrophic repercussions of insufficient designs make this especially true.

Foam properties are directly related to the relative density, whether the cells are open or closed, the degree of anisotropy of the foam, as well as the material properties of the ligaments (Gibson and Ashby 1997). These currently accepted assumptions may prove to be overly simplistic. To fully characterize the properties of aluminum foam, a combination of rigorous testing and analysis is necessary. Foam properties can be determined by analyzing their behavior during mechanical testing, applying the principles of elasticity and basic mechanics. In addition, computational analysis can be utilized to correlate testing results with idealized computer models created to replicate the geometry and microstructure of true foams. Using accurate computer models, parametric studies can be performed to determine how variation of different properties of the foam, such as cell shape or ligament geometry, and not just the relative density affect the properties of the material. Furthermore, computer models will allow for the microscopic behavior of foams to be investigated using small-scale representations. While the macroscopic behavior can be observed in mechanical testing, it is difficult to identify the response of individual elements within a physical network. Computer models allow tests to be run on networks with small numbers of cells and thus allow the response of each individual cell to be more apparent, potentially providing insight into the overall behavior of the material. With solid conclusions made about the material properties, the scope of testing can be expanded to include a measure of the fatigue behavior, specifically the relation of

6

applied strain to fatigue life, which is an essential characterization for the adaptation or design of aluminum for structural use.

1.2. Material Properties

Significant work has been performed with the goal of attaining a confident definition of the material properties of foam and the mechanics of its behavior. In their comprehensive work, *Cellular Solids: Structure and Properties*, Lorna Gibson and Michael Ashby address the properties of three-dimensional foam networks in great detail. In order to determine the mechanical properties of foams, it is necessary to first understand the deformation mechanisms of the material. The compressive response of foam is characterized by linear elasticity at low stresses followed by an extended collapse plateau and a period of densification in which the stiffness increases sharply, as shown in Figure 3.
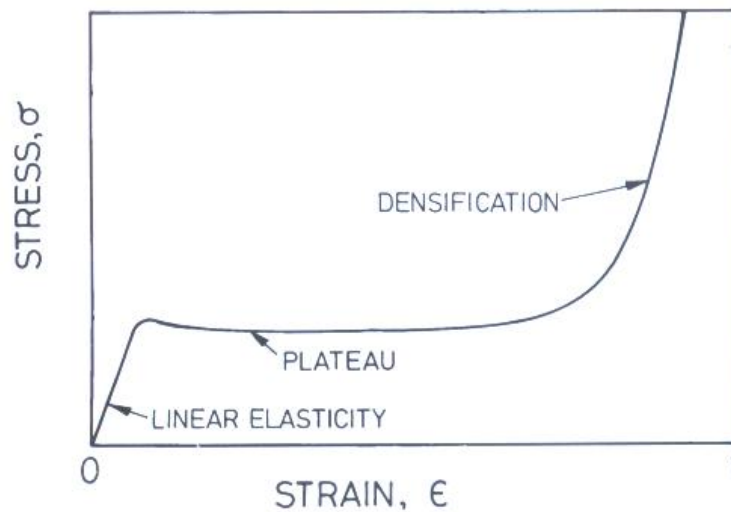
Figure 3: Typical compressive stress-strain response of cellular metal as defined in Cellular Solids (Gibson and Ashby 1997)

Linear elasticity in open cell foams is governed by cell wall deformation due to bending and axial forces and the elastic modulus of the foam can be determined by the initial slope of the stress-strain curve. The long plateau is a result of the collapse of the cells by elastic buckling, plastic collapse or brittle crushing. As the collapse progresses, the cell walls touch, resulting in the rapid increase of stress as the solid compresses and densification occurs (Gibson and Ashby 1997).

Because many applications of foam result in compressive loading, Gibson and Ashby formulate expressions for the mechanical properties of foams based on the compressive behavior. The expressions are derived using basic mechanics and simple geometry assuming a cubic unit cell with ligaments of length l and square cross section of side t, as shown in Figure 4.
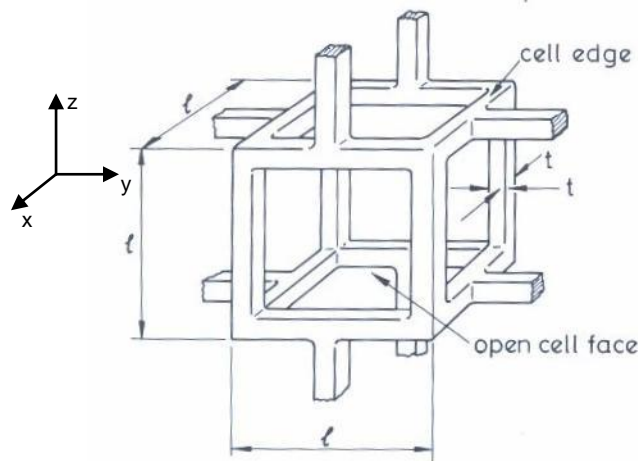
Figure 4: Cubic unit cell as provided in Cellular Solids by Gibson and Ashby

Figure 4 does not provide a realistic representation of physical foam cell geometry, but it is useful in that the deformation of the ligaments is easily understood and provides relatively straight forward geometry with which to derive equations. Cell

structure in actual foams is more complex and typically not uniform throughout the material.

While other options for unit cell definitions are available (see the Kelvin cell used in Section X.X) and equations could be obtained from more complicated, representative geometry, if the deformation behavior of the cell ligaments is consistent amongst different geometries, the properties can be adequately understood using this representation. Rather than properties derived explicitly, the expressions are presented as proportionalities that remain valid if the deformation mechanisms in real foam cells remain consistent with those assumed for the derivation. These proportionalities include constants that arise as the result of specific geometric cell configurations that are more representative of actual foam specimens.

Using this representation of a unit cell, the relative density and second moment of area of a ligament can be related to these dimensions by

$$\frac{\rho^*}{\rho_s} \propto \left(\frac{t}{l}\right)^2 \tag{1}$$

and

$$I \propto t^4 . \tag{2}$$

Gibson and Ashby derive their expressions for elastic properties using standard beam theory and the stress and strain relationship of the entire cell. Using beam theory, the deflection of the edge of a unit cell is proportional to Fl^3/E_sI. The global compressive stress is proportional to the force transmitted to the ligament as $\sigma \propto F/l^2$, while the global strain is proportional to the displacement as $\varepsilon \propto \delta/l$. These relationships are then

combined using Hooke's law of elasticity to determine expression for the elastic modulus,

$$E^* = \frac{\sigma}{\varepsilon} = \frac{F}{l^2} \cdot \frac{\delta}{l},$$

(3)

or,

$$E^* = \frac{C_1 E_s I}{l^4}.$$

(4)

Equations (1) and (2) and then substituted into Equation (4) to obtain

$$\frac{E^*}{E_s} = C_1 \left(\frac{\rho^*}{\rho_s} \right)^2$$

(5)

for open cell foams. The constant C_1, includes the constants of proportionality and is determined from tests data to be approximately equal to one.

The shear modulus is similarly derived. Deformation under an applied shear stress is again characterized by cell wall bending. The deflection, δ, is proportional to $Fl^3/E_s I$, and the overall stress, τ, and strain, γ, are proportional to F/l^2 and δ/ℓ, respectively. The shear modulus can be written as

$$G^* = \frac{\tau}{\gamma} = \frac{C_2 E_s I}{l^4}$$

(6)

or,

$$\frac{G^*}{E_s} = C_2 \left(\frac{\rho^*}{\rho_s} \right)^2.$$

(7)

Data suggests that C_2 is approximately equal to 3/8.

10

Poisson's ratio of a foam, v^*, is defined as the negative ratio of transverse to axial strain, both of which are proportional to δ/ℓ, as above. Therefore, it is determined that Poisson's ratio is a constant, independent of the relative density of the foam and a function only of the cell shape of the foam. Using Hooke's Law for isotropic material,

$$G = \frac{E}{2(1+\upsilon)},$$
(8)

Poisson's ratio for foam material can be determined to be

$$\upsilon^* = \frac{C_1}{2C_2} - 1 \approx 0.33 .$$
(9)

However, this definition of Poisson's ratio is valid only for isotropic materials like the network of cubic cells idealized by Gibson and Ashby. In foams comprised of a Kelvin cell microstructure as discussed in Section 6.1.1, this representation of Poisson's ratio is not necessarily applicable.

Gibson and Ashby derive the above expressions for the elastic properties of three-dimensional foams based on the deformation mechanisms of a unit cell that is not a truly representative of the cell structure found in real foams. While this method may be valid due to the expressions being written as proportionalities that include constants arising from more specific geometries, the only deformation considered in the derivation is the deformation as a result of ligament bending. Gibson and Ashby argue that ligament bending is the governing mechanism for failure of the entire network and exclude the deformations resulting from axial and shear forces. One of the aims of this project is to determine if it is valid to exclude axial and shear deformation considerations when

11

determining the properties of foam. To this end, the equations derived by Gibson and Ashby are rewritten to include axial deformations in Section 2.0.

In addition to using basic deformation mechanics to derive the effective elastic properties of cellular materials, the behavior of such materials during mechanical testing can be analyzed to determine their properties. In examining the crushing behavior of open cell aluminum foam, it is observed that the response under slow displacement rate is initially linear, followed by an extended plateau region (Jang and Kyriakides 2009). In compression tests performed, deformation was initially uniform throughout the specimen during elastic behavior. Collapse bands begin to form as the ligaments undergo plastic buckling until they come in contact with one another within the collapsed cell. This causes the deformation band to spread to neighboring cells without much further load being taken, eventually leading to densification and a gradual increase in stiffness.

Because most foams are not perfectly isotropic, they possess a difference in properties in different directions, defined mainly by the orientation of the cells. The rise direction is so called because in the process of manufacturing the material, a foaming agent is added to the metal causing air bubbles to "rise" to the surface of the material, creating an elongated cell in one direction. This can be most clearly seen in Figure 2(B) as the cells are obviously longer in the vertical direction. The mechanical properties in both the rise and transverse (perpendicular to the rise) directions can be determined from the testing results, with the transverse direction showing a lower elastic modulus and lower yield and plateau stresses (Jang and Kyriakides 2009).

True foams rarely contain the ideal morphologies used in the Gibson and Ashby derivations, as defects such as missing cell walls and ligaments of variable thickness are

often present. A 2003 study performed by Ramamurty and Paul investigates the dependence of mechanical properties on the variability of such foam characteristics as cell size, density and presence of morphological defects. This study contends that for closed cell aluminum foam the variability in the mechanical properties of the foam is directly related to the variability of the properties that characterize the foam, density and cell size distribution (Ramamurty and Paul 2004). While cell size distribution is much more easily characterized in closed cell foams in which the variation of cell sizes is greater and more apparent than in open cell material, it has been shown that the relative density of open cell foams has a major effect on the properties of the material. Because the variability of the properties of closed cell foam is much larger than the variability of the base material, in order to utilize the foam in applications where low failure probably and reliability are essential, the manufacturing process must be improved and made more consistent or safety margins must be increased. Similarly, in performing mechanical tests on the material, a number of experiments should be conducted in order to assure accurate behavior due to the variable nature of the foam (Ramamurty and Paul 2004).

1.3.   Fatigue Properties

To gain a useful idea of the capability of metal foams to absorb energy, it is necessary to study their response under fatigue testing. In many potential structural applications, foams would be subjected to cyclic compression/tension loading in an attempt to absorb energy created by loading such as that generated by wind or earthquakes. Much of the research performed on metal foams has dealt with cellular aluminum, due to its availability and desirable material properties compared to other commercially available cellular metals. Unlike fully dense materials, foams undergo progressive collapse under

compression-compression fatigue loading and can experience large strain accumulation prior to failure, a desirable quality in the absorption of energy (Harte et al 1999).

The fatigue life of aluminum foams is defined by a sharp increase in strain after a certain number of cycles. In closed cell foams, failure is governed by the formation of a deformation band within the material, approximately equal to the cell size. These bands originate as a result of the plastic buckling of cell walls, often near the largest cells of the network. As further cycles are applied, cracks that are formed from the cell wall buckling are allowed to propagate, causing the deformation band to grow and subsequently additional bands to form until full densification is experienced (Sugimura et al. 1999).

As in compression-compression fatigue, damage under fully reversed tension-compression fatigue is characterized by the formation of cracks. These cracks often initiate at pre-existing defects within the microstructure such as precracks or holes within in the cell walls. As the material is subjected to more and more cycles, these cracks grow, primarily in sections of cell walls where the thickness is smallest (Zettl et al. 2000).

In a study on the fatigue behavior of closed cell foam, Ingraham et al. (2008) found that foam samples tested over a range of applied strain amplitudes from 0.05 to 0.50% displayed consistent hysteresis loop shapes. This indicated that failure mode of closed cell foam in reversed cycle fatigue is independent of strain amplitude. Ingraham et al. (2008) used the ratio of pre peak compressive to tensile slopes on the hysteresis loop to define failure. As a crack developed within the foam microstructure, the pre peak tensile slope flattened out while the compressive pre peak slope increased as the crack closed. Once the ratio of the slopes increased above a defined threshold of 1.5, the foam

14

was said to have reached its fatigue life. This definition of failure, along with two others, is adopted for use in fatigue testing of open cell foam and results are compared to those found by Ingraham et al. for closed cell foam.

Specimens were observed to reach saturation stress, meaning that no further strain hardening would occur in successive cycles, after only a few cycles in all cases. Failure was governed by the formulation and growth of a crack. Digital image correlation performed in this study also showed that the crack propagation is enhanced by the compaction of the crack during the compression cycle. This compaction assisted crack propagation is characterized by plastic densification of the material in the compression cycle, shortening the specimen. Cracks are then required to open further during the tensile cycle in order to reach the defined strain amplitude.

Closed cell foam was determined to display a Coffin-Manson relationship of strain to fatigue life, which takes the form,

$$\varepsilon_p = \varepsilon_f' \left(N_f \right)^c.$$ (10)

In this equation, ε_p is the plastic strain amplitude, defined as half the width of the hysteresis loop at saturation stress and $2N_f$ is the number of reversals to failure. The curve fit parameters that define the relationship are the fatigue ductility coefficient, ε_f', and the fatigue ductility exponent, c. Results of the Ingraham et al. fatigue tests on closed cell foam are compared to results of similar testing performed on open cell foam.

Most of the work to date regarding fatigue properties of cellular materials has been performed on closed cell foams. A portion of this project will be to investigate the behavior of open cell aluminum foam under applied cyclic loading, specifically high

strain, low cycle fatigue. By performing fatigue tests on open cell foams, hysteretic and energy absorption characteristics can be obtained and compared to the existing data for closed cell material. Due to the less confined morphology of open cell foams, it is intuitive that they too would experience large strain accumulation prior to failure and full densification.

1.4. Computer Modeling

To date, there has been a good amount research performed in attempt to determine foam properties using computational modeling. In one such study, performed by Wen-Yea Jang, Andrew M. Kraynik and Stelios Kyriakides in 2009, open-cell aluminum foam was modeled based on the geometry and characteristics obtained from X-ray tomography. Several models were created with increasing levels of randomness to determine its effect on the elastic properties of the material. The most idealized model was created as a network of regular 14-sided Kelvin cells. A regular Kelvin cell is shown below in Figure 5.
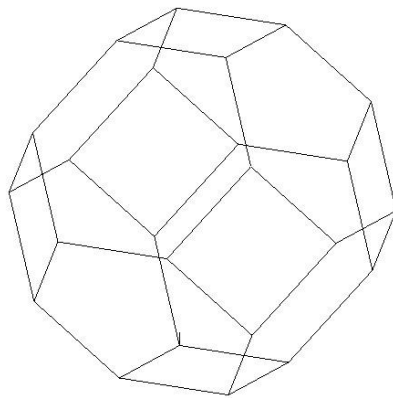
Figure 5: Regular 14-sided Kelvin cell used in computer models of 3-D foams

This geometry was used as the basis for the computer models created for this project and is described in further detail in Section 4.0.

Ligaments were modeled as elasto-plastic, shear deformable beams with non-uniform cross sections along the length. This method of defining the ligaments was utilized in place of three-dimensional solid elements for efficiency based on the size of the networks and magnitude of elements used in the models being analyzed (Jang and Kyriakides 2009). However, the use of beam elements introduced the existence of overlapping material at ligament intersection, which needed to be removed for accuracy in the model. Ligaments were assigned the properties of the base material of Al-6101-T6 aluminum alloy including an elastic modulus of 10,000 ksi. Using X-ray tomography, it was determined that a typical ligament in the foam being modeled was convex and had a varying thickness along the cross section. Because it was found that altering the cross sectional shape had no effect on the calculated elastic properties, a circular cross section was used in the model with a varying radius along the length. At low stresses, results from the model adequately matched results of physical testing on the appropriate samples (Jang and Kyriakides 2009). In elasto-plastic models, a reduction in stiffness associated with plastic action governed by limit load is observed at higher stresses. This is different from the buckling type instabilities associated with fully elastic models and when this plastic behavior is included, good agreement with measured foam yield stresses are observed (Jang and Kyriakides 2009). The correlation of these models with mechanical testing results indicates that the inclusion of axial and shear deformations, the variation of cross section along ligament length and the nodal end conditions are vital in determining elastic properties using computer models (Gong et al. 2005).

Most foam contains some level of anisotropy, commonly the elongation of cells in the rise (vertical) direction (Gong et al. 2005). The inclusion of this within reported

models also can be attributed to the accuracy of the results as it enhances the realism of the model to actual foam material, even in unperturbed networks. When modeling foams with random microstructure, it is essential to consider the effects of the network size on properties (Roberts and Garboczi 2002). If the created global model contains too few cells, the properties of the material will not be accurately represented. However in networks of adequate size (approximately 100 cells), it has been determined that the Kelvin cell model is an adequate method of replicating the initial elastic behavior of foams and thus determining their effective properties (Gong et al. 2005).

Most real foams are characterized by a random cellular microstructure rather than a perfectly ordered periodic geometry. For this reason, random foam models are the most realistic representations and yield results for elastic properties that most closely resemble the results of experimentation (Jang et al. 2008). Although, equivalent periodic foam models of ordered Kelvin cells are obviously unrealistically idealized, the predictions made for the elastic properties from these models are at most 24% higher than those found from mechanical tests. It was found that random networks of Kelvin cells produced 5-10% lower values for E^* than from ordered Kelvin networks. It has been reasoned that these results are within engineering accuracy for predictions of random foams and though irregular Kelvin models provide closer results, symmetric Kelvin models can be adequately used to predict the properties within a certain range (Jang et al. 2008).

CHAPTER 2

CELL WALL STIFFNESS RATIOS

Gibson and Ashby develop expressions for the effective elastic properties of a three-dimensional cellular network are based on the bending deformation of the cell wall ligaments. Their expressions do not take into account axial or shear deformations and are explicitly determined for ligaments with solid, rectangular cross sections. A portion of this research will be an effort to expand the current expressions to include axial and shear deformations and to loosen the assumption of rectangular ligament cross sections, instead expressing the equations in terms of ligament stiffnesses.

2.1.   Revised Gibson and Ashby expressions

In Gibson and Ashby's expressions for the elastic properties, the compressive stress is related to the global strain of a unit cell using Hooke's Law of elasticity. However, the strain as defined by the authors takes into account displacements as a result of bending only. In order to include axial deformations in the expression, the strain needs to be taken as proportional to total deformation, or $\varepsilon \propto \left(\delta_a + \delta_b \right) / l$. The axial and bending deformations are defined in equations (11) and (12) below,

$$\delta_b = C_{yb} \frac{Fl^3}{12 E_s I} \tag{11}$$

$$\delta_a = C_{ya} \frac{Fl}{AE_s} \tag{12}$$

where A is the cross sectional area of the ligament, E_s is the elastic modulus of the solid material from which the ligaments are comprised, and I is the bending moment of inertia of the ligament cross section. C_{yb} and C_{ya} are constants of proportionality that absorb

19

factors applied to the force and ligament length depending on the structure of the cell. Using Gibson and Ashby's cubic unit cell, these constants can be approximated using assumptions from basic mechanics.
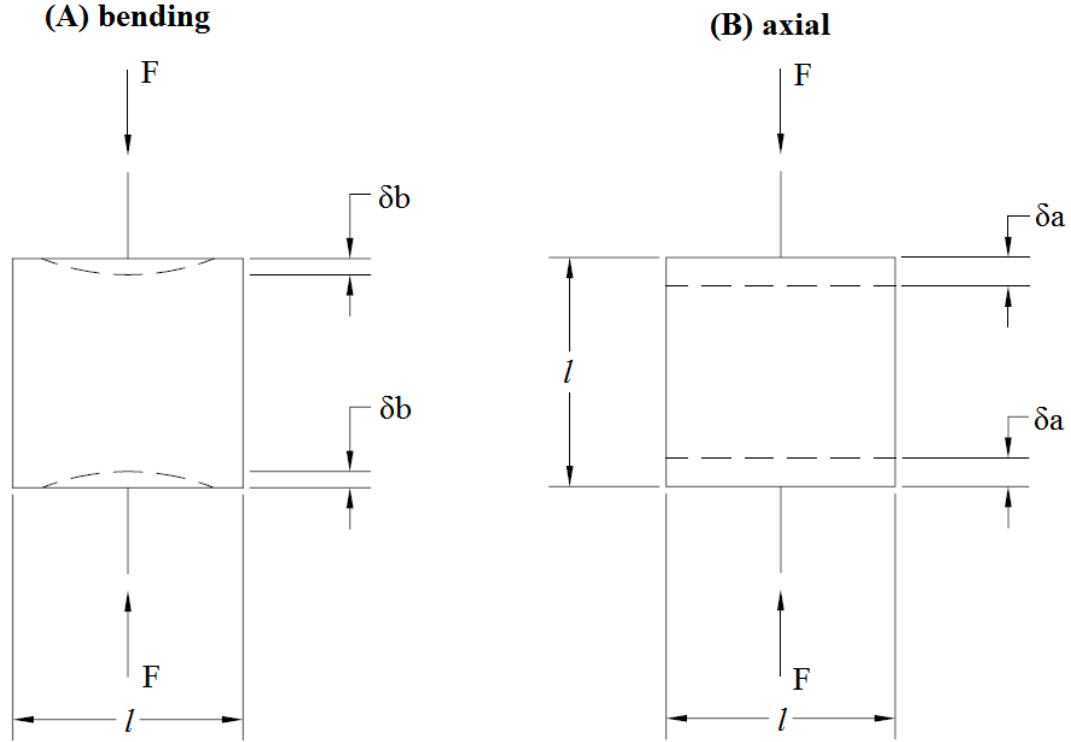
(A) bending   **(B) axial**

Figure 6: Two-dimensional respresention of unit cell deformation due to (A) bending and (B) axial forces

From Figure 6(A), the deflection due to bending, δ_b, is caused by one-half of the transmitted force, F, applied to one-half of the ligament length. This results in a proportionality constant, C_{yb} that is equal to 1/16. From Figure 6(B), the axial deformation, δ_a, is caused by one-half of the force transmitted through one-half of the length, yielding a proportionality constant, C_{ya} of 1/4.

2.2.   Stiffness Ratios

In order to relax the assumption of solid, rectangular ligament cross sections, the moment of inertia and cross sectional area are left as individual parameters in the elastic property expressions. To aid in this, the expressions will be rewritten in terms of the bending and axial stiffnesses. The bending stiffness of ligaments is

$$K_b = \frac{12E_sI}{l^3}.$$

(13)

The axial stiffness of ligaments is

$$K_a = \frac{E_sA}{l}.$$

(14)

These are related to each other by the stiffness ratio, defined as

$$R_k = \frac{K_a}{K_b}.$$

(15)

With these parameters defined, the expression for the elastic modulus can be rewritten to include bending and axial deformations in terms of the stiffness ratios as

$$E^* = \frac{C_E R_k K_b}{l\left(C_{ya} + C_{yb}R_k\right)}.$$

(16)

Similarly, the expression for the shear modulus is given by equation (17).

$$G^* = \frac{C_G R_k K_b}{l\left(C_{sa} + C_{sb}R_k\right)}.$$

(17)

These expressions can be plotted against R_k to determine the dependence of the elastic properties on the stiffness ratio, as shown in Figure 7. The properties are normalized by expressions determined based on bending deformation only, with $R_k \to \infty$.
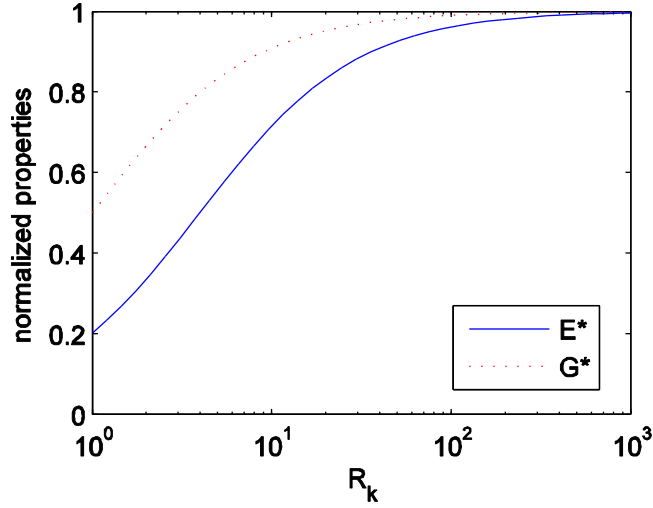
Figure 7: Variation of normalized properties with stiffness ratio, Rk

The value of R_k is shown to range from 10^0 to 10^3 as is typical in physical samples of aluminum open-cell foams. As expected, the properties converge to 1 as the value of R_k increases and the axial stiffness becomes large with respect to the bending stiffness. Variation of the stiffness ratio depends on the properties of the ligaments of the metal foam. Small values of R_k correspond to shorter, thin-walled tube-like ligaments in which the bending stiffness is much larger than the axial stiffness. Conversely, large R_k represents long, slender, cable-like ligaments with high axial stiffness and little resistance to bending.

In computing the stiffness ratios for the ligaments defined in the computer models discussed in Section 4.0, it was found that R_k is approximately 16 for the models. From Figure 7, this would correspond to an elastic modulus that is between 70 and 75% as stiff as one that was calculated based on bending deformation only. From this, it is reasonable to assume that the axial stiffness of ligaments has a definite effect on the behavior and properties of a foam network.

CHAPTER 3

COMPRESSION TESTING

In order to efficiently and confidently use any material for structural purposes, it is essential to have reliable knowledge of the material's properties and behavior. When the properties of a structural material are unknown or misrepresented, there is potential for inappropriate use and disastrous, occasionally dangerous consequences. Rigorous mechanical testing was performed to enhance understanding of the behavior of foam under common structural loading scenarios. Compression tests were performed on aluminum foam samples supplied by ERG Duocel. The samples had a reported relative density of 6 to 8% and the behavior of different porosity samples (both 20 and 40 pores per inch) was evaluated under monotonic compressive loads. The initial goal of the compression testing was to determine the effective elastic properties of open-cell aluminum foam and compare them to the predicted properties obtained from the Gibson and Ashby expressions defined in Section 1.2, as well as to the properties reported by ERG, the manufacturer of the foam samples tested. Furthermore, compression tests were used to illustrate the energy absorption properties of foam and highlight its strength in this area, a valuable structural characteristic.

Two sets of compression tests were performed. The goal of the first set was to gain an estimate of the elastic modulus of different porosity foams. However, the specimens used in this set of tests were very slender and therefore produced somewhat unreliable results due to the tendency of the specimens to buckle prior to the crushing that normally characterizes compression failure in foams. While the elastic modulus was measured in each of these tests and reported in the following section, only one test at

each porosity was able to be performed, an inadequate amount of data from which to extract confident conclusions. Furthermore, a complete representation of the compressive behavior of foam was impossible. The second set of tests, while not conducive to elastic modulus measurement due to dimensional constrictions, provided an opportunity to test the foam to densification and gain insight on the full compressive collapse behavior of the material.

3.1. Elastic Modulus Tests

To determine an initial approximation of the modulus of elasticity, monotonic compression testing was performed on three aluminum foam samples. This set of tests allowed the material to be loaded elastically and the stress strain response to be measured for the purposes of determining the elastic properties. The Gibson and Ashby equation for determining the elastic modulus of an open-celled foam, defined in Equation (5) of Section 1.2, is restated below.

$$\frac{E^*}{E_s} = C_1 \left(\frac{\rho^*}{\rho_s} \right)^2.$$
(18)

The expression states that the foam modulus, E^*, is dependent solely on the relative density, ρ^*/ρ_s, of the material and the elastic modulus of the solid material, E_s, of which the ligaments are comprised (with C_1 as a constant of proportionality equal to one). In an effort to broaden this assumption, tests were performed on three different porosities of foam to determine if the porosity of the foam has any relationship with the elastic modulus. Testing was limited to only three samples, one of each porosity, and therefore a robust set of data from which to draw meaningful, overarching conclusions is impossible. The results do provide a sound basis for estimating the elastic properties and allow for

further testing to be planned. Through additional testing, information necessary for determining potential structural use for foam can be provided.

3.1.1. Setup and procedure

Elastic modulus tests were performed on three aluminum foam specimens of porosities of 10, 20 and 40 ppi. The samples tested were relatively small scale, specified as being 88.9 mm in height with a 38.1 mm by 12.7 mm cross section. A schematic showing the dimensions of the samples tested is provided in Figure 8.
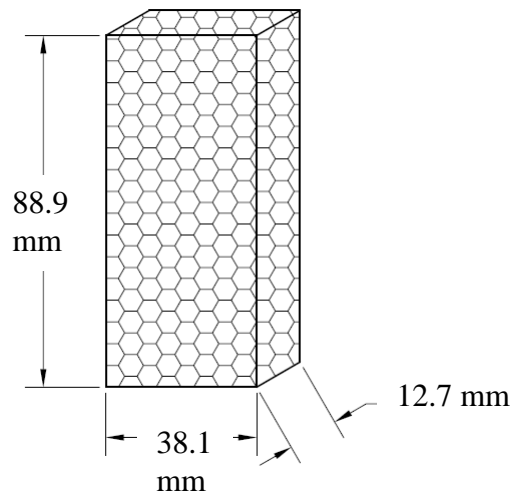
Figure 8: Example test specimen dimensions

As stated, the samples were reported by the foam manufacturer, ERG Duocel, as having a relative density between 6 and 8%. The exact relative densities of the 10 and 40 ppi samples were determined to analyze the accuracy of the Gibson and Ashby predictions and to ease in comparison of results between different specimens. The determination of the exact relative density values is discussed in Section 1.1.2.

The orientation required for precise strain measurement such that the effective length was defined as the maximum specimen dimension, in conjunction with the

slenderness of the specimens, made global buckling of the samples a concern during testing. In order to discourage buckling during loading, a fixture was implemented at the base of the specimen being tested. Two steel angles were positioned at the base of the specimen to provide rotational restraint, shortening the effective length of the specimen and therefore increasing the applied load that would cause global Euler buckling. The load required to induce Euler buckling is defined as

$$P_e = \frac{\pi^2 EI}{(kL)^2}. \tag{19}$$

The Euler buckling capacity of the aluminum foam specimens tested was calculated to be 7.32 kN. This value was calculated using Equation (X) assuming the specimen dimensions given in Figure 1, an elastic modulus of 441.6 MPa (determined from the Gibson and Ashby expression in Equation (5) of Section 1.2 for 8% relative density) and an effective length factor, k, of 0.7, a result of the steel angle restraints shown in the photograph of the test setup in Figure 9.
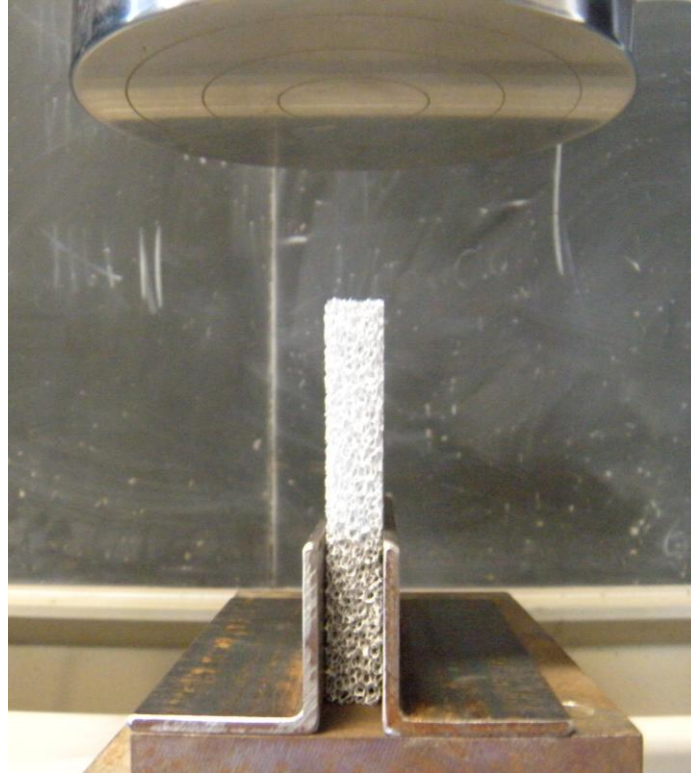
Figure 9: Monotonic compression test setup

It was assumed that the angles at the base of the specimen would provide rotational restraint, while the top of the specimen would be free to rotate at the platen where load is applied. Because the critical buckling load of 7.32 kN was determined to be greater than the predicted compressive load to cause yielding of the material, 1.2 kN, it was determined that buckling was not a concern for these tests. The critical yield load was calculated using the yield stress reported by the foam manufacturer, ERG Duocel, of 2.53 MPa, and the cross sectional properties of the specimen, shown in Figure X.

For each test, load and displacement data was captured directly from the testing machine as well as strain recorded by an extensometer, and a stress and strain relationship was obtained using the measured dimensions. From this, an elastic modulus

value could be approximated by determining the slope of the linear portion of the stress-strain curve.

The foam specimens were subjected to monotonic compression using an Instron Testing machine. Tests were displacement controlled with strain measured by the extensometer while in the elastic region and by the vertical crosshead displacement of the machine as the foam approached and progressed passed yield point. The extensometer had a gage length of 50.8 mm and a maximum displacement value of 12.5% strain so it was removed at about 8 to 10% strain to avoid damage as the sample experienced larger levels of deformation.

The 40 ppi and 20 ppi samples were loaded at a displacement rate of 0.0127 mm per minute, controlled by the vertical movement of the machine's crosshead, which in turn applied a corresponding compressive load on the sample. In the test of the 10 ppi sample, the load rate was decreased to 0.0889 mm per minute. The first two tests resulted in the failure of the specimens at lower than expected loads, so the slower load rate was instituted to allow for closer monitoring of the applied load.

Tests were stopped shortly after yield of the material, prior to densification, at approximately 10-15% strain because it was anticipated that this would provide enough data for determining an initial estimate of the elastic modulus. Full behavior of foam as it underwent progressive collapse and densification was captured in the second set of tests, described in Section 3.2.

3.1.2. Results

To analyze the elastic response of aluminum foam, load and displacement data was captured electronically from the test machine and manipulated to obtain a stress-strain relationship for each test. The linear portions of the stress-strain curves were used to approximate the elastic modulus of each sample and are compared to one another in Figure 10.
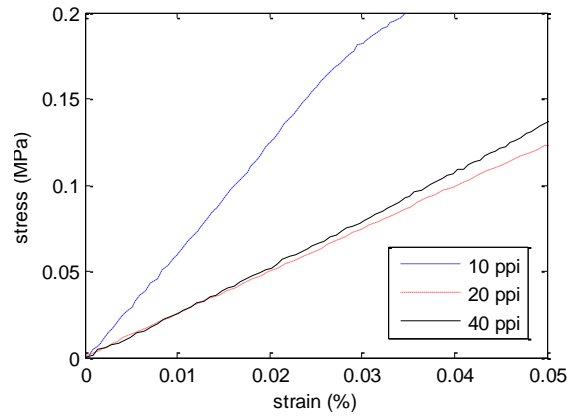
Figure 10: Comparison of linear portion of stress-strain curves

As discussed, strain measurement for this response was taken using an extensometer due to crosshead displacement data being unreliable due to lack of calibration at the time of testing. The calculated values for the elastic modulus of each foam sample, determined by the slope of the linear portion of the stress-strain curve, are shown in Table 1.

Table 1: Experimentally measured values of elastic modulus

Porosity, *ppi*	Elastic modulus,MPa
10	588
20	261
40	265

Figure 10 and Table 1 show that the 20 and 40 ppi samples have similar elastic modulus values while the 10 ppi displays much stiffer behavior. However, the comparison of these samples to one another may not be significant as their relative densities are vastly different. According to the Gibson and Ashby relationship, larger relative density would result in the stiffer behavior observed here. To gain a more contextual understanding of the elastic modulus results, the precise value of relative density for the specimens was determined and the elastic modulus values found from testing were compared to values predicted using the expressions developed in *Cellular Solids* by Gibson and Ashby.

The expression developed by Gibson and Ashby in Equation (5) concludes that the elastic modulus of foam depends directly on the relative density and the elastic modulus of the base material ($E_{aluminum}$ is 69 MPa). The foams tested were reported by the manufacturer to have relative densities between 6 and 8%. Based on the expressions, foams with relative density within this range would result in a predicted elastic modulus anywhere within a range of 248 to 441 MPa. To more accurately predict the elastic modulus of each specimen for more useful comparisons with test results, the relative density of each specimen was calculated directly. Relative density, ρ^*/ρ_s, is defined as

$$\frac{\rho^*}{\rho_s} = \frac{\text{Density of cellular material}}{\text{Density of solid material}} = \frac{m^*/V^*}{m_s/V_s} \; , \tag{20}$$

where m^* and V^* are the mass and volume of the foam and m_s and V_s are the mass and volume of the solid material.

The mass of each specimen was measured using a digital scale with accuracy to the tenth of a gram. The volume of each specimen was measured to be 43 cubic centimeters based on the initial dimensions and the density of the solid material (aluminum alloy 6101-T6) was 2.7 g/cm^3 (Ugural and Fenster 2003). The calculated relative densities as well as the predicted elastic modulus from the Gibson and Ashby expressions and the percent difference of the predictions from the test results for the 10 and 40 ppi specimens are given in Table 2, with percent difference defined as

$$\frac{\left| E^*_{pred} - E^*_{test} \right|}{\left(E^*_{pred} + E^*_{test} \right)/2} \times 100\% \ . \tag{21}$$

In this equation, E^*_{pred} is the predicted value of elastic modulus based on the average relative density of all specimens tested as listed in the table and E^*_{test} is the elastic modulus value determined from the mechanical testing results

Table 2: Initial test specimen dimensions

Porosity, ppi	Mass, g	ρ^*/ρ_s, %	Predicted E*, MPa	Measured E*, MPa	% difference
10	10.7	9.14	584	588	0.68
40	7.7	6.61	306	265	14.4

The larger relative density value for the 10 ppi specimen above the range reported by the manufacturer explains the stiffer behavior illustrated in the test as it shows good correlation to the modulus value predicted by the Gibson and Ashby formula. Furthermore, the modulus measured from the test results of the 40 ppi foam also compares favorably to the predicted value using the calculated relative density. The mass and therefore the relative density of the 20 ppi sample were not measured prior to testing,

31

as deviation from the specification of the manufacturer was not anticipated. However additional samples were measured to determine an appropriate range of values for relative densities for a given porosity and are shown below in Table 3.

Table 3: Comparison of relative density for each specimen porosity

Porosity, *ppi*	Mass, *g*		ρ^*/ρ_s, %		Predicted E*, *MPa*	
	Mean	**Std. Dev.**	**Mean**	**Std. Dev.**	**Mean**	**Std. Dev.**
10	8.4	0.94	7.23	0.81	366	90.2
20	8.8	0.15	7.52	0.13	395	11.8
40	7.7	0.69	6.69	0.60	318	58.8

The values in Table 3 are the averages of at least three samples of each porosity, not including the specimens that were tested whose relative densities are reported in Table 2. It is shown that while the average relative density for available 10 ppi foams was within the reported range, this porosity has the highest standard deviation and therefore the 9.14% density sample is explained as an outlier from the expected density. Furthermore, the 20 ppi foams measured were all found to be within a range of 6.5 to 7.5% relative density with the least amount of variation of all the porosities. Therefore, it does not seem to be an unreasonable assumption that the 20 ppi sample tested could have had a similar relative density to the 40 ppi foam. This would explain the similarity in their respective measured elastic modulus values. Table 4 provides a summary comparing values measured from compression tests, predicted from equations and those reported by ERG Duocel, the foam manufacturer.

Table 4: Comparison of elastic modulus values

Porosity, *ppi*	Measured, *MPa*	Predicted, *MPa*	Reported, *MPa*
10	588	584	93.1
20	261	395	93.1
40	265	306	93.1

In Table 4, the measured values are those found from the slope of the linear portion of the stress-strain response of the mechanical compression tests performed. The predicted values are based on Equation (5) of Section 1.2 as derived by Gibson and Ashby in *Cellular Solids* (1997) and based solely on the computed relative density of the samples. The densities of the 10 and 40 ppi samples were computed for the specific specimens that were tested, but the density of the 20 ppi was not found prior to testing and this prediction is based on the average of three other available samples of the same porosity. As mentioned above, it is possible that the actual relative density of the sample was lower than assumed and thus yielded a prediction that is closer to the test result. The reported value in Table 4 is the modulus listed by the manufacturer of the foam, ERG Duocel, on their website for 6101-T6 aluminum foam with 8% relative density.

The measured values show relatively good agreement with those predicted by the Gibson and Ashby equations, but both values are much greater than those reported by ERG. While the larger relative density measured in the tested specimens than that reported by ERG undoubtedly played some role in the discrepancy, the difference in the densities is not large enough to result in the extreme difference observed between the values. Another possible suggestion for the inconsistent values is the size of the networks that were tested. Each of the specimens tested featured a rectangular cross section of 25.4 mm by 12.7 mm. However, it has been suggested by ERG that thicker samples be used

for crush testing in order to obtain results free from edge effects. Though the 12.7 mm thickness would provide the appropriate number of cells (8-10) suggested by other studies to give accurate compression behavior for the 20 and 40 ppi specimens, it would be worthwhile to investigate behavior for a larger cross sectional area with much more cells in each direction to increase the margin for error and decrease edge effects experienced by the samples. The 10 ppi sample would seemingly yield inaccurate results as it provides only about 5 cells through the thickness of the specimen. Furthermore, it seems from relative density measurements of the samples that ERG Duocel's assumption of a constant elastic modulus value, regardless of porosity, is inaccurate. While porosity itself may not directly impact the modulus, it seems to have an influence on the density of the material, which in turn impacts the elastic properties. While relative density and, by association, porosity have a clear effect on the compressive elastic modulus of the aluminum foam tested, this most likely is a result of the existing ligament properties of the foam. Observations of the three samples indicated that the ligaments in the 10 ppi foam had larger diameters than those in either the 20 or 40 ppi samples. This is apparent in Figure 1 of Section 1.0. The thicker ligaments in the 10 ppi foam result in more material within the sample and thus the larger measured relative density. Furthermore, because deformation of foam is governed by ligament bending, the thicker ligaments result in a stiffer response of the global material. This is the primary underlying reason for the difference in elastic response of the different porosity samples. Because of the good agreement between the measured values and those predicted by the Gibson and Ashby equations, it would seem most likely that the values provided by ERG may not be true to the actual material supplied. The fact that relative density varies a great deal from

sample to sample makes designing for a specific stiffness of foam a difficult proposition, especially when small volumes of material are used.

3.2. Densification Tests

The first set of tests was used to measure the elastic modulus of different porosity aluminum foams. However, these results may not be conclusive due to the lack of adequate dimensions in each direction in order to encapsulate true foam behavior free from edge effects. Though the second set of tests provided adequate number of cells to achieve representative behavior of a larger volume of foam, accurate strain measurements were not possible. For this reason, though elastic modulus measurement is addressed here, it is revisited during the results for fatigue testing and more reliable measurements of the modulus are provided.

3.2.1. Setup and Procedure

To observe foam behavior as it approaches and completes densification, cuboidal specimens were tested in compression to upwards of 80% strain. The specimens used had an initial cross section of 50.8 mm by 50.8 mm and a height of 25.4 mm, resulting in at least 10 cells being present in each direction. This size specimen would allow the test to encapsulate foam behavior free from edge effects and illustrate the densification of the material without danger of global buckling of the specimen. In order to allow for Poisson expansion during the test, a layer of thick grease was applied to each of the test platens. Figure 11 shows the test setup of a typical compression test on these specimens.
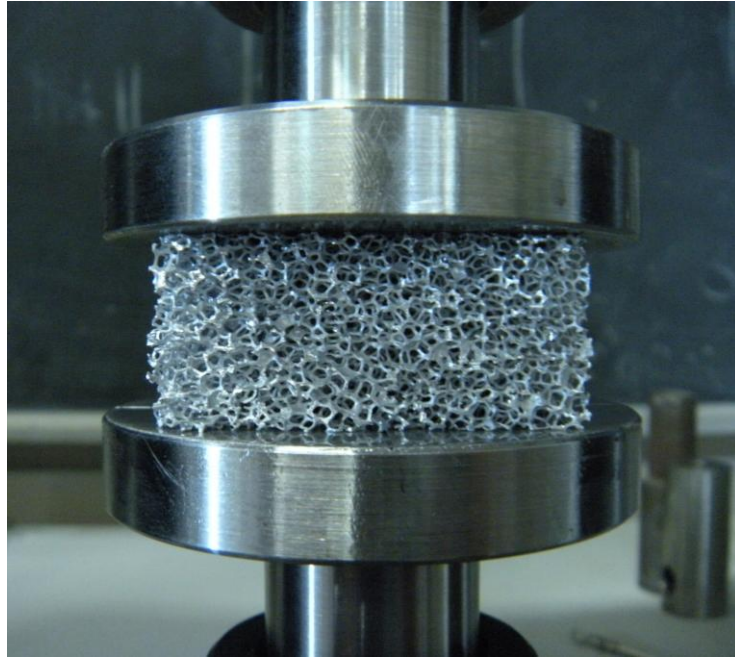
Figure 11: Monotonic compression test setup on cuboidal specimen

Like the first set of compression tests, an Instron Testing machine was used to apply monotonic compressive loading to the cuboidal specimens. Tests were displacement controlled to ensure that full response of the material was captured. Although the specimens used for these tests provided the necessary 10 cells in each direction to fully capture behavior free from edge effects, the dimensions of the specimens were not adequate to allow the use of the extensometer to measure strain. The gage length of the extensometer was 50.8 mm and thus too large to be attached to the cuboidal specimens without potential damage occurring during testing. Strain was thus measured using the crosshead displacement of the testing machine which, as discussed, was not a reliable method. For this reason, the elastic modulus could not be measured during this set of tests.

3.2.2. Results

Compression tests of cuboidal specimens were performed beyond the point of densification of the foam, upwards of 80% strain, in order to fully illustrate the response of the material under extended loading. Full behavior of foam in compression is characterized by a long stress plateau after yield followed by a dramatic increase in stiffness after densification. Although the strain in this set of tests, as previously noted, was not able to be measured accurately, the specimens were used to highlight the full compressive behavior of the material, shown in Figure 12.
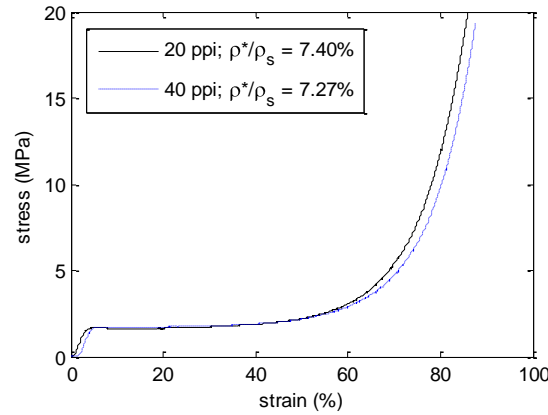
Figure 12: Full stress-strain response of 20 and 40 ppi aluminum foam under compressive loading

As illustrated by the stress-strain curves, when foam is loaded in compression, yielding occurs at approximately 5% strain followed by a long densification plateau to about 60% strain. During this densification phase, the foam undergoes a large amount of deformation without a substantial increase in stress. At about 60% strain, collapse of the ligaments in the foam microstructure is complete and the voids that were initially present in the material no longer exist. With densification complete, the stress-strain relationship shows a drastic increase in stiffness as the foam takes on the elastic properties of the base

material. That is, the slope of the stress-strain curve of the foam after densification is equal to the elastic modulus of aluminum. While the elastic properties, though not measured in this set of tests, have been shown to be dependent on porosity, Figure 12 shows that this behavior in response to compressive loading is largely independent of porosity. Both the 20 and 40 ppi samples demonstrate the extended collapse plateau followed by dramatic increase in stiffness after densification. The long progressive collapse plateau of aluminum foam makes it an extremely attractive material for use in applications where energy absorption is desirable. The capability of the material to undergo extensive deformation without loss of strength is vital in several structural capacities. The potential for use in energy absorption applications makes aluminum foam a strong candidate for use in such structural endeavors as impact absorbing siding or as a bracing member of a building frame.

CHAPTER 4

TENSION TESTING

Many of the potential structural applications of foam, such as in the core of a sandwich beam, can result in tensile forces being applied to the material. For this reason, it is essential to understand the tensile response of aluminum foam. To do this, monotonic tensile testing was performed on samples of different porosities to measure the elastic properties and investigate tensile behavior, especially at failure.

While compressive failure of foam is characterized by progressive collapse due to ligament bending and buckling, tensile failure is sudden and brittle, governed by fracture of the ligaments. Tensile testing was performed to compare the elastic response in tension to that in compression as well as to examine the peak strength and strain that the material can undergo. The results of tensile tests were then used to shape the plan for cyclic testing in which to study the fatigue properties of foam, also essential in determining its potential for structural use.

4.1 Material and Setup

Monotonic tension tests were performed on 20 and 40 ppi samples of ERG Duocel open-cell aluminum foam. The 10 ppi samples were not tested because their microstructure was such that it did not provide enough cells through the cross section to not only ensure true behavior, but also even provide a useful representation of behavioral properties. The samples used in the elastic modulus compression testing (initial dimensions of 88.9 by 38.1 by 12.7 mm) were machined into dogbone specimens for tensile testing. The cross section of the specimens was reduced to 25.4 mm by 12.7 mm, promoting failure within

this area of the sample rather than at the connections. Figure 13 shows a schematic of the tensile specimens used in testing.
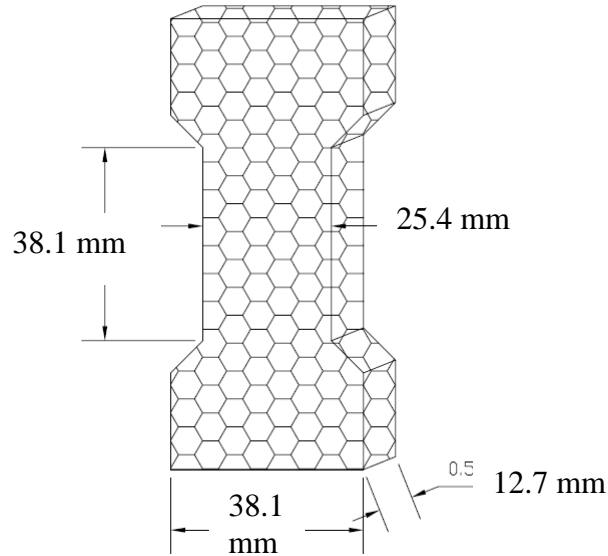
Figure 13: Example tensile test specimen dimensions

Typical tensile grips clasp onto the ends of the specimen and tighten when load is applied. However, because of the cellular composition of the material and potential for crushing under applied compressive forces, typical grips of this type could not be used in this testing approach. Instead, specimens were bonded to stainless steel platens using epoxy adhesive called JB Weld (tensile strength of about 27 MPa). The adhesion strength of the epoxy is about 12 MPa, stronger than the assumed tensile strength of the foam, ensuring that failure of the material would occur prior to separation of the foam from the platen, provided epoxy is mixed and applied correctly. Strain, as in compression testing, was measured using an extensometer attached to the specimen at the boundaries of the reduced cross section. The Instron Testing machine was again used to perform displacement controlled tests on the dogbone specimens. A photograph of the test setup

showing the extensometer attached to the specimens and the epoxy adhesion of the specimen to the grips is provided in Figure 14.
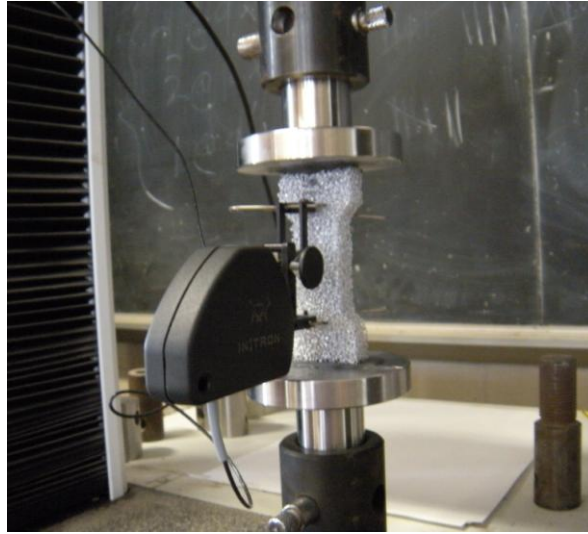
Figure 14: Test setup for monotonic tension testing of aluminum foam

Although, as in the compression tests, these specimens do not provide enough cells in each direction to achieve behavior representative with that of larger samples of the material, the tests do provide an informative measure of both the elastic modulus in tension and ultimate tensile strength. It is anticipated that larger volume specimens, featuring more cells in each direction to fully encapsulate behavior would display stiffer behavior and higher strength than the slender specimens tested. Furthermore, the tests highlight the failure mechanism of aluminum foam in tension and allow for comparison of the behavior of two different porosities.

4.2.   Results

Two tests at each porosity (20 and 40 ppi) were performed and stress-strain response of the foam in tension was recorded. The tensile stress-strain responses for the 20 ppi samples are shown in Figure 15.
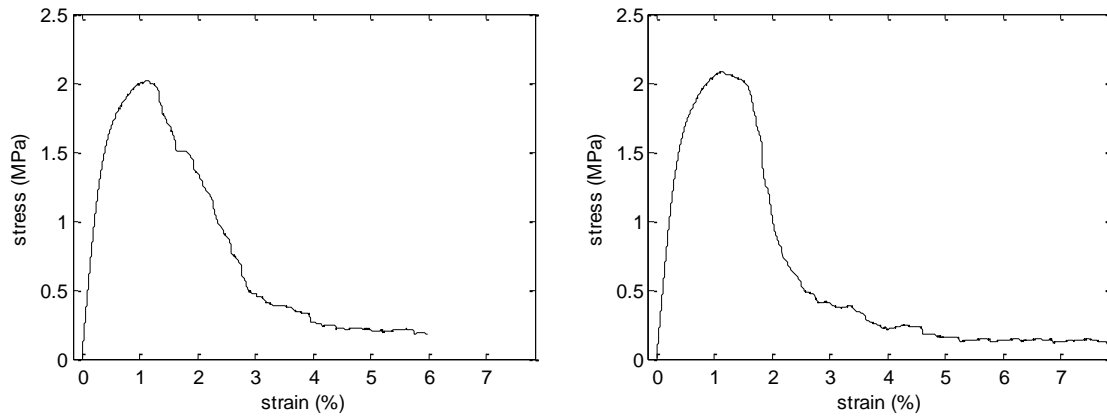
Figure 15: Stress-strain response of 20 ppi foam under monotonic tensile loading for (A) specimen 2-20-1 (B) specimen 2-20-2

Figure 15 highlights the sudden, brittle failure of aluminum foam in tension as the curves show the material losing significant strength almost immediately after yield. Table 5 shows the results for the elastic modulus, ultimate strength and the strain at peak stress for the 20 ppi specimen tests.

Table 5: Results of 20 ppi tensile tests

Specimen	$\rho*/\rho_s$ (%)	$E*$ (MPa)	$E_{pred}*$ (MPa)	% Difference	σ_u (MPa)	ε_u (%)
2-20-1	8.16	394	459	15.2	2.02	1.15
2-20-2	8.41	452	488	7.7	2.08	1.13

Table 5 shows that the elastic modulus measured from the tensile response of the 20 ppi aluminum foam sample showed good correlation with the predicted elastic modulus from the Gibson and Ashby expressions, $E_{pred}*$. Elastic modulus results from tensile testing are compared to compressive elastic modulus in Table 7. Percent difference was calculated using Equation (21). The tensile stress-strain responses of the 40 ppi samples tested are shown in Figure 16.
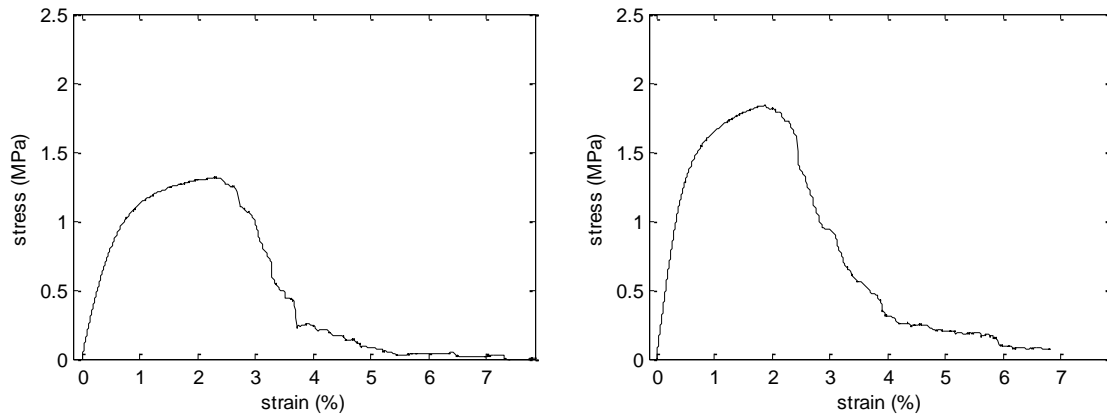
Figure 16: Stress-strain response of 40 ppi foam under monotonic tensile loading for (A) specimen 2-40-1 (B) specimen 2-40-2

Table 6 shows the results for the elastic modulus, ultimate strength and strain for the 40 ppi specimen tests.

Table 6: Results of 40 ppi tensile tests

Specimen	ρ^*/ρ_s (%)	E^* (MPa)	E_{pred}^* (MPa)	% Difference	σ_u (MPa)	ε_u (%)
2-40-1	7.42	148	380	87.9	1.32	2.33
2-40-2	7.92	288	433	40.2	1.84	1.88

While the 40 ppi specimens tested also displayed a very abrupt, brittle failure, they showed slightly larger strain at failure than the 20 ppi specimens, a softer response in the linear elastic region, and lower ultimate strength. However, not only do the 40 ppi results show a much greater variability between the two tests than the results for the 20 ppi samples, albeit in a small sample size, but both tests also yield elastic modulus values that are significantly different from the Gibson and Ashby predictions. This suggests that porosity affects the tensile elastic properties of foam, most likely due to the difference in ligament geometry. Because tensile failure is governed by fracture of individual ligaments, properties of the ligaments such as cross sectional diameter or thickness and

length can greatly affect the behavior of the material. Therefore, the difference in ligament geometry that exists between porosities greatly influences the elastic properties of foam.

As anticipated, tensile loading caused specimens to fail in a sudden, brittle manner. The tensile fracture surface occurred on a diagonal plane through the reduced cross section of the specimen in each test, as shown in the 40 ppi specimen in Figure 17.
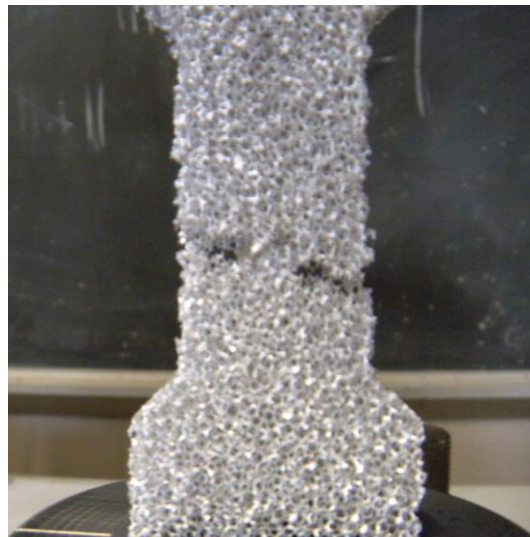
Figure 17: Diagonal tensile crack in 40 ppi specimen

From observation during testing, as foam is loaded in tension, ligaments bend and straighten vertically until fracture occurs. Much like crack propagation in solid material, tensile cracks in foam begin at an initial defect in the microstructure and propagate across the cross section at points of weakness or existing defects.

As stated, it is important to understand both the tensile and compressive properties of foam in order to successfully apply the material towards structural uses. Specifically, the differences between the behavior of foam in tension and compression provide insight on the type of use the material is best suited for and how it will respond to

different structural applications. Gibson and Ashby (1997) state the elastic response of a foam in tension is identical to its response in compression. Confirmation of this assumption can be achieved by comparing the elastic modulus results of the tensile tests with the results of the elastic modulus compression tests described in Section 3.1. Table 7 details this comparison using the average values of relative density and elastic modulus from all tests performed on the porosity specified.

Table 7: Comparison of monotonic testing resuts for 20 and 40 ppi aluminum foam samples in tension and compression

		20 ppi	40 ppi
Tension	ρ^*/ρ_s **(%)**	8.29	7.67
	E_T^* **(MPa)**	423	218
	Pred E_T^* **(MPa)**	481	412
	% Difference (%)	12.8	61.6
Compression	P^*/ρ_s **(%)**	7.52	6.69
	E_C^* **(MPa)**	261	265
	Pred E_C^* **(MPa)**	396	313
	% Difference (%)	41.1	16.6

The comparison between tensile and compressive behavior in Table 7 is highlighted by the percent difference, defined in Equation (21) of Section 3.1.2, between the elastic modulus from testing and the predicted elastic modulus from the Gibson and Ashby relationship in Equation (5).

As the comparison in Table 7 illustrates, while the prediction for tensile elastic modulus of the 20 ppi foam was fairly accurate (12.8% difference), the prediction for the tensile modulus of the 40 ppi specimen was vastly different (61.6%) from the result of testing. Conversely, the compression test comparisons showed the opposite relationship

in which the 40 ppi prediction was substantially closer (16.6% difference) to test results than the 20 ppi results (41.1% difference).

While, the discrepancy between predictions for compressive elastic modulus and results of compressive testing is likely a result of specimen dimensions and insufficient numbers of cells in each direction to capture representative behavior, the disagreement between predictions and tensile test results is much more surprising. To this point, the elastic modulus measured in tension and compression has been assumed to be the same. The inconsistency in variation from predictions across porosities suggests that more rigorous investigation into tensile foam mechanics is needed.

To this end, the results of tensile testing could be used to outline the test matrix for fatigue testing of aluminum foam. Due to the brittle response of foam in tension, the strain at which failure occurred in tension could be used to determine a maximum threshold for strain amplitudes of cyclic testing. In order to ensure tests provide the most useful sense of the fatigue life of the material, tests with strain amplitudes greater than the failure strain of the material in monotonic testing would cause failure prior to adequate cycling of the load to provide useful data in measuring the fatigue life.

CHAPTER 5

FATIGUE TESTING

Understanding of the behavior of open cell aluminum foam under cyclic loading is substantially more limited than that of monotonic loading or either compression-compression or tension-tension fatigue. With this in mind, tests were performed in an attempt to characterize the relationship between strain amplitude and fatigue lifetime for open cell foams under fully reversed loading over a range of 0.30 to 1.25% applied strain amplitude. Through a relatively small number of cycles, these high amplitude tests provide insight into not only the behavior and mechanism of failure under fatigue loading, but also into potential definitions for failure of the material, after which point structural capacity is no longer reliable.

Many structural engineering applications of foam, such as the absorption of energy from an earthquake or impact resistance, will result in both tensile and compressive forces being applied to the material. For this reason, tests were performed such that foam was subjected to equal amplitude tensile and compressive cycles. The results of the high amplitude tests can be extrapolated to hypothesize the potential results of low amplitude, high cycle fatigue tests, which to this point have not been performed on open cell foam. The results of the tests can also be compared to the results of closed cell aluminum foam testing performed by Ingraham et al. (2008) to highlight the effects of cell structure on fatigue properties, and conclusions can be made about the potential of the material for use in structural, cyclic energy absorbing applications.

5.1.   Test Setup and Procedure

Fatigue tests were performed on open cell aluminum foam using the same Instron Testing Machine as used in the monotonic tension and compression tests. Because this is not a hydraulic loading machine, testing frequency could not exceed 0.10 Hz, which severely influenced the length of tests and limited the magnitude of strain amplitude that could be realistically utilized. Dog bone specimens were used with reduced cross sectional dimensions of 38.1 inches by 50.8 mm and a gage length of 50.8 mm. An example test specimen used for fatigue testing as well as a photograph of the test setup is shown in Figure 18.
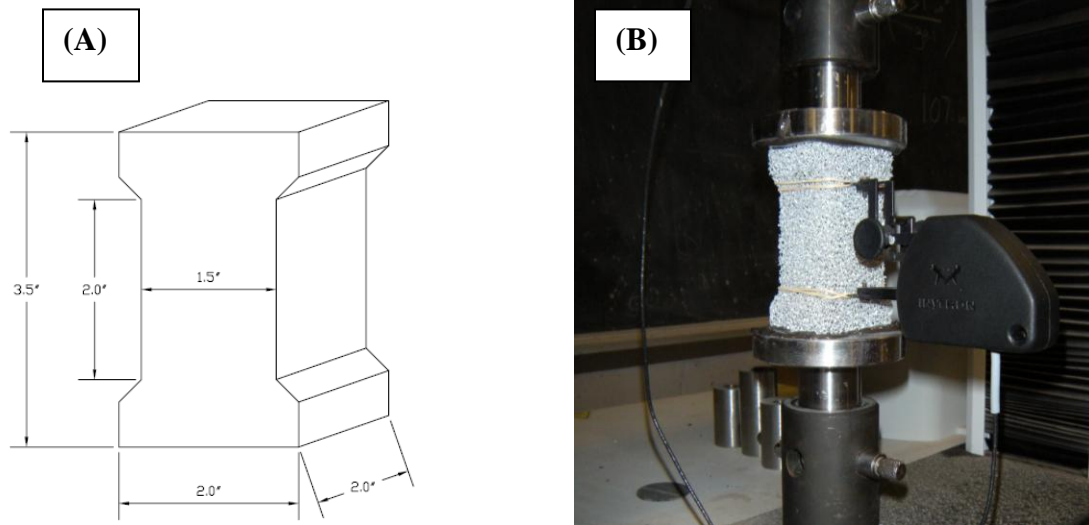
Figure 18: (A) Example fatigue test specimen dimensions and (B) Photograph of test setup for 20 ppi foam sample in Instron Testing Machine with strain measured using an extensometer

Strain was measured using the extensometer attached to the specimens using elastic bands. The gage length of the specimen was chosen to match the gage length of the extensometer, which is illustrated in Figure 18(B). In order to transmit both tensile

and compressive forces into the foam, the specimens were affixed to circular platens using an epoxy adhesive called JB Weld.

Strain controlled tests were performed for high amplitude, low cycle fatigue. Specimens were tested at 0.30, 0.40, 0.50, 0.75, 1.00 and 1.25% applied strain amplitudes. Though investigation of high cycle fatigue is necessary, the conclusions developed from high applied strain amplitude testing is valuable as low cycle properties are not currently known for the material. The tests performed herein are the first step in fatigue characterization of open cell aluminum foam.

5.2. Failure Criteria

Ingraham et al. (2008), in their work regarding the fatigue behavior of closed cell foams, found that foams subjected to reversed cyclic loading will develop a tensile crack at a pre-existing defect. The crack will then propagate through the material until failure. However, when foams are subjected to relatively low strain amplitudes, failure of a specimen may not be obvious or will be difficult to discern. For this reason, criteria for defining the failure of a specimen must be defined so that a distinct value for the fatigue life of foams can be determined and analyzed. To this end, four distinct criteria for the fatigue failure of open-cell foams have been defined: the increase of the ratio of pre-peak slopes, the degradation of peak compressive and tensile stress and the formation of a kink in the compression curve of the hysteresis loop.

Figure 19 illustrates the four failure criteria outlined for fatigue testing of open cell foam. Two hysteresis cycles are shown for a 0.75% strain amplitude test, both before and after failure has occurred. In the failure cycle shown, each of the failure criteria has

been reached, though obviously not simultaneously. This cycle was chosen so as to obviously highlight each of the criteria.
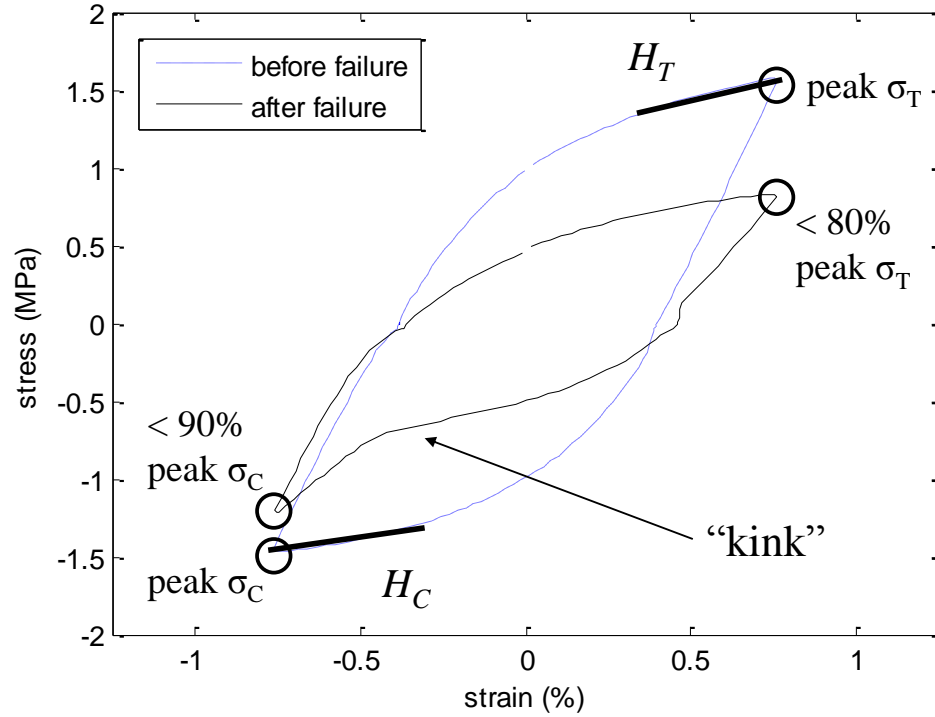
Figure 19: Definition of failure criteria for fatigue testing of aluminum foam

5.2.1. H_C/H_T ratio

The first failure criterion for fatigue testing of open cell aluminum foam was adopted from the work of Ingraham et al. (2008). In performing fatigue testing on closed cell foam, Ingraham et al. used the ratio of compressive and tensile pre-peak slopes in the hysteretic relationship to determine failure of a specimen. With an increase in cycles, the tensile pre-peak slope of the stress-strain hysteresis curve will decrease as the specimen undergoes tensile yielding until a tensile crack has formed in the foam. The compressive pre-peak slope will correspondingly increase as the specimen returns to elastic behavior after the closing of the crack. When the ratio of these slopes, henceforth known as the H_C/H_T ratio, exceeds 1.5, fatigue failure is said to have occurred by Ingraham et al. This

threshold was proposed in the study of closed cell fatigue behavior as it was determined that at this point a significant amount of damage had accumulated in the specimen, specifically a significant number of ligaments having reached the point of tensile fracture or compressive yield.

5.2.2. Degradation of peak tensile stress

An important characteristic of foam behavior in fatigue is the effect that increased applied loading cycles has on the tensile stress of the material. The most common mode of failure of foam subjected to cyclic loading is the formation of tensile cracks. These cracks develop when individual ligaments fracture in tension as discussed in Section 4.2 and open and close as the material continues to undergo cyclic loading. As cycles increase, the crack expands until failure occurs. As more ligaments are loaded to failure and ultimately fracture, the overall tensile stress experienced by the specimen decreases. To quantify this relationship between fatigue life and peak stress within a cycle, the second criterion of failure is defined to measure the degradation of the peak tensile stress with increased cycles. When the peak tensile stress in a cycle has decreased to less than 80% of the maximum peak tensile stress in all cycles, failure is said to have occurred. This threshold of failure was chosen because it was found to produce similar results for fatigue lifetime as the Ingraham et al. (H_C/H_T ratio) criterion. While this arbitrary threshold defining failure may not produce results for fatigue life that are representative of the actual ability of the material to perform under fatigue loading applications, the overarching behavior of the degradation of tensile stress is a valid and worthwhile measure with which to analyze fatigue behavior and properties.

5.2.3. Degradation of peak compressive stress

Similar to the degradation of the peak tensile stress, the peak compressive stress in each cycle is compared to the maximum peak compressive stress experienced in any cycle in order to determine when it has decreased to a point that failure is said to have occurred. A threshold was created in similar fashion to the tensile stress criterion that produced results of the same order of magnitude as the other methods of determining failure. When the peak compressive stress has dropped to 90% of the maximum stress, the foam is said to have reached failure. The failure mechanism of foam under fatigue is such that failure is less dependant on the compressive strength than on the tensile strength. As discussed in Section 4.2, yield strength in tension of open cell foam is less than the compressive yield strength and failure in tension is much more brittle. Therefore, when subjected to fully reversed cyclic loading, the ligaments of the foam will fail in tension prior to compression in general and result in a more rapid degradation in the overall tensile strength. For this reason, the threshold of compressive strength degradation for definition of failure was defined as a less dramatic decrease than the corresponding criterion for tensile strength.

5.2.4. Formation of "kink" in compression curve

When a tension crack forms in open-cell foam, the presence can be identified by a specific characteristic of the hysteresis curve. As a specimen with an initial crack is loaded in tension, the crack is opened by the applied forces. When the load reverses, the specimen undergoes elastic unloading followed by compressive yielding as the crack closes. Once the crack is fully closed, the foam undergoes plastic compaction, and the material is shortened. Elastic behavior returns prior to load reversal after the compression

band is fully densified and load is redistributed to other ligaments outside the local densified band. The crack then opens further on the successive cycle in order to maintain the required applied strain amplitude. This mechanism, observed in the tests of Ingraham et al. (2008) on closed cell foam is known as compaction assisted crack propagation. This specific failure mode is illustrated in the hysteresis loop as a "kink" that forms in the compression curve, highlighting the crack closure, yield, and return to elastic behavior.

The presence of a kink in the compression curve proved to be the most difficult of the four failure criteria to identify. While a kink is exaggerated and obvious after a number of cycles beyond development of a crack, the initial formation of a kink, which would suggest the existence of a crack and thus define failure, is often imperceptible. In order to locate the cycle at which the kink first exists, a procedure was created to determine when any portion of the compression curve of the hysteresis loop in a cycle was concave down.

The method created a cubic trend line of the bottom half of the hysteresis curve for each progressive cycle. Data points were plotted along the cubic trend line. A parabolic trend line was then fit to small segments (i.e. windows of five to ten data points) of the cubic trend and the second derivative of the parabolic relationship was found. When the sign of the second derivative was found to be negative, it indicated that a "kink" existed in the cycle and the first such cycle where this occurred was defined as the fatigue life.

However, it was found that this procedure worked best with larger strain amplitude tests and those with strain amplitudes less than 0.075% provided unreliable results. For this reason, results for the kink failure criterion were not reported but are

discussed where applicable to highlight the relationship between the formation of a kink, and therefore the presence of a crack, and the other failure criteria for failure.

Note that the kink indicated by the arrow in Figure 19 is the one described that indicates the existence of a fatigue crack. The second, more concentrated kink that exists at around 0.5% strain in the after failure curve is not related to failure of the material. Rather, this kink exists as a result of the manner in which the testing machine loads the specimen. Platens were fixed to the testing machine using pins as shown in Figure 18. This resulted in a temporary loss of load data recording at load reversal due to the small gap around the pins. When the load changes from tensile to compressive, there is a small period during which the specimen experiences no change in strain because of the space that exists at the pin connection at the test platens. Once the machine picks up load again, the hysteresis curve continues, but the kink shown in Figure 19 remains on the curve. The existence of this "hitch" in data collection is one of the reasons that quantifying the formation of the actual failure kink was so difficult.

Despite the evidence of the loss of data collection due to the "play" of the pins during load reversal, the use of the extensometer for strain measurement is vastly superior to the option of measuring strain by the movement of the machine crosshead. Figure 20 shows a comparison of hysteresis loops with strain measured by the extensometer and the crosshead movement.
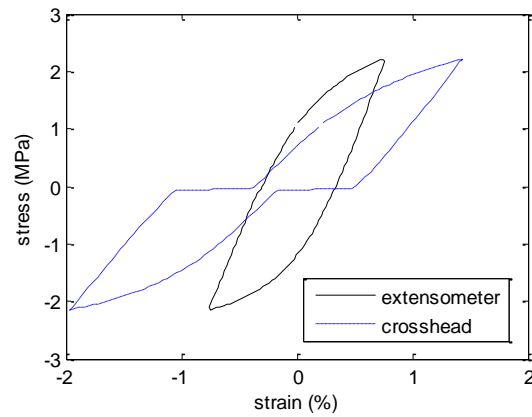
Figure 20: Comparison of hysteresis loops for strain measured by machine crosshead movement and the extensometer for 0.75% applied strain amplitude cycle

The curve illustrates the first cycle of a 20 ppi foam test at 0.75% applied strain amplitude and clearly shows the superiority of extensometer measurement as the inaccuracy in correlation between stress and strain experienced by the specimen is much less exaggerated than in the crosshead movement strain data.

5.3. Results

Three replications of each strain amplitude test were performed on both 20 and 40 ppi samples. Table 8 shows the results for fatigue life of 20 ppi specimens as defined by three of the four failure criteria. The cycle at which the kink indicating the existence of a crack criterion is omitted due to the described difficulty in identifying the kink in low amplitude tests.

Table 8: Fatigue test results for 20 ppi aluminum foam specimens

Specimen	$\rho*/\rho_s$ (%)	ε_a (%)	$H_C/H_T >$ 1.5	< 80% peak σ_T	< 90% peak σ_C
20-12	7.87	0.30	2316	1131	2316
20-17	7.53	0.30	2706	1351	3648
20-18	7.53	0.30	1081	902	126
20-05	7.93	0.40	589	481	602
20-10	7.41	0.40	796	454	695
20-11	7.41	0.40	666	377	613
20-04	7.53	0.50	111	101	123
20-06	7.35	0.50	173	171	295
20-14	8.05	0.50	161	131	109
20-03	7.41	0.75	11	13	14
20-07	7.18	0.75	31	36	40
20-09	7.70	0.75	29	36	40
20-01	7.29	1.00	15	16	17
20-02	7.47	1.00	13	9	10
20-16	7.53	1.00	11	11	12
20-08	7.18	1.25	6	3	3
20-13	7.58	1.25	7	4	4
20-15	7.47	1.25	8	7	8

Table 9 shows the results for 40 ppi tests.

Table 9: Fatigue test results for 40 ppi aluminum foam specimens

Specimen	ρ^*/ρ_s (%)	ε_a (%)	$H_C/H_T >$ 1.5	< 80% peak σ_T	< 90% peak σ_C
40-12	7.24	0.30	1380	1205	226
40-13	7.41	0.30	1536	1068	192
40-18	7.58	0.30	1800	1145	62
40-09	7.18	0.40	232	220	356
40-14	7.18	0.40	456	391	524
40-20	7.87	0.40	271	212	244
40-02	7.12	0.50	110	116	185
40-08	7.18	0.50	79	86	94
40-16	7.64	0.50	107	88	82
40-06	7.53	0.75	9	9	9
40-07	7.24	0.75	13	15	17
40-17	7.18	0.75	37	32	35
40-01	7.58	1.00	9	10	10
40-05	7.35	1.00	10	11	11
40-15	7.24	1.00	16	15	14
40-03	7.41	1.25	6	4	3
40-04	7.35	1.25	10	5	5
40-19	7.47	1.25	6	4	3

In general, the 40 ppi samples produced shorter fatigue life results than the 20 ppi tests, especially at low strain amplitudes. This is illustrated in Table 10 in which the average percent difference between 20 and 40 ppi results for each failure criterion at each applied strain amplitude. The average percent difference for each failure criterion is defined as the average difference between fatigue life results of 20 and 40 ppi samples divided by the average fatigue life across both 20 and 40 ppi samples for a given strain amplitude, or

$$\frac{\left(\dfrac{\sum N_{f_{20}} - \sum N_{f_{40}}}{3}\right)}{\left(\dfrac{\sum N_{f_{20}} + \sum N_{f_{40}}}{6}\right)} \times 100\% \ . \tag{22}$$

Table 10: Average percent difference of fatigue life for 20 and 40 ppi tests

ε_a (%)	Average percent difference of N_f		
	$H_C/H_T > 1.5$	< 80% peak σ_T	< 90% peak σ_C
0.30	25.6	-1.0	170.8
0.40	72.6	45.8	51.8
0.50	40.2	32.6	37.4
0.75	18.5	41.1	42.6
1.00	10.8	0.0	10.8
1.25	-4.7	7.4	30.8

As previously stated, fatigue failure is highlighted by the formation of a tensile crack. The tension tests in Section 4.0 indicated that the ultimate tensile strength in 40 ppi foams was lower than in 20 ppi foams. This is most likely a result of the ligament cross section properties of the different porosity specimens, and therefore the relative density.

While Tables 8 and 9 show the overall trend of a decrease in cycles to failure as strain amplitude increases, it is interesting to note the difference in fatigue life results across the four definitions of failure. Specifically, the difference in number of cycles required to decrease the peak compressive stress in low amplitude (0.30%) tests is vastly different than the fatigue life defined by the other criteria. Furthermore, the nature of this difference is not consistent for the different porosities. Results for the 20 ppi tests show that foams tested at 0.30% amplitude had a larger fatigue life as defined by the compressive stress failure criterion. The 40 ppi samples tested at this amplitude displayed the opposite effect, with much shorter fatigue life defined by compressive stress degradation. A possible explanation for this occurrence is the nature of fatigue failure being more dependent on tensile strength than on compressive stress. As discussed, fatigue failure is characterized by the formation of tensile cracks. Therefore, the point at which the compressive stress degrades past a certain threshold may not have a bearing on

the number of cycles it is subjected to, especially as the applied amplitude is decreased and the length of the test is increased.

The results for each criteria of failure are analyzed individually to compare the fatigue behavior of the different porosities.

5.3.1. H_C/H_T ratio

Figures 21 and 22 show the progression of the H_C/H_T ratio increase with the increase in cycles in fatigue tests on 20 and 40 ppi aluminum foams.
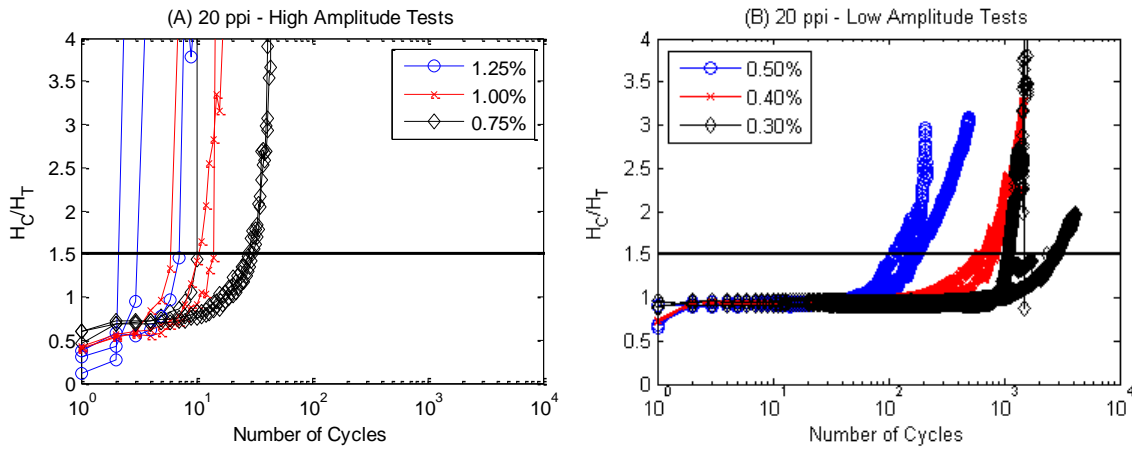
Figure 21: Increase of HC/HT ratio used to define failure as cycles increase for 20 ppi cyclic test with (A) high and (B) low strain amplitudes
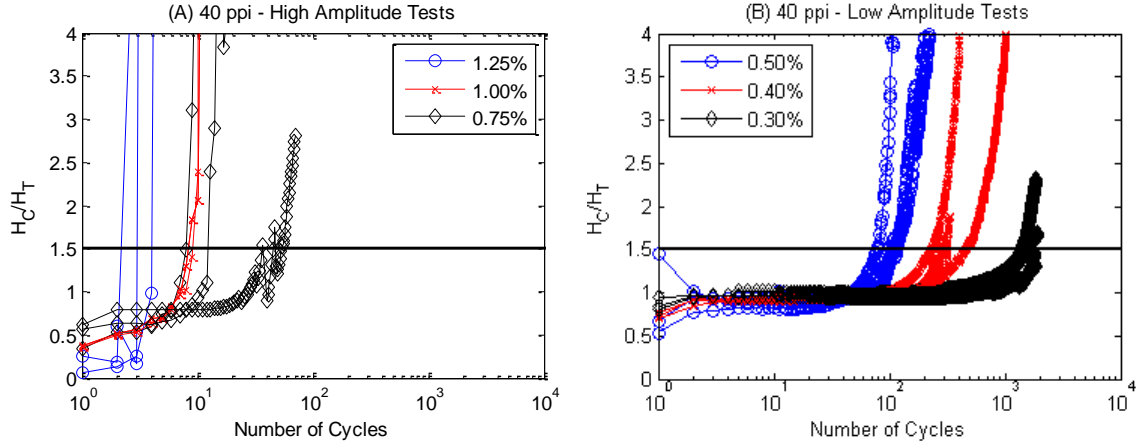
Figure 22: Increase of HC/HT ratio used to define failure as cycles increase for 40 ppi cyclic test with (A) high and (B) low strain amplitudes

As these figures show, the H_C/H_T ratio stays essentially constant during the majority of the test to the point when failure approaches. As discussed, the rise in the ratio is a result of both an increase in the pre-peak compression slope and a decrease of the pre-peak tension slope. This occurs due to the formation of a crack in the material. When a crack is present and the foam undergoes tensile load, the slope of the stress-strain curve flattens out as more ligaments yield and fracture, allowing the crack to further propagate though the material. When loaded reverses, the material is unloaded elastically, followed by a decrease in the stress experienced by the material as the crack closes. When the load is such that the crack is fully closed and the foam is experiencing applied compression, the slope of the compressive stress-strain response increases dramatically. Figures 21 and 22 highlight the rapid change of the H_C/H_T ratio as failure of the foam approaches. When a crack exists in the material, the ratio rapidly increases towards the defined failure threshold of 1.5. Prior to the formation of the crack, the pre-peak slope remained essentially constant. Once the crack formed and began to expand towards failure, each progressive cycle featured an increase in the H_C/H_T ratio.

60

The effect of the H_C/H_T ratio progression on the hysteresis relationship of foam is illustrated in Figure X.

(A) H_C/H_T=0.79

stress (MPa) vs strain (%)

cycle1

(B) H_C/H_T=0.79

stress (MPa) vs strain (%)

cycle1
cycle10

(C) H_C/H_T=0.91

stress (MPa) vs strain (%)

cycle1
cycle25

(D) H_C/H_T=1.54

stress (MPa) vs strain (%)
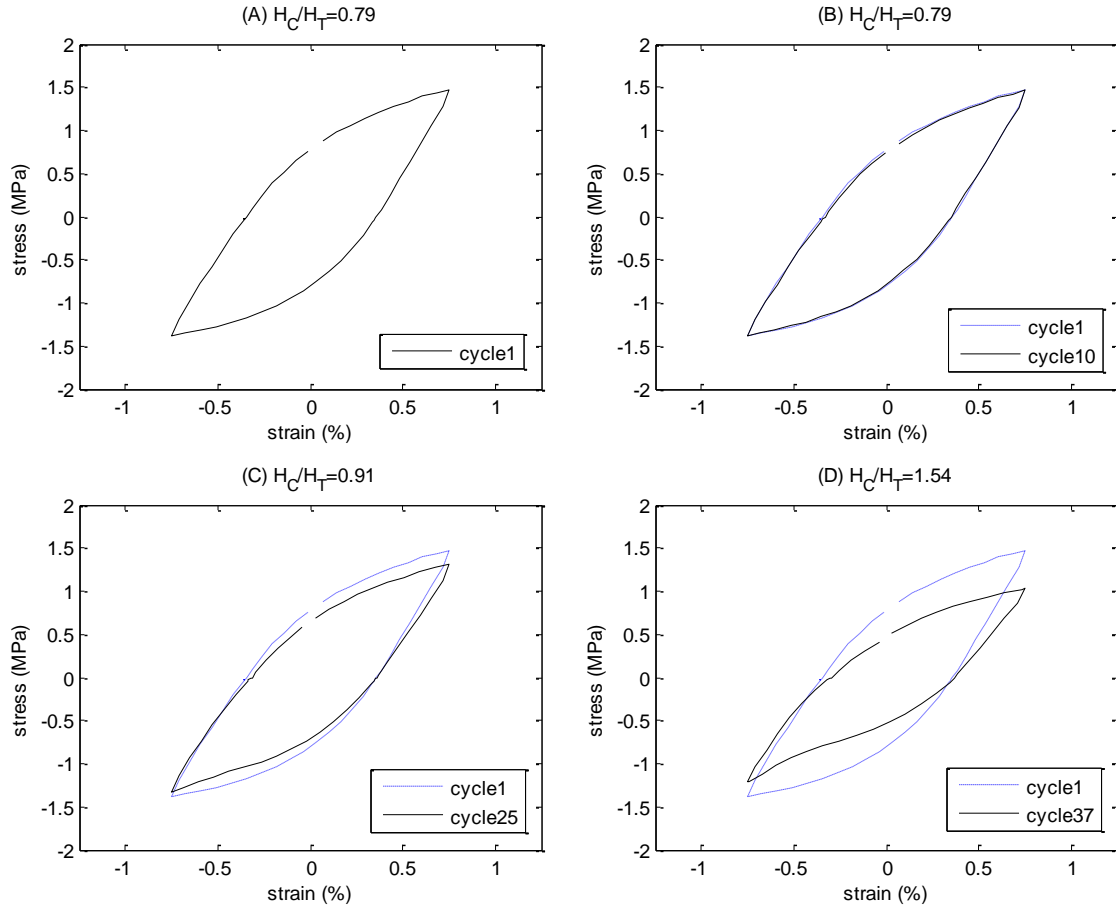
cycle1
cycle37

Figure 23: Progression of hysteresis response for 40 ppi aluminum foam tested at 0.75% applied strain for (A) cycle 1: HC/HT = 0.79 (B) cycle 10: HC/HT = 0.79 (C) cycle 25: HC/HT = 0.91 and (D) cycle 37 (failure): HC/HT = 1.54

As Figure 23 shows, the H_C/H_T ratio increases dramatically as the foam approaches failure. Figure 23(A) and (B) illustrate that the foam tested had identical H_C/H_T ratios at cycles 1 and 10, while the ratio increases drastically from cycle 10 to 25 and again from cycle 25 to 37 (failure). This increase in the H_C/H_T ratio is indicated in the stress-strain hysteresis relationship by pinching of the curve at higher cycles. Figure

23(D) clearly illustrates the change in the pre-peak slopes at failure as the plot shows a clear increase in the pre-peak compressive slope and decrease in pre-peak tensile slope.

The relationship of applied strain amplitude to fatigue life for 40 ppi foams tested is shown in Figure 24. A regression curve was fitted to the data for comparison with 20 ppi results as well as with the results for closed cell foam fatigue testing performed by Ingraham et al.
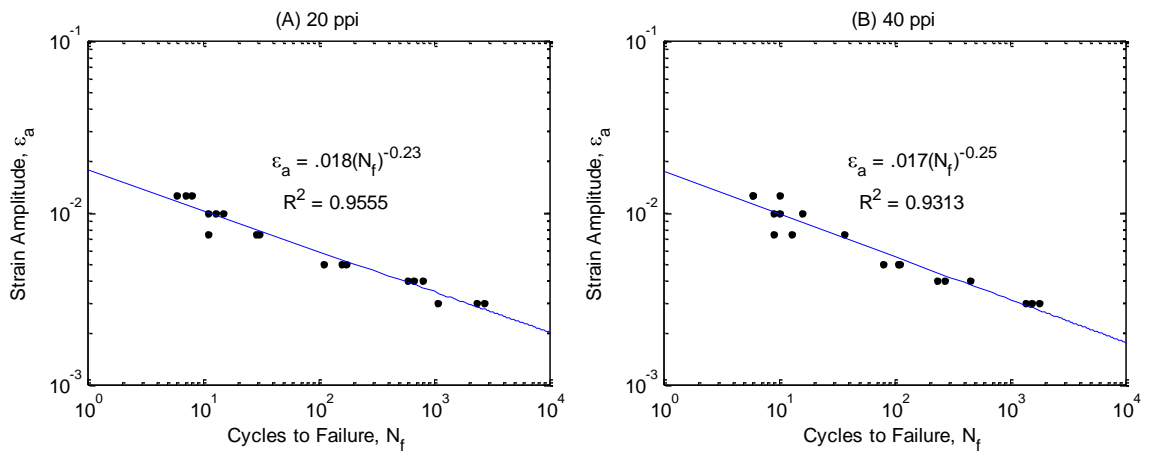
Figure 24: Coffin-Manson relationship for strain amplitude with fatigue life, Nf defined by increase of HC/HT ratio for (A) 20 ppi and (B) 40 ppi aluminum foam

Applied strain and fatigue life illustrate a Coffin-Manson relationship, just as observed in the Ingraham et al. (2008) data on closed cell foams. Comparison of this data will be described in Section 5.4.

The regression curves for both the 20 and 40 ppi strain-life relationships take the form,

$$\varepsilon_a = \varepsilon_f' \left(N_f \right)^c. \tag{23}$$

In this equation, ε_a is the applied strain amplitude, N_f is the fatigue life, ε'_f is the fatigue ductility coefficient and c is the fatigue ductility exponent. These relationships can be used to predict fatigue life for higher cycle tests.

5.3.2. Degradation of peak tensile strength

This failure criterion measures the number of cycles required for foam to lose significant peak tensile strength under constant strain amplitude. Figure 25 shows the degradation of peak tensile strength with fatigue life for 20 ppi foam tests.

Figure 25: Degradation of peak tensile stress as cycles increase for 20 ppi cyclic tests with (A) high and (B) low strain amplitudes

These plots can also be presented as the decrease in the fraction of peak tensile stress for each cycle. Figure 26 illustrates the degradation of tensile stress in this fashion, as well as highlights the threshold of 80% of maximum peak tensile stress used to define failure.

Figure 26: Degradation of peak tensile stress as a fraction of maximum peak tensile stress as cycles increase for 20 ppi foam tested at (A) high and (B) low amplitudes

The same trend is observed for the 40 ppi foam tests in Figure 27.

Figure 27: Degradation of peak tensile stress as cycles increase for 40 ppi cyclic tests with (A) high and (B) low strain amplitudes

Figure 28: Degradation of peak tensile stress as a fraction of maximum peak tensile stress as cycles increase for 40 ppi foam tested at (A) high and (B) low amplitudes

Figures 25 and 27 show that the degradation of peak tensile strength shows a similarly sharp drop as failure approaches as for the H_C/H_T ratio failure criterion. While the peak tensile strength remains at a fairly constant level until a crack forms in the cross section, at which point the peak strength begins to aggressively drop with each cycle, some hardening is observed. This is especially evident in the low strain amplitude tests, Figures 25(B) and 27(B), where the peak tensile strength remains at a constant level for the majority of the test, with some slight strengthening shown in later cycles, until a sharp drop at failure. Though strengthening of the material would be expected for low amplitude tests in early cycles, it is surprising to see this occur immediately prior to failure, as observed in the 0.30% amplitude tests for both 20 and 40 ppi.

The high amplitude test figures, 25(A) and 27(A), highlight the large decrease in peak strength from cycle to cycle during the decline. During each reversal, more ligaments are loaded to fracture, thus vastly reducing the strength in the proceeding cycle.

65

The fatigue-life curves for both 20 and 40 ppi tests are again plotted and illustrate a Coffin-Manson relationship, as described for the H_C/H_T ratio criterion. Figure 29 provides the curves for both sets of tests.

(A) 20 ppi
$$\varepsilon_a = .018(N_f)^{-0.25}$$
$$R^2 = 0.9744$$

(B) 40 ppi
$$\varepsilon_a = .017(N_f)^{-0.25}$$
$$R^2 = 0.9606$$

Figure 29: Coffin-Manson relationship for strain amplitude with fatigue life, Nf defined by degradation of peak tensile strength for (A) 20 ppi and (B) 40 ppi aluminum foam

Unlike for the H_C/H_T ratio failure criterion, where there is a significant difference in the fatigue ductility exponents, the fatigue ductility parameters are nearly identical for 20 and 40 ppi foams. The sensitivity of the fatigue ductility parameters with regards to expected fatigue life at a given strain amplitude is illustrated in Section 5.4.2.

5.3.3. Degradation of peak compressive stress

The degradation of peak compressive stress as cycles increase is shown in Figures 30 and 31 for 20 ppi and Figures 32 and 33 for 40 ppi foam tests. As described in Section 5.2.3, the threshold for degradation of compressive stress for failure definition is 90% of the peak compressive stress. Similar to the criteria for degradation of peak tensile stress, the fraction of peak compressive stress for each cycle is plotted as a fraction of the maximum peak compressive stress and the threshold of 90% used to define failure is highlighted.
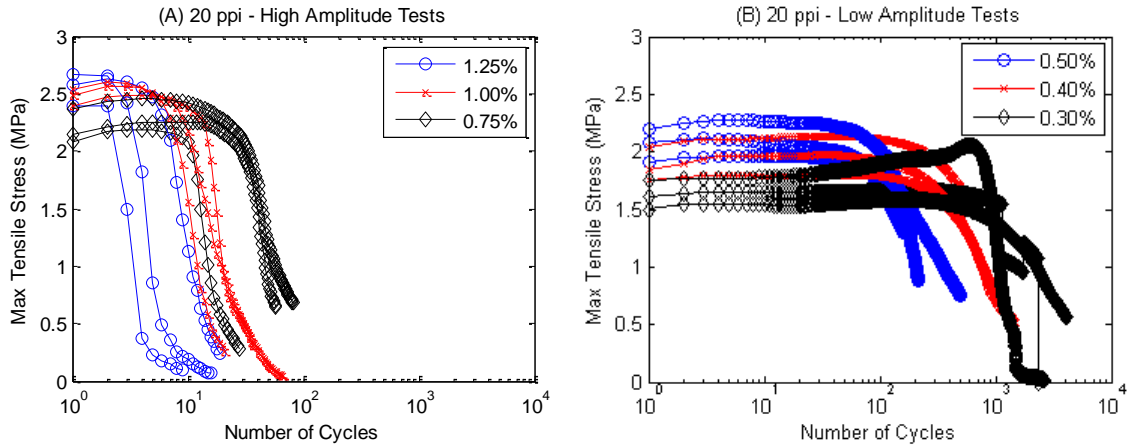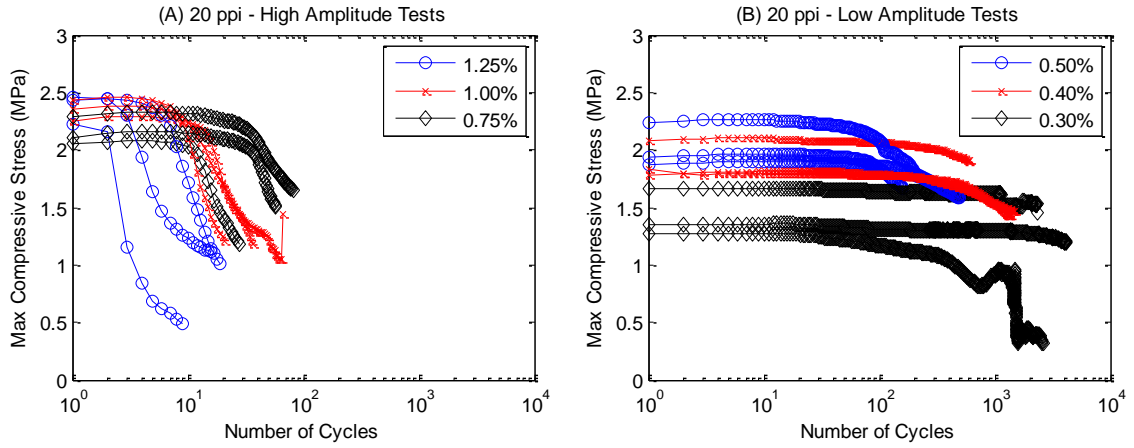
Figure 30: Degradation of peak compressive stress as cycles increase for 20 ppi cyclic tests with (A) high and (B) low applied strain amplitudes
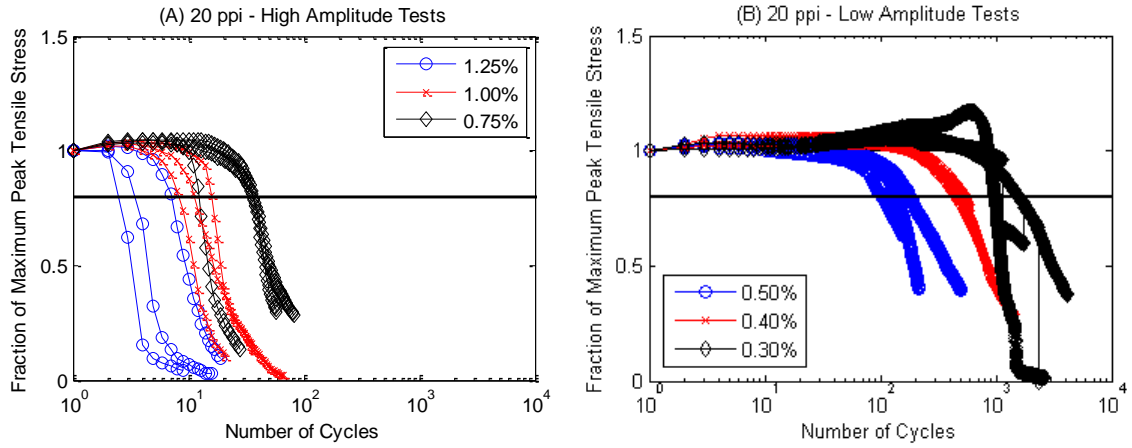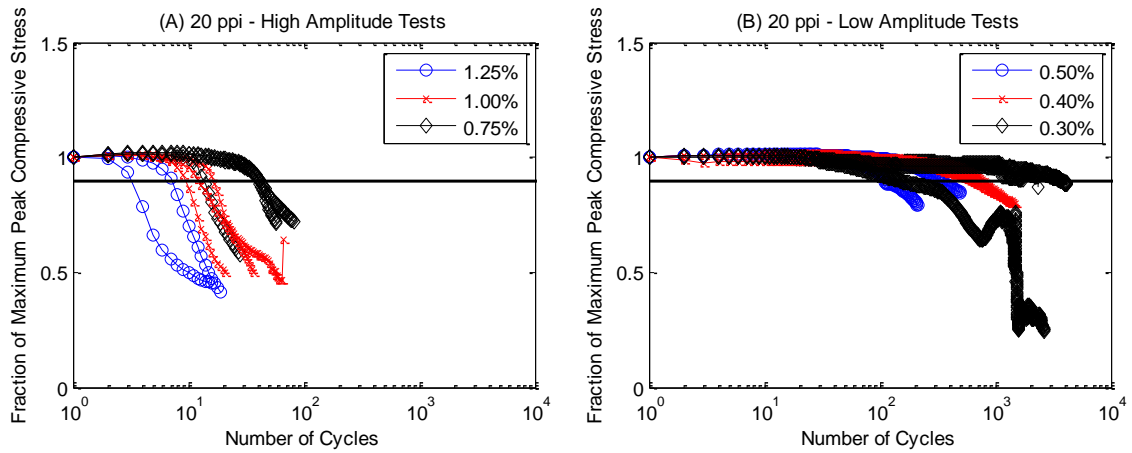

Figure 31: Degradation of peak compressive stress as a fraction of maximum peak compressive stress as cycles increase for 20 ppi foam tested at (A) high and (B) low applied strain amplitudes
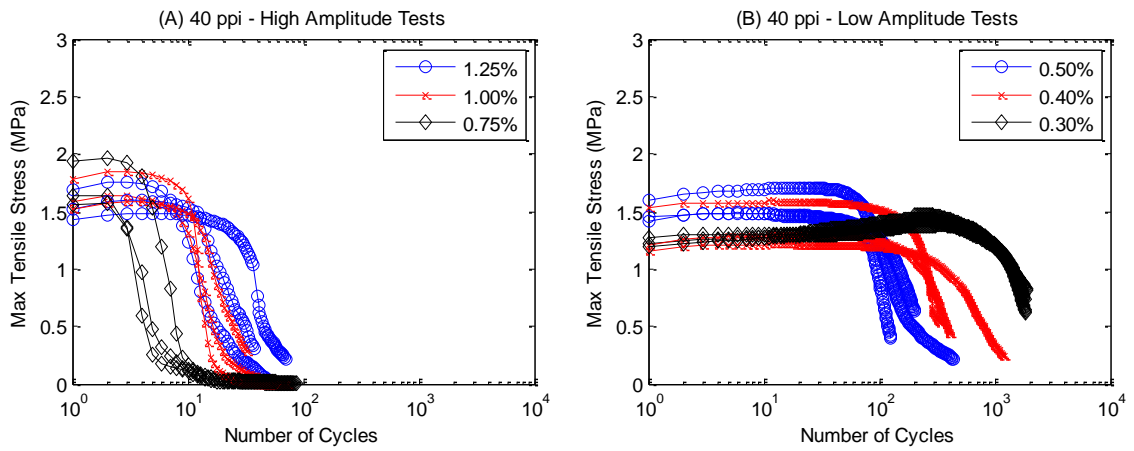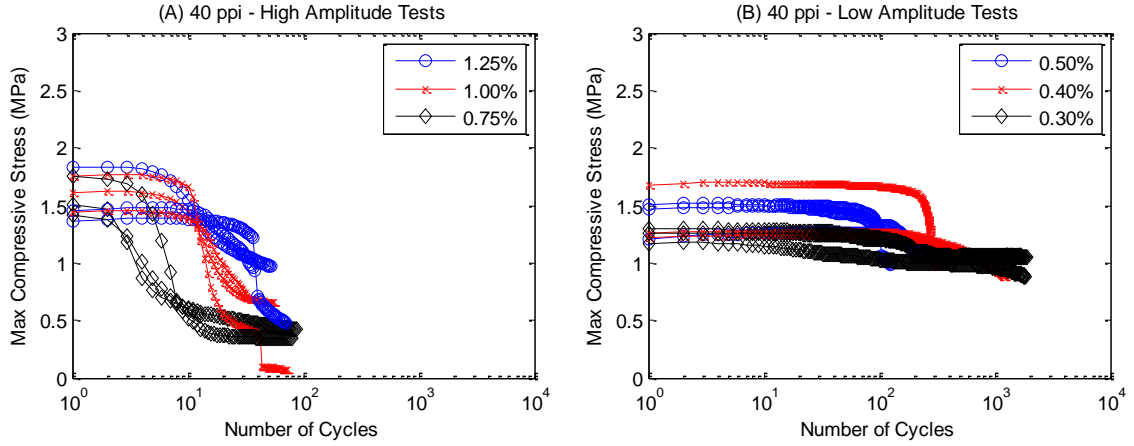
Figure 32: Degradation of peak compressive stress as cycles increase for 40 ppi cyclic tests with (A) high and (B) low applied strain amplitudes
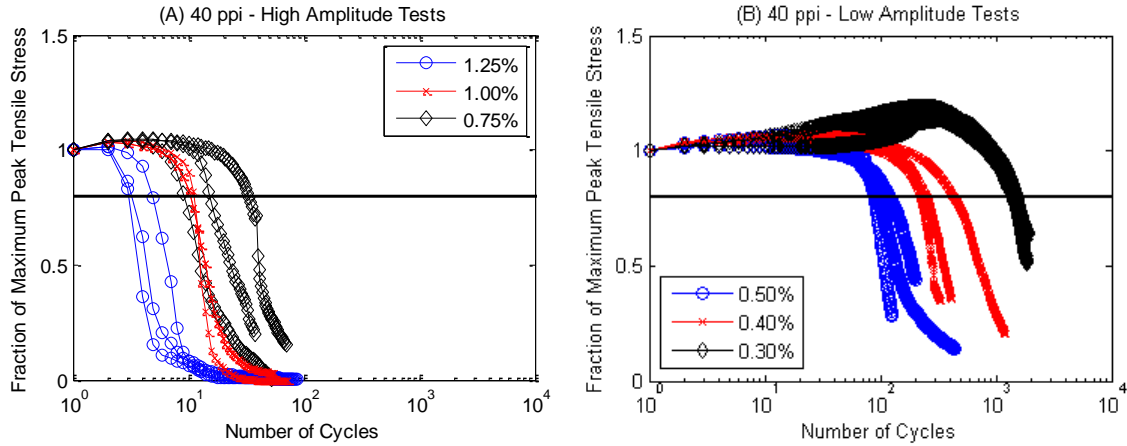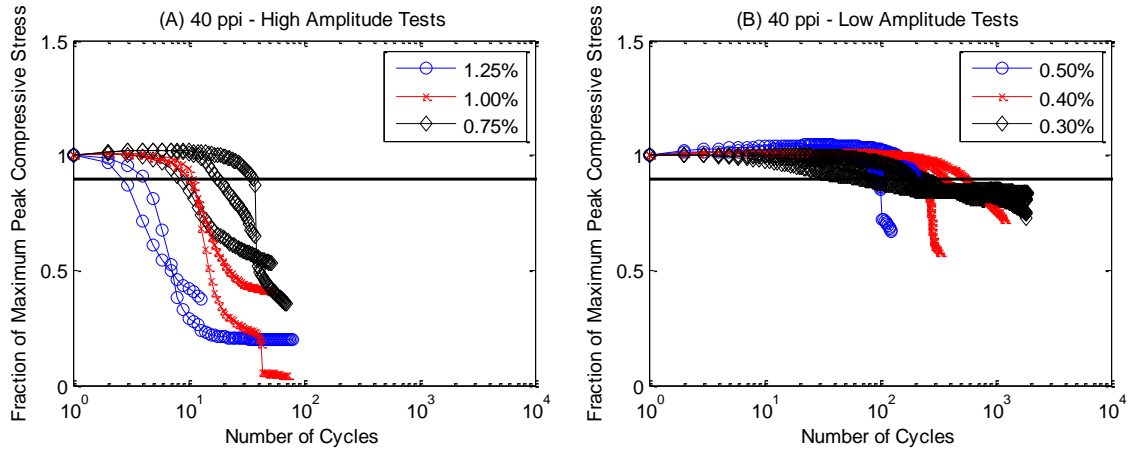

Figure 33: Degradation of peak compressive stress as a fraction of maximum peak compressive stress as cycles increase for 40 ppi foam tested at (A) high and (B) low applied strain amplitudes

The results for high amplitude tests, shown in Figures 30(A) and 32(A), demonstrate similar behavior for the degradation of peak compressive strength as that for peak tensile strength. While large degradation of strength does occur as failure approaches in high amplitude tests, the decline is not as rapid or severe as for the degradation of tensile strength. This is even more obvious in Figures 30(B) and 32(B) for the results of low amplitude tests. These plots show a more gradual reduction of strength with increase of cycles than for the tensile strength criterion.

This more gradual degradation of strength for peak compressive values than observed for peak tensile strengths is again due in large part to the failure mechanism. Failure of foam ligaments in tension, as described in Section 4.0, is sudden and brittle and characterized by fracture of the ligament. As this occurs during cyclic loading of the material, once a ligament fractures, its tensile strength can never be recovered. In compression meanwhile, behavior is characterized by a long collapse plateau during which time the material undergoes large strains without any loss of strength. For this reason, even after a fatigue crack has formed during cycling, the peak compressive strength of the material is not as severely affected as the tensile strength, as highlighted by Figures 30 to 33. This also results in less reliable data for fatigue life results as defined by this criterion.

The fatigue-life curves for the degradation of compressive strength failure criterion are provided in Figure 34.
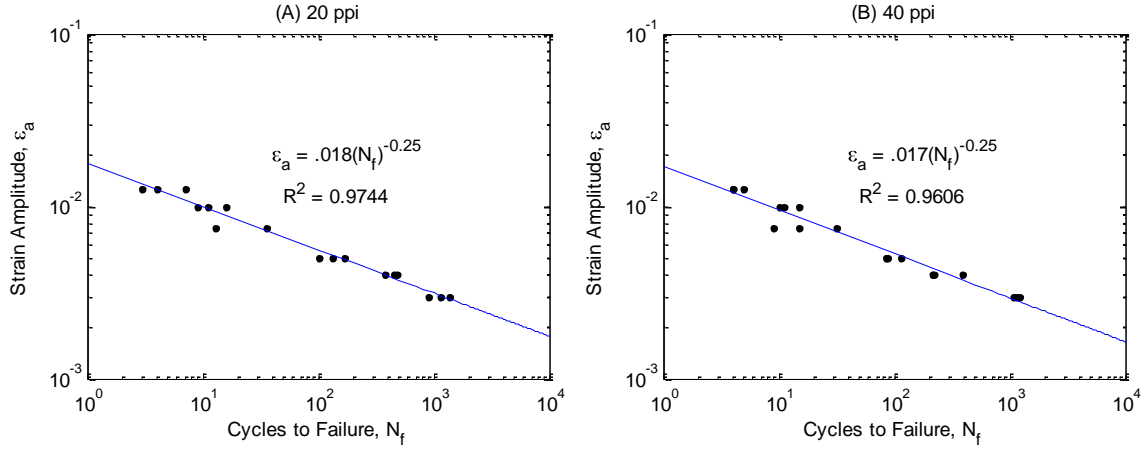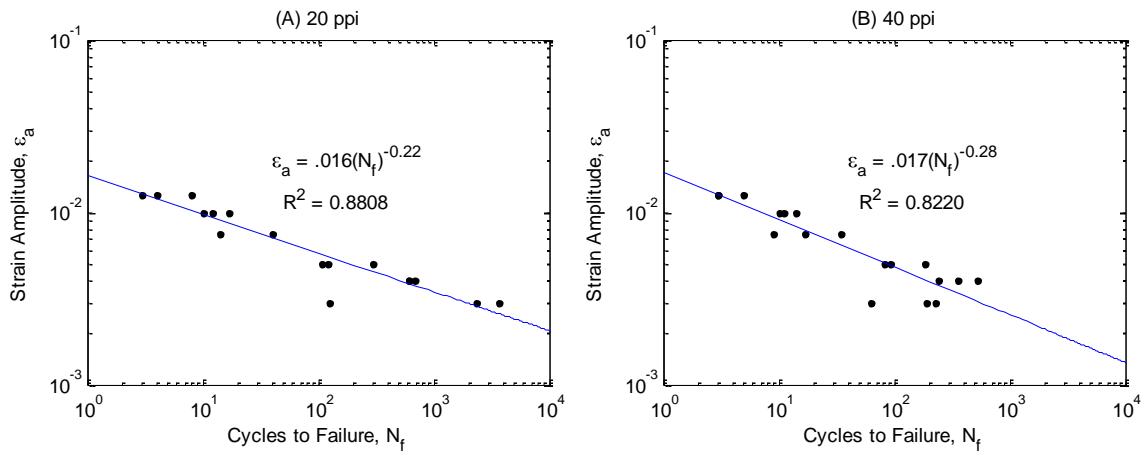

Figure 34: Coffin-Manson relationship for strain amplitude with fatigue life, Nf defined by degradation of peak compressive strength for (A) 20 ppi and (B) 40 ppi aluminum foam

69

Though the results for the degradation of peak compressive strength illustrate the same form of relationship of applied strain amplitude to fatigue life as the other criteria, it is important to note differences of Figure 34 to the similar plots in Figures 24 and 29 for the other criteria. As Tables 8 and 9 highlight, the results for the compressive strength criterion are significantly different, lower in most cases, than the results for the other criteria. This is evident in examining at the fatigue ductility exponents for each failure criteria. For the H_C/H_T ratio, exponents were -0.25 and -0.23 for 20 and 40 ppi respectively. For the degradation of tensile strength, the exponent for both porosities was -0.25. For the criterion defined by the degradation of peak compressive strength however, the fatigue ductility exponents were -0.22 and -0.28 for 20 and 40 ppi foams respectively. Not only is there are larger discrepancy between the compression strength criterion and the other two, but the exponent is less consistent across the different porosities than the other criteria illustrate. The difference observed across criteria is again most likely driven by the failure mechanism of the material when subjected to cyclic loading, while the difference in exponents for different porosities for the compressive strength failure criterion is due to the ligament cross section geometry and relative density statistics of the specimens tested.

Furthermore, the results of the compressive strength failure show a much larger distribution across a given strain amplitude, reducing the confidence of the trend. This is confirmed by the R^2 values computed for the regression lines. While the test results for the H_C/H_T ratio and degradation of peak tensile strength fit tightly along the trend line for the data with R^2 values of 0.9744 and 0.9606, the results for the compressive strength

degradation are more variable along the trend with R^2 values of 0.8808 and 0.8220, for 20 and 40 ppi tests respectively.

5.4.   Comparison of Results

To assess the consistency and agreement between the different defined failure criteria, the fatigue ductility parameters determined from test results can be used to make predictions of fatigue life. Using predictions rather than the actual parameters, results for different failure criteria can be compared more easily. Additionally, the difference in fatigue life results for both different porosities tested and to compare with result from closed cell foam fatigue testing in a similar fashion.

5.4.1.   Failure criteria results comparison

As discussed earlier, three distinct failure criteria (kink cycle proved to yield unreliable results) are defined to determine the point at which open cell foam has reached its fatigue life capacity. The strain-life relationships for the three different criteria are compared in Figure 35, illustrating that seemingly small changes in the fatigue ductility parameters can have dramatic effects on the fatigue life at lower applied strain amplitudes.
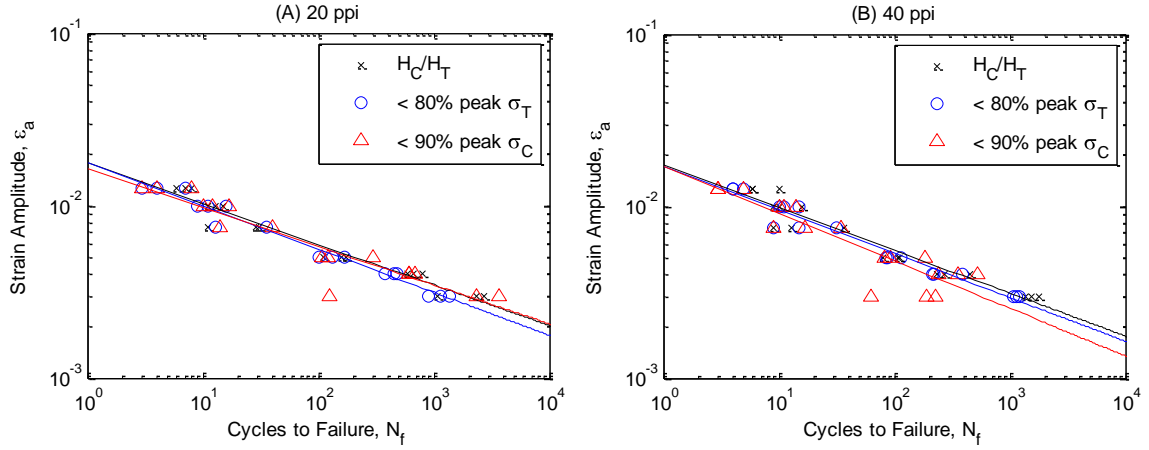
Figure 35: Comparison of strain-life relationships for different failure criteria for tests on (A) 20 ppi and (B) 40 ppi open cell aluminum foam

The results from the different criteria can also be evaluated to assess differences in fatigue life across definitions by comparing predictions for fatigue life based on the Coffin-Manson relationship results. These predictions from each criterion are compared in Table 11 where ε_f' is the fatigue ductility coefficient and c is the fatigue ductility exponent defined in Equation (23) of Section 5.3.1.

Table 11: Comparison of predicted fatigue life results for 20 ppi foam at applied strain amplitudes of 0.30% and 0.50%

	ε_f'	c	$N_f\ (\varepsilon_a = 0.30\%)$	$N_f\ (\varepsilon_a = 0.50\%)$
H_C/H_T	0.018	-0.23	2417	262
$\sigma_T > 80\%$ **peak**	0.018	-0.25	1296	168
$\sigma_C > 90\%$ **peak**	0.017	-0.28	490	79

Table 11 shows that the predictions for fatigue life based on 20 ppi foam tests do not produce consistent results across the criteria. The difference in predictions for the H_C/H_T ratio criterion and the degradation of peak strength criteria show that the peak strengths, both compressive and tensile, decrease past the threshold point for failure definition prior to the formation of a fatigue crack. This suggests ductile failure of the

72

material as the ligaments approach and surpass the yield point as cycles increase, but do not reach tensile fracture in enough ligaments to cause significant changes in the pre-peak slopes to promote increase in the H_C/H_T ratio. This is potentially due to the specific geometric properties of the ligaments as 20 ppi foams generally contain stockier and thicker ligaments. Therefore, despite plastic behavior is experienced by the ligaments during cyclic testing, actual fracture to cause fatigue cracking occurs significantly after the tensile and compressive peak strengths decrease.

Similar predictions for the fatigue life based on the 40 ppi foam tests are provided in Table 12.

Table 12: Comparison of predicted fatigue life results for 40 ppi foam at applied strain amplitudes of 0.30% and 0.50%

	ε_f'	c	$N_f\,(\varepsilon_a = 0.30\%)$	$N_f\,(\varepsilon_a = 0.50\%)$
H_C/H_T	0.017	-0.25	1031	134
$\sigma_T > 80\%$ **peak**	0.017	-0.25	1031	134
$\sigma_C > 90\%$ **peak**	0.016	-0.22	2016	198

Unlike the predictions made for 20 ppi foam, results based on the H_C/H_T ratio and the degradation of peak tensile strength failure criteria show good agreement with one another. This would suggest that the threshold for degradation of tensile strength is surpassed in close proximity to the formation of a tensile crack. As mentioned for the 20 ppi foam, the geometric properties of the ligaments could dictate this behavior, explaining the difference in results for 40 ppi foams versus the 20 ppi samples.

Predictions made from the results of the loss of compressive strength criterion, on the other hand, produced immensely different values for predicted fatigue life than the other criteria for the 40 ppi foam. This is also observed in the 20 ppi predictions as the

degradation of compressive strength failure criteria suggests vastly different fatigue life than the other criteria. However, the different porosities demonstrate opposite results for the compressive strength criteria predictions. While the 20 ppi predictions suggest a much shorter fatigue life based on compressive strength degradation, the 40 ppi predictions indicate a significantly longer fatigue life.

This difference implies that the degradation of compressive strength has no impact on the actual, physical failure of the foam. Because the failure mechanism of foam in fatigue is defined by the formation of a tensile crack, the H_C/H_T ratio and degradation of tensile strength criteria are much more useful in determining when a foam has reached its true fatigue life.

5.4.2. Comparison of results for different porosity and cellular structure

This predicted data for fatigue life results of open cell foams can also be compared to the findings of the research performed by Ingraham et al. on the strain-life relationship of closed cell aluminum foam. However, strain-life relationships in this study are determined using the plastic strain amplitude, defined as half the width of the hysteresis curve at zero stress after saturation. To compare the results from these tests with those performed on both 20 and 40 ppi open cell foams, the results for fatigue life must be compared to the total applied strain amplitude to develop a relationship analogous to those for the open cell foam. The results for fatigue life of closed cell from the tests of Ingraham et al. are plotted against total applied strain amplitude in Figure 36 and a Coffin-Manson relationship is illustrated.
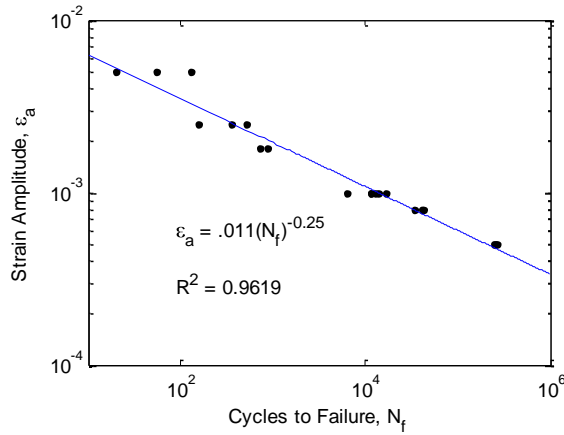
Figure 36: Coffin-Manson relationship for applied strain amplitude with fatigue life, Nf for closed cell foam fatigue testing performed by Ingraham et al. (2008)

The data from the closed cell foam testing provided a fatigue ductility coefficient of 0.011 and a fatigue ductility exponent of -0.25. These values were then compared to the results from the H_C/H_T ratio failure criterion results for the open cell foam testing, which illustrated a similar relationship. The H_C/H_T ratio failure criterion results were used for the comparison as this was the criterion used by Ingraham et al. for definition of failure in their tests on the closed-cell material. The 40 ppi foam tests yielded fatigue ductility parameters of $\varepsilon_f' = 0.018$ and $c = -0.23$, while the 20 ppi tests produced parameters of $\varepsilon_f' = 0.017$ and $c = -0.25$.

The similarity in the fatigue ductility exponents for the closed and open cell foam suggests that the affect of strain amplitude on the fatigue life is the similar in both materials. However, the smaller value for the fatigue ductility coefficient suggests that open cell foam material has inherently longer fatigue life than the closed cell foam, independent of applied strain amplitude.

The relative density of the materials is not the cause of the difference in fatigue life as the average relative density of the closed cell samples was 8.7%, higher than the

75

average relative density of both the 20 and 40 ppi open cell samples, 7.53% and 7.38% respectively. A higher relative density, as determined in previous sections for both testing and computer modeling would suggest a stronger material, at least for open cell foams. It is reasonable to conclude that relative density is not the cause of the shorter fatigue life for closed cell foam.

When the relationship developed from large amplitude open cell foam testing is applied to smaller amplitudes to promote higher cycle fatigue, the predicted fatigue life is significantly longer than observed for closed cell foam. Despite the same relationship between fatigue life and applied strain amplitude for the two materials, open cell foam seems to be capable of undergoing significantly higher number of cycles prior to the formation of a critical fatigue crack that causes failure. Low amplitude, high cycle fatigue testing on open cell foam is needed to confirm that the relationship developed for applied strain and fatigue life is consistent for amplitudes similar to those applied to closed cell foam.

As in section 1.4.1, fatigue ductility parameters defining the Coffin-Manson relationship for fatigue life with applied strain amplitude are used to make predictions for fatigue life. These predictions, along with the parameters used to generate them given in Table 13 for 20 and 40 ppi open cell foams tested and the closed cell foam tests performed by Ingraham et al.

Table 13: Comparison of fatigue ductlity parameters and predictions for fatigue life for open cell and closed cell aluminum foam

	ε_f'	c	$N_f (\varepsilon_a = 0.30\%)$	$N_f (\varepsilon_a = 0.50\%)$
Open – 20 ppi	0.018	-0.23	2417	262
Open – 40 ppi	0.017	-0.25	1031	134
Closed cell	0.011	-0.25	181	23

Table 5 shows that predictions based on closed cell foam tests yield fatigue lifetimes that are a full order of magnitude lower than results from open cell foam tests, considering the same definition of failure. This is likely a result of the cellular structure of the closed cell foam in comparison of the open cell material. Failure in open cell foam is governed by the fracture of individual ligaments and the propagation of a fatigue crack due to increased stress in ligaments in close proximity to those that have already experienced fracture. At the same relative density, the walls of closed cell foam will likely be thinner than the ligaments of open cell foam, thereby making them more susceptible to the initiation of a fatigue crack. The cellular structure of the closed cell foam therefore promotes failure at fewer cycles than the open cell material.

5.5. High Cycle Fatigue on Open Cell Foam

Much of the testing on closed cell foam was performed at much lower applied strain amplitudes than the open cell foam testing described above. To obtain a better basis for comparison between the two materials, high cycle fatigue tests (low applied strain amplitude) must be performed on open cell foam. Due to the method of testing performed on open cell foam, namely the use of the Instron Testing Machine rather than a hydraulic machine capable of higher testing frequencies, the length of tests becomes a concern as the applied strain amplitudes decreases. For this reason, it is useful to analyze predictions for fatigue life of open cell foams at lower applied strain amplitudes.

Using the Coffin-Manson strain-life relationship developed in the testing described, predictions for fatigue lifetimes of both 20 and 40 ppi open cell foams can be determined for prospective strain amplitudes to match those applied to the closed cell

foams in the tests of Ingraham et al. The fatigue ductility parameters used to make these predictions were derived from the results of the H_C/H_T ratio failure criteria, as this was the definition of failure used in the closed cell foam tests. As discussed in Section 5.4.2, the Coffin-Manson relationship for strain-life was developed using total applied strain amplitude and not the plastic strain amplitude used by Ingraham et al. High cycle fatigue life predictions for 20 and 40 ppi foams corresponding to low applied strain amplitude values are given in Table 14 and compared to closed cell estimations for the same amplitudes as the Ingraham et al. tests.

Table 14: Comparison of predicted fatigue life for open and closed cell aluminum foam under low applied strain amplitude cycles

	Predicted N_f					
	Closed cell		**Open cell – 20 ppi**		**Open cell – 40 ppi**	
ε_a (%)	ε_f'=0.011	c=-0.25	ε_f'=0.018	c=-0.23	ε_f'=0.017	C=-0.25
0.05	234256		5841611		1336336	
0.08	35745		756928		203909	
0.10	14641		286884		83521	
0.18	1395		22275		7956	
0.25	375		5340		2138	
0.50	23		262		134	

Table 14 shows that the strain-life relationships determined in Figure 13 produce predictions for fatigue life for the closed cell foam very similar to those determined by Ingraham et al. testing. Furthermore, the predictions for open cell foam in Table 14 suggest that the open cell material will have substantially longer fatigue life at lower amplitude than the closed cell foam. However, physical tests must be performed at these amplitudes to ensure that the strain-life relationship developed in the current round of testing is consistent for higher cycle fatigue behavior.

CHAPTER 6

COMPUTATIONAL MODELING

A goal of this project was to create and use computer models to examine the properties and behavior of open-celled aluminum foam. By creating computer models of cellular networks based on the geometry and microstructure of actual foams, the properties and behavior can be investigated using finite element analysis to determine what features have the most dramatic effect on the properties. Despite challenges in creating the computer models such as the definition of a unit cell and unexpected size effects, the simulations performed provided valuable insight on foam mechanics. Models were created with increasing complexity from those with a perfectly regular and ordered cellular structure to those with random geometry in which no cells were identical within the network.

6.1. Finite Element Modeling

Finite element modeling is a process in which the governing equations of elasticity for a given domain are discretized and solved numerically using a powerful computer program. Finite element modeling was used to investigate the effective elastic properties of a three dimensional foam network as well as the effects of geometry and irregularity on the forces and stresses developed within the network microstructure. The results obtained from the computer models were then compared to the results of mechanical testing as well as predicted values from existing sources to determine their validity and usefulness more expansive predictions. Additionally, more specific details about the behavior and response of the material not evident in even small scale mechanical testing can be

identified and studied using finite computer models. The finite element program ADINA was used for all simulations.

6.1.1. Unit cell

The simplest method for modeling foam for finite element analysis is to create periodic networks of unit cells. To do this, a unit cell that is able to be periodically replicated in three dimensions needs to be established. An obvious possibility is provided by Gibson and Ashby, the cubic shape shown in Figure 4.

However, this representation does not satisfy the requirements of a unit cell as it is unable to be repeated in all three directions. Though its structure promotes axial, bending, and shear behavior that leads to the proportionality expressions for material properties discussed in Section 1.2, it was not intended for use in a three dimensional model. Therefore, to model a cellular network and achieve the most accurate results, a polyhedron that is a true unit cell with the ability periodic repetition in the three primary directions must be determined.

When modeling a network cells in three dimensions, there are surprisingly few options that allow for perfect periodicity without any irregular voids between cells (i.e. the spaces that exist between cells in a network comprised of spheres). For this reason, the unit cell that provides the option for modeling a foam network is the polyhedron known as a Kelvin cell. A Kelvin cell is a tetrakaidecahedron (fourteen-sides) featuring six square and eight hexagonal sides. Figure 37 shows a regular, unit Kelvin cell in which each of the ligaments making up the cell are of uniform length and thickness.
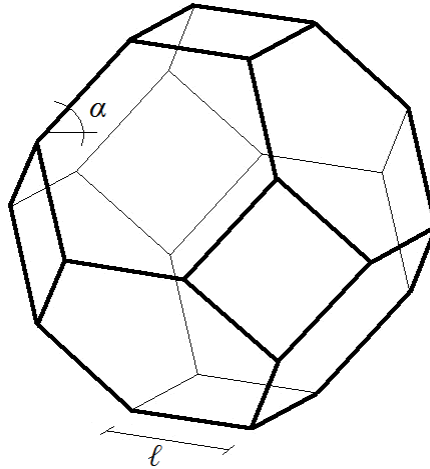
Figure 37: Regular 14-sided Kelvin cell used in 3-D finite element models of aluminum foam

The Kelvin cell provides the advantage of potential for repetition in three-directions as well as the existence of planar boundary surfaces (in that the Kelvin could be inscribed within a cube and each of the square faces on the Kelvin cell would be parallel to a corresponding face of the cube) which is convenient for the application of boundary conditions. Aggregates of these Kelvin cells (shown in Figure 38 of Section 6.1.3) were created and used in ADINA to perform simulations in an effort to characterize the effective elastic properties of the modeled networks and further examine the effects of network microstructure on behavior.

6.1.2. Model input parameters

Gibson and Ashby's expressions for effective elastic properties were based on a unit cell with cell wall struts with solid, rectangular cross sections. In examining physical samples of aluminum foam however, the assumption of such cross sectional properties may not be universally applicable. In an attempt to determine if it is acceptable to relax the assumption of rectangular ligament cross sections, solid cylindrical cross sections were used in the finite element model.

Gibson and Ashby's expressions show that the elastic properties of three-dimensional foam directly depend on the foam's relative density. It was also determined that the relative density of a computer model directly depends on the properties of the cell wall struts, specifically the ratio of the cross section diameter to the ligament length. Therefore, in order to create a model with a desired relative density (generally between 6 and 8% to simulate samples provided by ERG Duocel), a specific diameter to length ratio could be determined and kept constant throughout simulations.

6.1.3. Boundary conditions

To find the effective elastic properties of aluminum foam, displacement loads were applied to opposite faces of the global network, meaning each node on the extreme faces normal to the axis of loading are subjected to an applied displacement. A translation was applied at each node in the extreme planes to cause the desired strain of the entire network. This method of load application is beneficial in that it allows a controlled amount of strain to be applied to the network and because elastic analysis is being performed, the resulting forces that are developed can be used to calculate the desired results.

To prevent rigid body rotation of the network, one node within the network was restrained for both translation and rotation in each direction. Figure 38(A) below shows an isotropic view of a 10 by 10 by 10 cell network, while Figure 38(B) shows an elevation view of the same network with displacement loads applied to global exterior faces of the network.
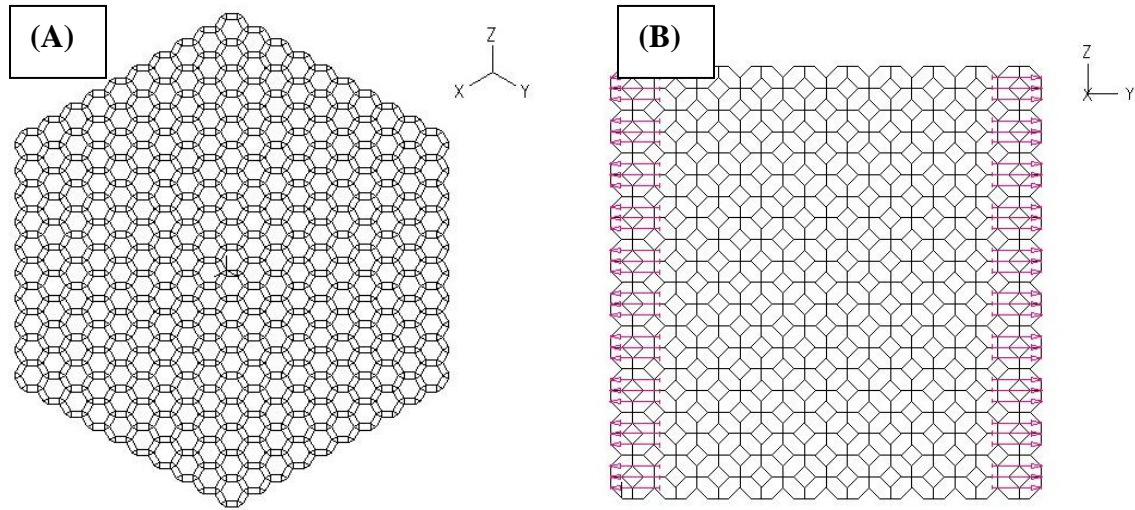
Figure 38: 10x10x10 network of Kelvin cell aggregates used to model aluminum foam (A) isotropic view (B) elevations view

6.2. Regular Foam Network

Initially, the model used to investigate the effective elastic properties of the foam network was constructed of perfectly regular, isotropic Kelvin cells. Although this was an overly idealized representation, it provided adequate insight on the overall behavior of the foam and produced results from which relevant conclusions could be made. The cell walls, or ligaments, of the network were created with uniform length and diameter throughout the model.

The foam was modeled in ADINA using beam elements defined with the properties of aluminum. Because the elastic properties of foam depend at least somewhat on the relative density, the relative density of the computer networks generated needed to be determined. Relative density is defined as the density of the density of the cellular material divided by the density of the solid material comprising the cell ligaments. When the mass of the foam is equal to the mass of the solid, this equation reduces to a ratio of the volumes,

$$\frac{\rho*}{\rho_s} = \frac{m*/V*}{m_s/V_s} = \frac{V_s}{V*} . \tag{24}$$

For the model networks with ligament length, ℓ, and ligament diameter, D, the relative density is defined as

$$\frac{\rho*}{\rho_s} = \frac{N_e\ell\frac{\pi}{4}D^2}{\lambda\left(N_c\ell\sqrt{2}\right)^3} \times 100\% , \tag{25}$$

where N_e is the number of elements in the network, N_c is the number of cells in each direction, and λ is the anisotropy ratio, defined in Equation (29) of Section 6.2.1. This relationship for relative density proves to only be valid for larger networks, but provides a basis for defining ligament geometry for a target relative density of a computer model.

Ligaments had an initial length of 1.25 mm and a solid circular cross section of diameter 0.356 mm. These values were selected using Equation (25) to create a model with a relative density as close to 8% as possible (to match actual specimens that were tested). Values for ligament length and diameter that yielded a desired model density were compared to measurements of ligament properties of a physical foam specimen to ensure realistic representation in the model.

As the size of the network increases, the amount of time required to generate the network geometry and complete a simulation increases exponentially. This is illustrated in Figure 39 below by plotting network size against time required to run a simulation.
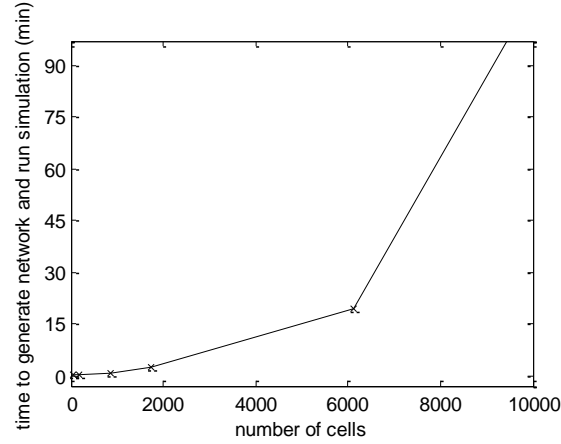
Figure 39: Time to run computer simulation as a function of network size

For this reason, it is important to determine the appropriate size of network on which to perform all future analysis that will maximize time efficiency while maintaining accurate results free from size effects. To do this, a convergence study was performed to investigate the effect of network size on the calculated elastic modulus. The results for networks with increasing size including relative density and the computed elastic modulus are given in Table 15 below.

Table 15: Convergence investigation results

Network size	Number of cells	Generation time, *sec*	ρ^*/ρ_s, *%*	Run time, *sec*	E*, *MPa*
3 x 3 x 3	35	2	8.01	0.39	269.0
5 x 5 x 5	189	9	7.55	1	227.2
8 x 8 x 8	855	44	7.30	7	207.7
10 x 10 x 10	1729	112	7.21	21	201.8
15 x 15 x 15	6119	861	7.10	298	194.3
30 x 30 x 30	51389	41057	6.98	23600	187.1

An unexpected result of this convergence investigation is the influence of network size on the relative density of the network. Because the ligament diameter to length ratio was the same in each network analyzed in the convergence study, they were assumed to

85

have had equivalent relative densities. The relationship between relative density and network size is shown in Figure 40 below.
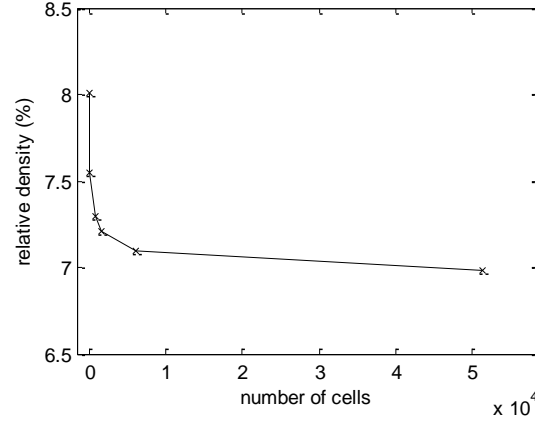
Figure 40: Relative density as a function of network size

The fact that the relative density is decreasing as network size increases is contributing to the subsequent decrease in the effective elastic modulus. One method to determine whether the simulation results are actually converging towards an acceptable value is to examine the difference between the predicted elastic modulus from Equation (5) as derived by Gibson and Ashby and the value as computed using the model at the given relative density. This error measure,

$$\left| E^*_{simulation} - E^*_{predicted} \right|,\tag{26}$$

is plotted against network size in Figure 41 to illustrate possible convergence.
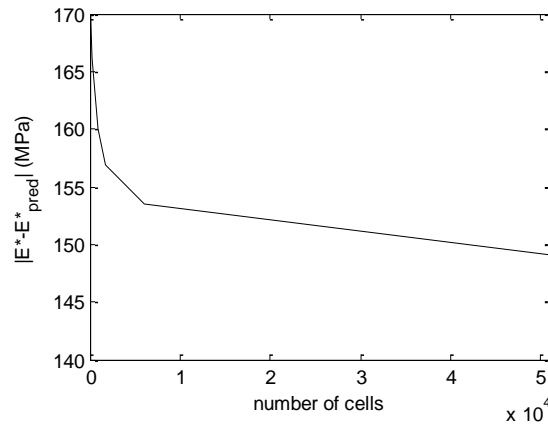
Figure 41: Difference between predicted E* from Gibson and Ashby relationship and model results as network size increases

Figure 41 shows that as network size increases, the elastic modulus computed by computer simulations is becoming closer to the value predicted by Gibson and Ashby's expression for the same relative density. The magnitude of the difference between the values is less important than the rate at which the difference is decreasing. The difference in magnitude between predicted and computed modulus is due characteristics of the model that can be investigated after the existence of convergence is confirmed. Because Figure 41 shows that the decrease in difference becomes less dramatic as network size increases suggests that the model results are converging. The difference between predicted and computed values begins to taper off after a steep initial decrease at a network size of around 10,000 cells. The change in relative density shows a similar drop off in the severity of change at a similar network size. Therefore, a network size of 10 cells in each direction is adequate in proceeding towards the analysis of the mechanical properties of foam.

6.2.1. Anisotropy

The unit Kelvin cell used to create three-dimensional foam networks has a geometrically isotropic microstructure in which the height of the cell is equal to the width (see Figure 42) and each of the ligaments comprising the cell is of equal length. Cells in actual metal foams are not perfectly isotropic, as evident in the 20 ppi foam in Figure 1 of Section 1.2. Rather, the cells of open cell foam are generally elongated in the rise direction as a result of the foaming process during manufacturing as described in Section 1.4. To investigate the effects of the anisotropy of cells on the behavior of foam networks, cells were elongated in one direction, to varying degrees and the resulting effects on their properties were analyzed.

In an isotropic Kelvin cell, ligaments are either oriented at an angle of $\pi/4$ with respect to a plane or parallel to that plane. This can be seen in the Kelvin cell in Figure 37 of Section 6.1.1. When the cells are stretched in one direction to create anisotropy, this angle, denoted as α, is altered throughout the cell. This causes the height of the cell in the direction being stretched to become

$$h_1 = 2\sqrt{2}\ell \tan\alpha,$$
(27)

while the height in both orthogonal directions remains

$$h_2 = 2\sqrt{2}\ell.$$
(28)

Thus, the measure of the anisotropy of a cell can be defined as

$$\lambda = \frac{h_1}{h_2} = \tan\alpha,$$
(29)

where λ is the aspect ratio of the cell, hereby called the anisotropy ratio. For isotropic cells, λ will be equal to 1.0, increasing as the cell is elongated in the rise direction (as defined in Section 1.4) and decreasing as cells are "squashed" (or elongated in an orthogonal direction). A comparison of a network of isotropic cells to one with cells elongated in the rise direction is given in Figure 42 as illustrated by Gong et al. (2005).
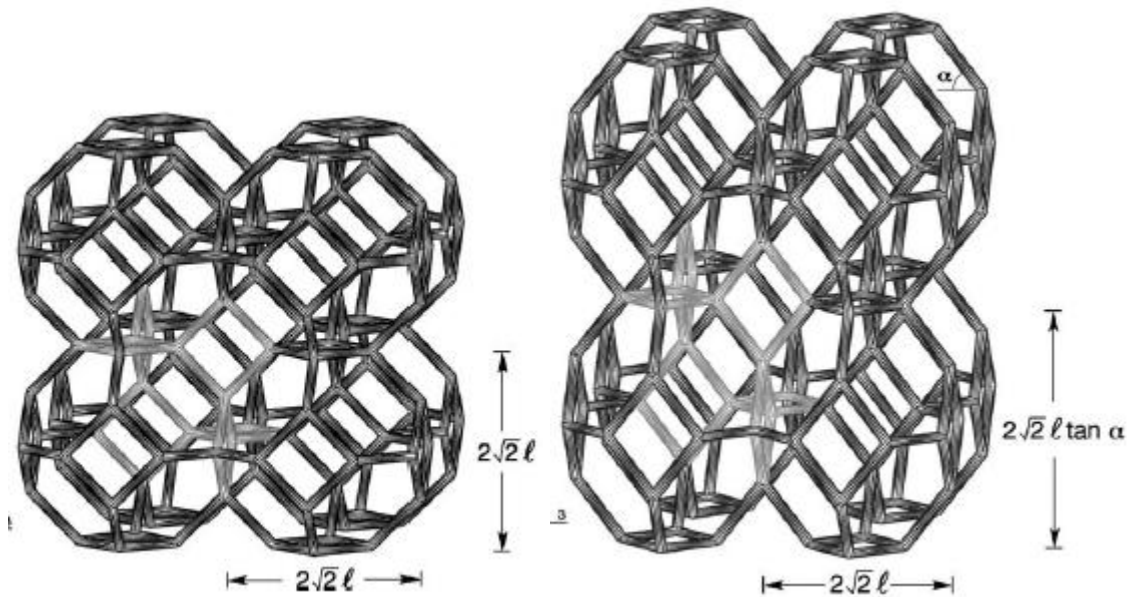
Figure 42: Comparison of cellular networks as illustrated by Gong, Kyriakides and Jang (2005) (A) isotropic (B) anisotropic

The relationship of the effective elastic modulus with the anisotropy of cells in the network is illustrated in Figure 43. Ligament diameter was altered slightly for each simulation in an effort to maintain a constant relative density (about 8%) and therefore highlight only the effect of anisotropy on the effective elastic modulus. The results illustrate another example where relative density cannot fully predict the mechanical properties of foam.
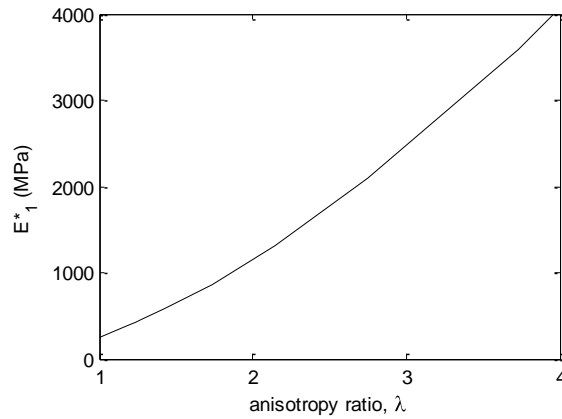
Figure 43: Effective elastic modulus as a function of the anisotropy ratio for a 10x10x10 cellular network computer model

It is clear from this figure that the shape of cells has a significant effect on the stiffness of a foam network. Anisotropy ratios for aluminum foams were found to range from 1.18 to 1.27 by Jang, Kraynik and Kyriakides (2008). In that study, anisotropic networks were created based on aluminum foam samples from the same source as this project, ERG Duocel. Using the anisotropy ratios defined by Jang et al for 20 and 40 ppi foams, anisotropic models were created and the effective elastic modulus was compared to the modulus measured from mechanical testing. The results are given in Table 16.

Table 16: Comparison of effective elastic modulus values for aniotropic computer model simulations and mechanical testing results

	20 ppi		40 ppi	
	Model	**Test**	**Model**	**Test**
λ	1.23	-	1.19	-
ρ^*/ρ_s (%)	7.18	7.18	7.59	7.58
E^* (MPa)	334.3	543.1	342.5	426.8

Even with anisotropy introduced to the computer models to more accurately simulate foam microstructure, the elastic modulus computed by the finite element simulations is 48% and 22% different from the mechanical testing results for the 20 ppi

and 40 ppi foams respectively (with percent difference measured using Equation (21) of Section X.1.2 with E^*_{model} replacing E^*_{pred}). These results indicate that the computer models still do not provide accurate representations of actual foam behavior. One explanation for this is the effect that individual ligament geometry has on both the stiffness of that ligament and the stiffness of the network as a whole.

6.2.2. Rigid end zones

In the initial finite element model, the elements that make up the microstructure of the foam are defined to have a constant cross section along their length. Upon close investigation however, this is found to be an over idealization of the ligaments in an actual foam. Rather than solid cylinders with constant cross-sectional thickness, the ligaments instead possess a dogbone-like shape with flared ends occurring where multiple ligaments converge to form a joint. A single ligament of this type is shown in Figure 44 below as illustrated by Jang and Kyriakides (2009).
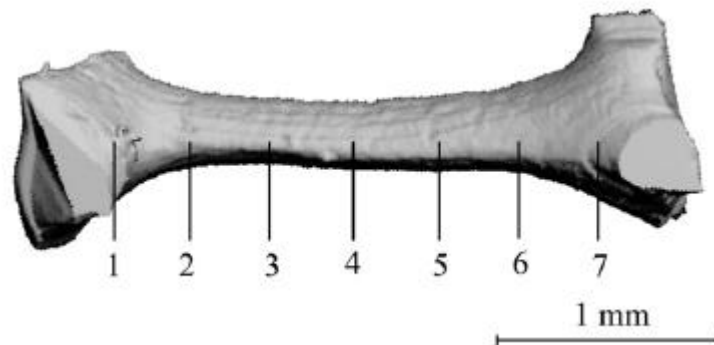

Figure 44: Example aluminum foam ligament as illustrated by Jang, Kraynik, and Kyriakides (2007) to show dogbone shape

The excess material at the joints acts to restrict rotation at the ends of ligaments, resulting in increased axial and bending stiffness for each individual ligament. This, in turn, would seemingly result in a stiffer overall response by the entire network. To

account for the presence of this thickening of material where ligaments meet in the finite element model, the Rigid End Zones (REZ) function in ADINA can be utilized. This function defines an area at the ends of an element to be infinitely rigid, thus accounting for the rotational restraint occurring in actual foam ligaments. By defining rigid end zones of a certain length throughout the network, the effective length of each element was decreased, thereby increasing the stiffness of the ligament and thus the stiffness of the network as a whole.

In order to ensure the most accurate representation of the rigid end zones, it was necessary to determine what portion of the original ligament length should be defined as rigid to result in the most realistic behavior of the network. Furthermore, it is important to note how this affects the behavior of the network as a whole. The rigid end length is defined as,

$$\text{rigid end length} = \frac{\text{length of ligament defined as rigid}}{\text{total length of ligament}} \times 100\% . \tag{30}$$

As defined by the equation above, the length of the ligament defined as rigid is the total rigid length, or the sum of the rigid lengths on each side of the ligament. Figure 45 below shows the relationship of the effective elastic modulus, E^*, with the rigid end length.
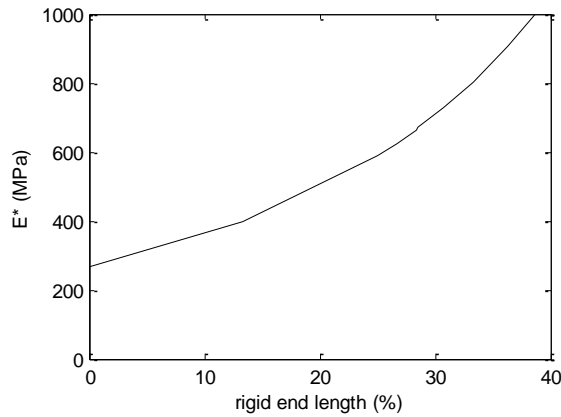
Figure 45: Effective elastic modulus as a function of rigid end length

As shown in Figure 45, the length of each element that is defined as infinitely rigid has a significant effect on the overall stiffness of the network. To determine what percentage of the ligament should be defined as rigid end zones, measurements of actual foam ligaments were used. Measurements were taken from center to center of ligament joints to obtain total length. Measurement of the "unrestrained" length of the ligaments where the cross section remained essentially constant were then taken. By comparing these two measurements for a number of ligaments within in actual foam sample, a baseline definition for the rigid end length to be used in computer models was determined.

When rigid end zones are applied to networks with anisotropic cells as described in section 6.2.1, the results for the effective elastic modulus become even closer to the mechanical testing results, as shown in Table 17 below.

Table 17: Comparison of results from computer model simulation and mechanical testing results for anisotropic networks with rigid end zones

	20 ppi		40 ppi	
	Model	**Test**	**Model**	**Test**
REZ (%)	10.0	-	10.0	-
λ	1.23	-	1.19	-
ρ*/ρ$_s$ (%)	7.18	7.18	7.59	7.58
E* (MPa)	462.3	543.1	471.2	426.8

With the introduction of rigid end zones that define 10% of the total ligament length to be infinitely rigid, the elastic modulus computed by simulations for both 20 ppi and 40 ppi foam models are shown to be much closer to the mechanical testing results of the foam samples. The percent difference between the modulus computed by the model and measured in testing drops from 48% to 16% for 20 ppi foam and from 22% to 10% for 40 ppi foam. Jang et al performed similar comparisons and found that their results for elastic modulus of computer models with perfectly ordered Kelvin cells differed by 13% and 12% with mechanical tests for 20 and 40 ppi foams respectively. It can be concluded that in addition to relative density, both the connectivity of ligaments at joints and the shape, specifically isotropy, of cells within the network have a significant effect on the elastic properties of the global network. It is expected, as noted in Jang and Kyriakides (2009), that irregular network simulations would provide even truer representations of actual foam (3% and 2% for 20 and 40 ppi foams respectively) and thus closer results to actual behavior. However, rather than further investigation of elastic properties, this project will instead use random network models to investigate the stresses that develop in the individual ligaments and how they are affected by the foam microstructure.

6.3. Irregular Foam Networks

Although ordered Kelvin cell networks are adequate in modeling the behavior of foams, irregular models provide the opportunity to investigate the effects of representative foam microstructure on the manner in which the forces that govern behavior develop within the network. Insight into ligament behavior that is not apparent in ordered microstructures is possible through analysis of randomly perturbed networks. Foam behavior is governed by the failure of individual ligaments. For this reason, it is important to investigate the forces that develop within these ligaments and the effects of foam microstructure, such as ligament orientation and level of randomness of the network have on the magnitude and distribution of forces.

In order to create finite element foam models with random microstructure, the nodes of the model network can be perturbed to create irregular geometry, which promotes a variety of ligament lengths and orientations throughout the network. The manner in which these microstructural variations influence specifically the axial and bending forces, as well as the combined tensile and compressive stresses in the ligaments of the network can go a long way in further understanding and predicting foam behavior.

6.3.1. Perturbation of nodes

To create an irregular foam network of disordered geometry, each of the nodes in a regular network was perturbed. With this approach, the element connectivity of the network remains the same, while each of the nodal coordinates is altered to create variable ligament lengths throughout the network. The diameter of the ligaments remained constant throughout the network. To ensure connectivity and continuity, each nodal coordinate was perturbed within a spherical boundary defined by the input

parameter, p. Let θ_o, φ_o, and r_o represent the spherical coordinates of the nodes of the unperturbed network, as defined in Figure 46.
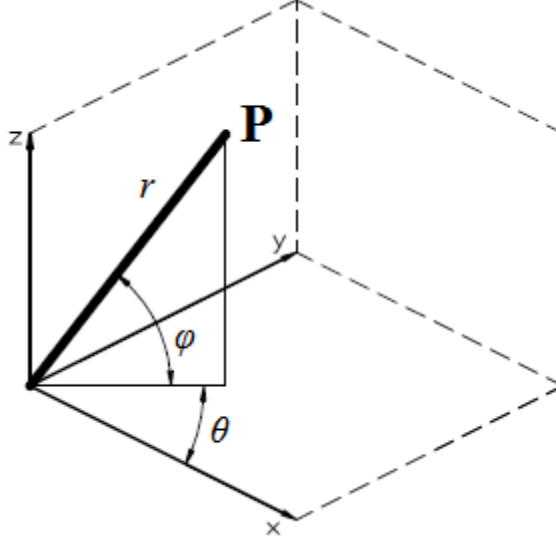
Figure 46: Definition of spherical coordinates used to perturb nodes in random foam model

The final coordinates in the perturbed configuration are given by

$$\theta = \theta_o + \xi_\theta, \quad 0 \le \xi_\theta \le 2\pi, \tag{31}$$

$$\varphi = \varphi_o + \xi_\varphi, \quad -\frac{\pi}{2} \le \xi_\varphi \le \frac{\pi}{2}, \tag{32}$$

and

$$r = r_o + p\xi_r\ell, \quad 0 \le \xi_r \le 1, \tag{33}$$

where ξ is the amplitude of disturbance for each directional coordinate, p is a perturbation factor defined to be between 0 and 1, and ℓ is the initial ligament length to scale perturbation.

The effect of randomness on the 10x10x10 networks analyzed is illustrated in Figure 47 for different values of the perturbation factor.
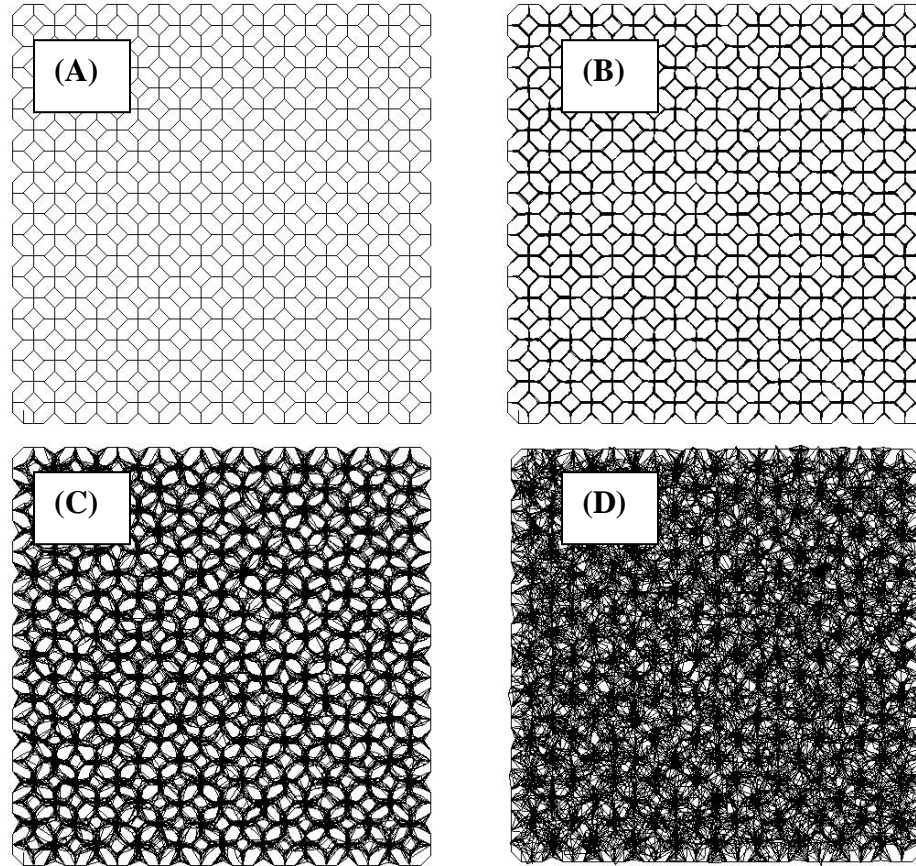
Figure 47: Elevation view of 10x10x10 computer generated networks with perturbation factors of (A) p = 0 (B) p = 0.10 (C) p = 0.50 and (D) p = 1.00

In order to maintain the planar boundary surface of the global network, the nodes on each exterior face of the network were left unaltered from their original geometry. For this reason, ligaments defined by a node on the face of the network were excluded from reported results and statistics to avoid the inclusion of edge effects that would not encapsulate true behavior of the network.

Initially, the average results of multiple simulations were to be used for analysis in similar fashion to previous studies performed on the computer modeling of random

foam networks such as Jang and Kryiakides (2009). However, the necessity of this was checked using the Kolmogorov-Smirnov test (K-S test) to avoid performing more time-consuming simulations than necessary. The K-S test compares two sets of data to determine if they were drawn from the same distribution. The simulation results of three different randomly generated networks with 10 cells in each direction were compared to each other using the K-S test. Results for axial force of over 25,000 elements for each test were compared at it was determined that the data sets were not drawn from three unique distributions. Therefore, it was decided that only one simulation at each of the intended parameters was necessary.

6.3.2. Relationship of axial force to ligament orientation

Foam networks fail in compression when the axial force in the ligaments is great enough to cause them to buckle or crush. Because of this controlling failure mechanism, the magnitude of axial force experienced by ligaments in random networks was investigated. One of the main parameters governing the magnitude of axial force experienced by a ligament is its orientation within the network with respect to the axis of loading. It is expected that ligaments more closely oriented along the axis of loading would experience greater axial force.

In the simulations described, the network was loaded along the z-axis and therefore, the orientation of a ligament is defined as the angle of the element with respect to the x-y plane, ranging from 0 to $\pi/2$. This definition of orientation is illustrated in Figure 48.
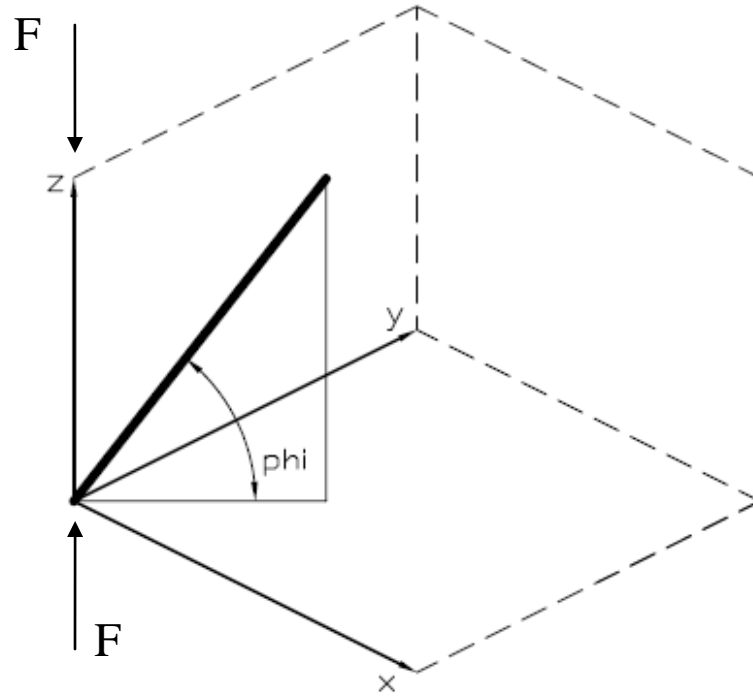
Figure 48: Definition of ligament orientation (phi)

In Figure 48, the thick black line represents an individual ligament and its orientation is defined by the angle, *phi*. According to this definition of ligament orientation, it was expected that ligaments with orientations approaching pi/2 (that is, parallel to the axis of loading) a greater magnitude of axial force would be experienced. Figure 49 shows the relationship of ligament orientation to the axial force in the ligament for different degrees of randomness. The horizontal line on the plots indicates the boundary between tensile and compressive forces. All points above the line indicate that the ligament experienced tension, while points below the line indicate ligaments in compression.

Figure 49: Axial force normalized by mean axial force in isotropic unperturbed network with respect to ligament orientation for perturbed network under 10% applied strain with (A) p=0 (B) p=0.10 (C) p=0.25 (D) p=0.50 (E) p=0.75 (F) p=1.00
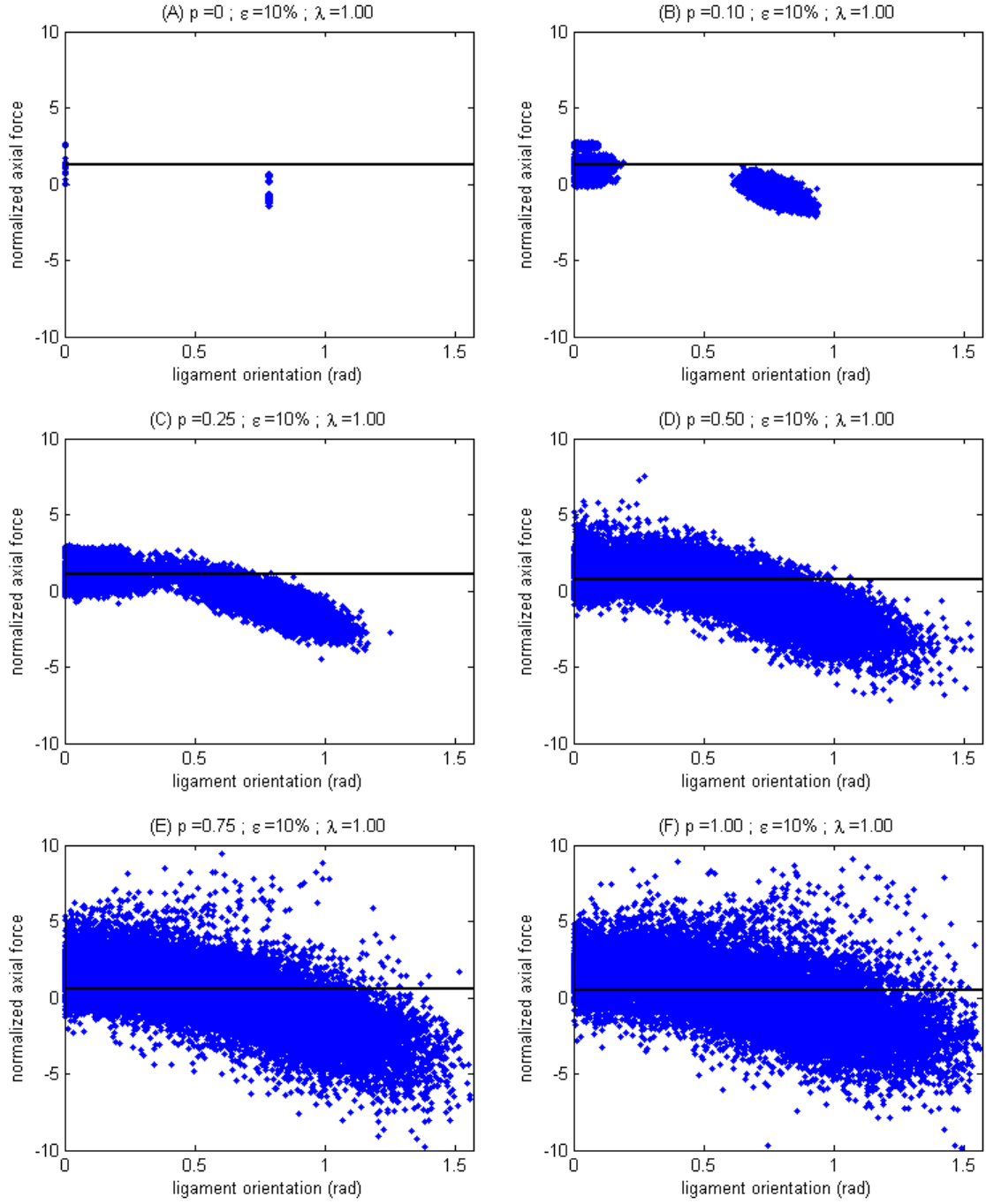
Normalized axial force is used in these figures for ease of comparison between networks of different degrees of perturbation or anisotropy. The normalized axial force in Figure 49 is defined as,

$$F_{normalized} = \frac{F - \mu_{unperturbed}}{\sigma_{unperturbed}},$$
(34)

where F is the axial force in the ligament, $\mu_{unperturbed}$ is the mean axial force experienced in ligaments of an unperturbed, isotropic network, and $\sigma_{unperturbed}$ is the standard deviation of the axial force in an unperturbed, isotropic network. This method of normalization scales the axial force data so that the distribution of the axial force in an unperturbed isotropic network has a mean of zero and a standard deviation of one. The means and standard deviations of perturbed networks can then be easily compared to the unperturbed isotropic network to highlight the difference in magnitude of axial forces in the networks. Histograms of unique ligament orientations that exist in the network for different perturbation factors, as well as histograms of normalized axial force experienced by ligaments in such networks are shown in Figures 50 and 51.
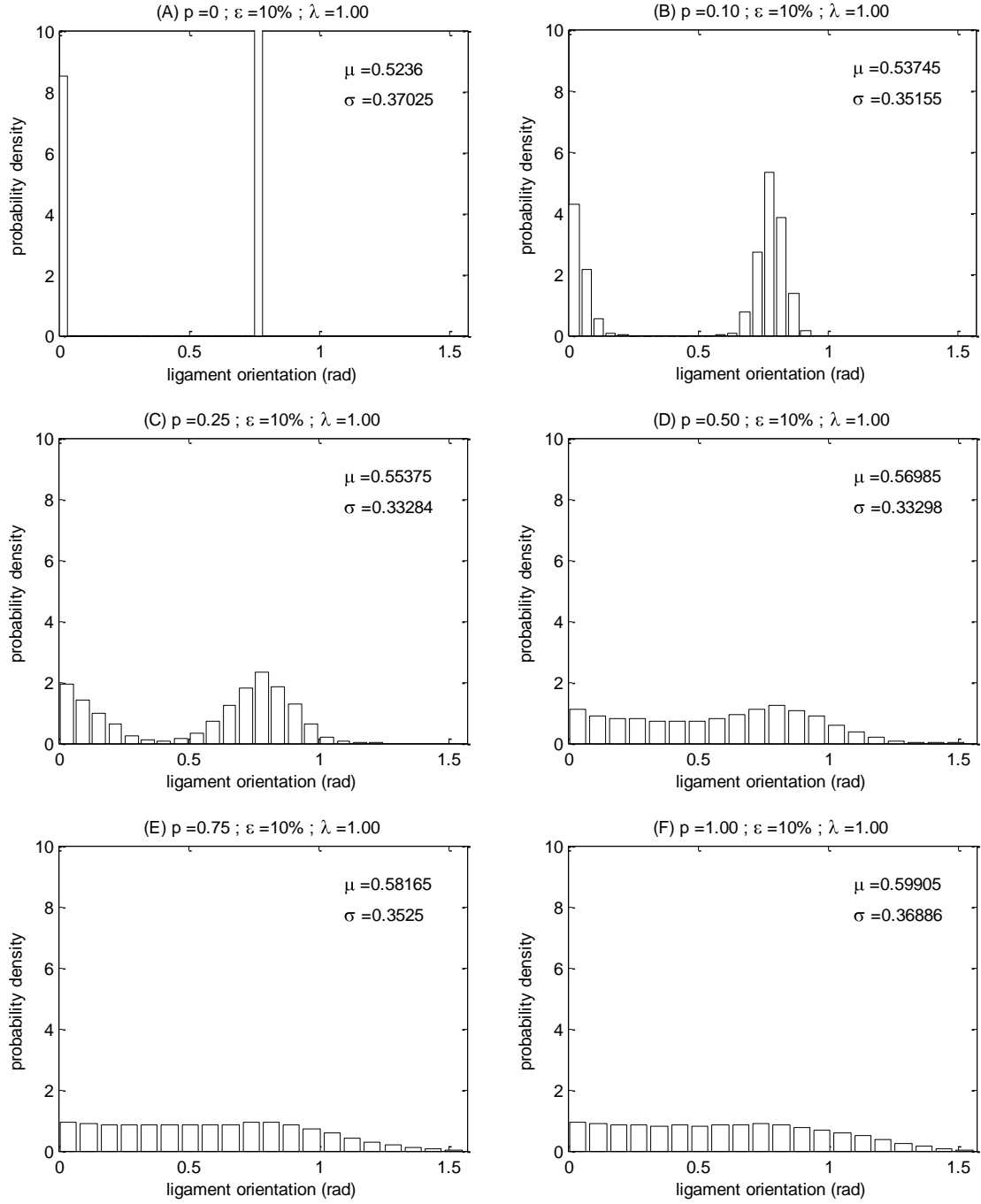
Figure 50: Histograms of ligament orientation in 10x10x10 networks with perturbation of (A) p=0 (B) p=0.10 (C) p=0.25 (D) p=0.50 (E) p=0.75 and (F) p=1.00
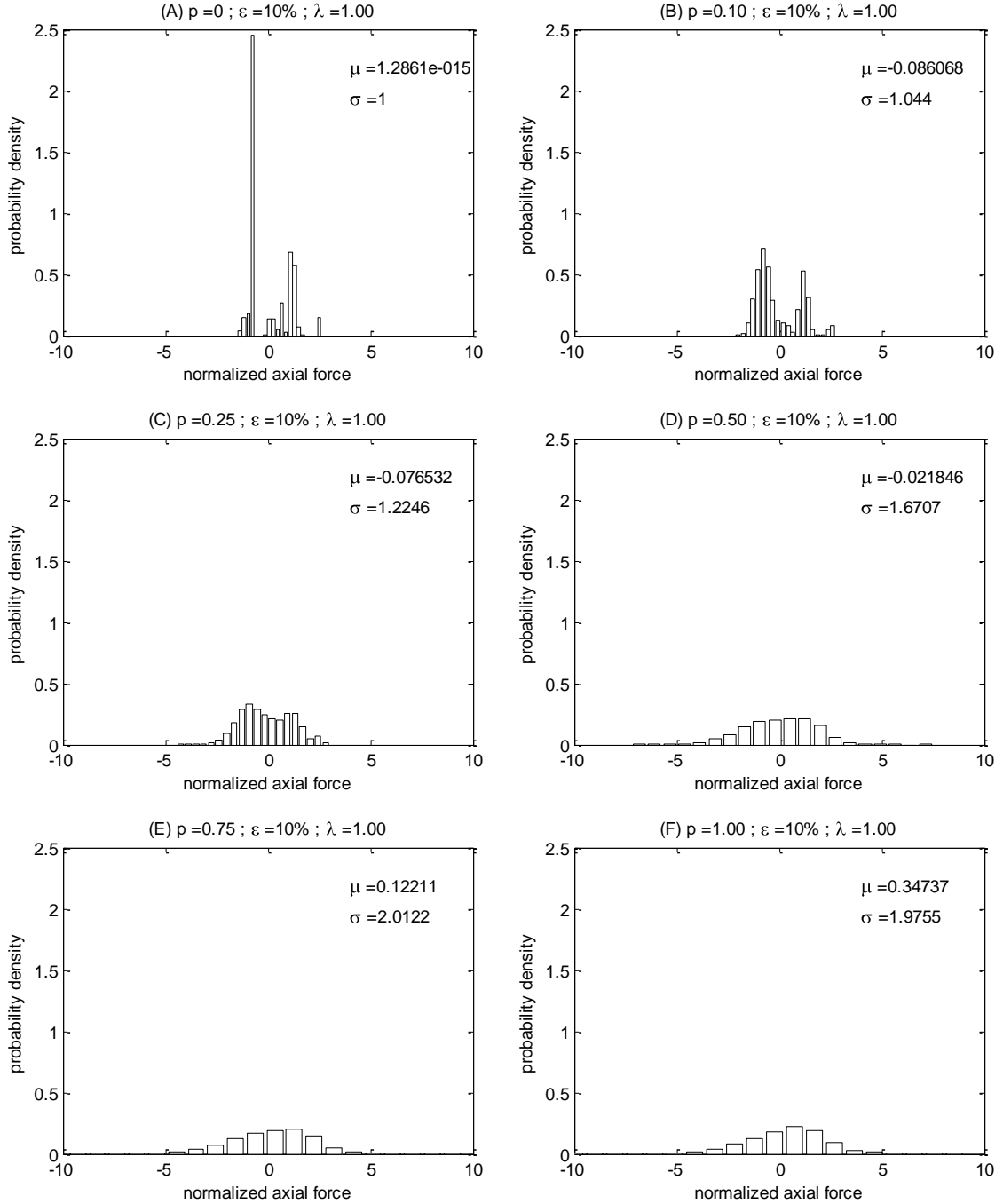
Figure 51: Histograms of normalized axial force for isotropic networks under 10% applied strain for (A) p=0 (B) p=0.10 (C) p=0.25 (D) p=0.50 (E) p=0.75 (F) p=1.00

Figure 50(A) shows that in a regular, unperturbed network only two distinct ligament orientations exist, resulting in the relationship shown in Figure 49(A). Though only two ligament orientations exist, Figure 49(A) indicates that more than two values for

axial force are observed. This illustrates that even in a deterministic network with perfectly ordered Kelvin geometry, ligament orientation is not sufficient information for predicting axial force.

Figure 49 shows that as the degree of randomness of the network increases, the number of different orientations present tin the network increases. As expected, Figure 50 shows that as the number of orientations that exist in the network increases, the axial forces experienced by ligaments in the network trend towards normal distribution. Figure 49 shows that the compressive axial force is greater in ligaments that are oriented more closely along the axis of loading but with a large amount of scatter for networks with higher degrees of randomness, described by the parameter, p. Figures 52, 53, and 54 show how the relationship of axial force with ligament orientation changes with anisotropy for randomness levels of $p=0.10$, 0.50, and 1.00 respectively. Perturbation of nodes is performed after cells are stretched to induce anisotropy, so randomness levels are comparable to those applied to isotropic networks. Again, the horizontal line on each of the plots indicates the boundary between tension and compression with points above the line corresponding to ligaments in tension and points below the line to ligaments in compression.

Figure 52: Axial force normalized by mean axial force in isotropic unperturbed network with respect to ligament orientation for perturbed network (p=0.10) under 10% applied strain with (A) λ=0.27 (B) λ=0.58 (C) λ=1.00 (D) λ=1.73 (E) λ=3.73

Figure 53: Axial force normalized by mean axial force in isotropic unperturbed network with respect to ligament orientation for perturbed network (p=0.50) under 10% applied strain with (A) λ=0.27 (B) λ=0.58 (C) λ=1.00 (D) λ=1.73 (E) λ=3.73

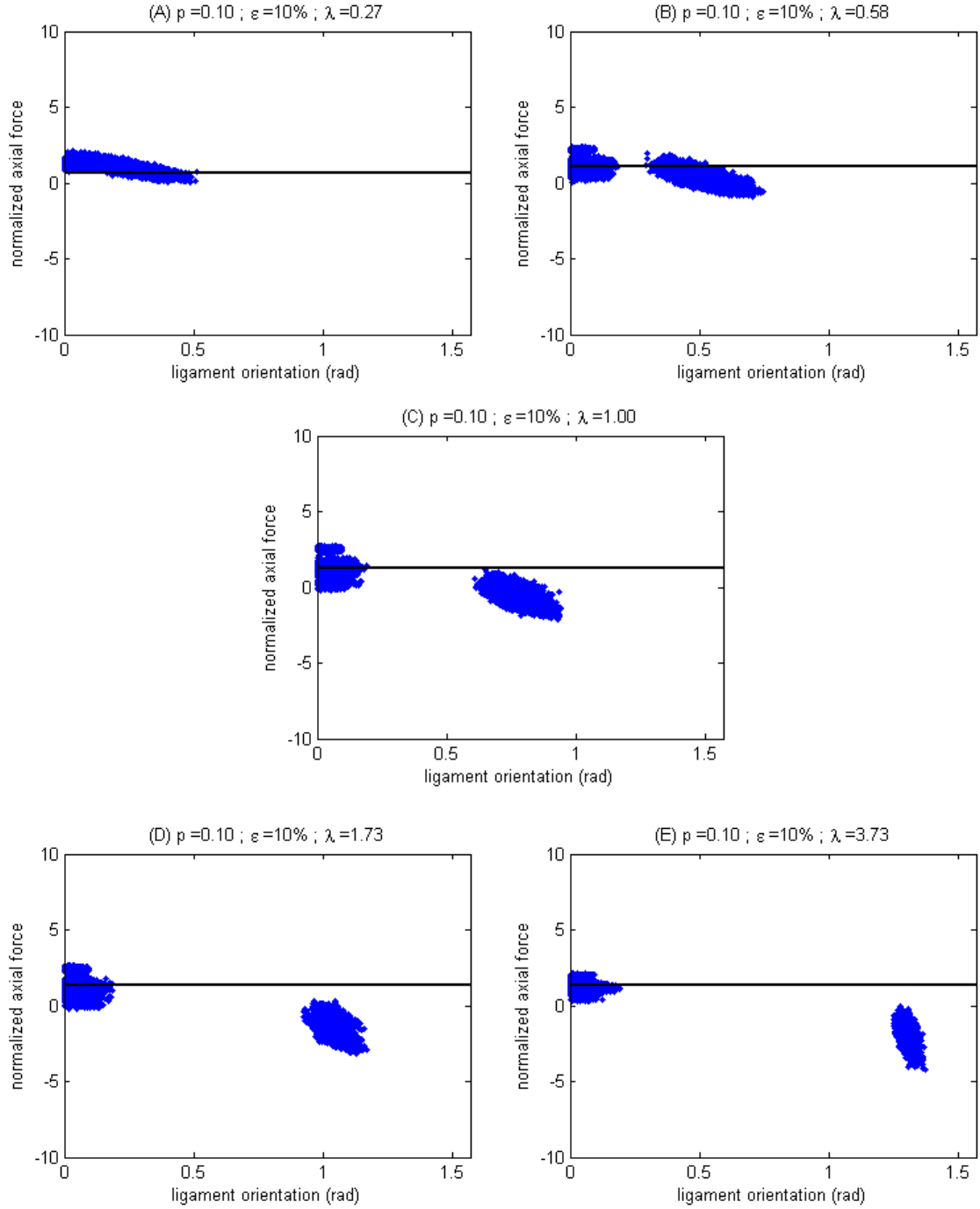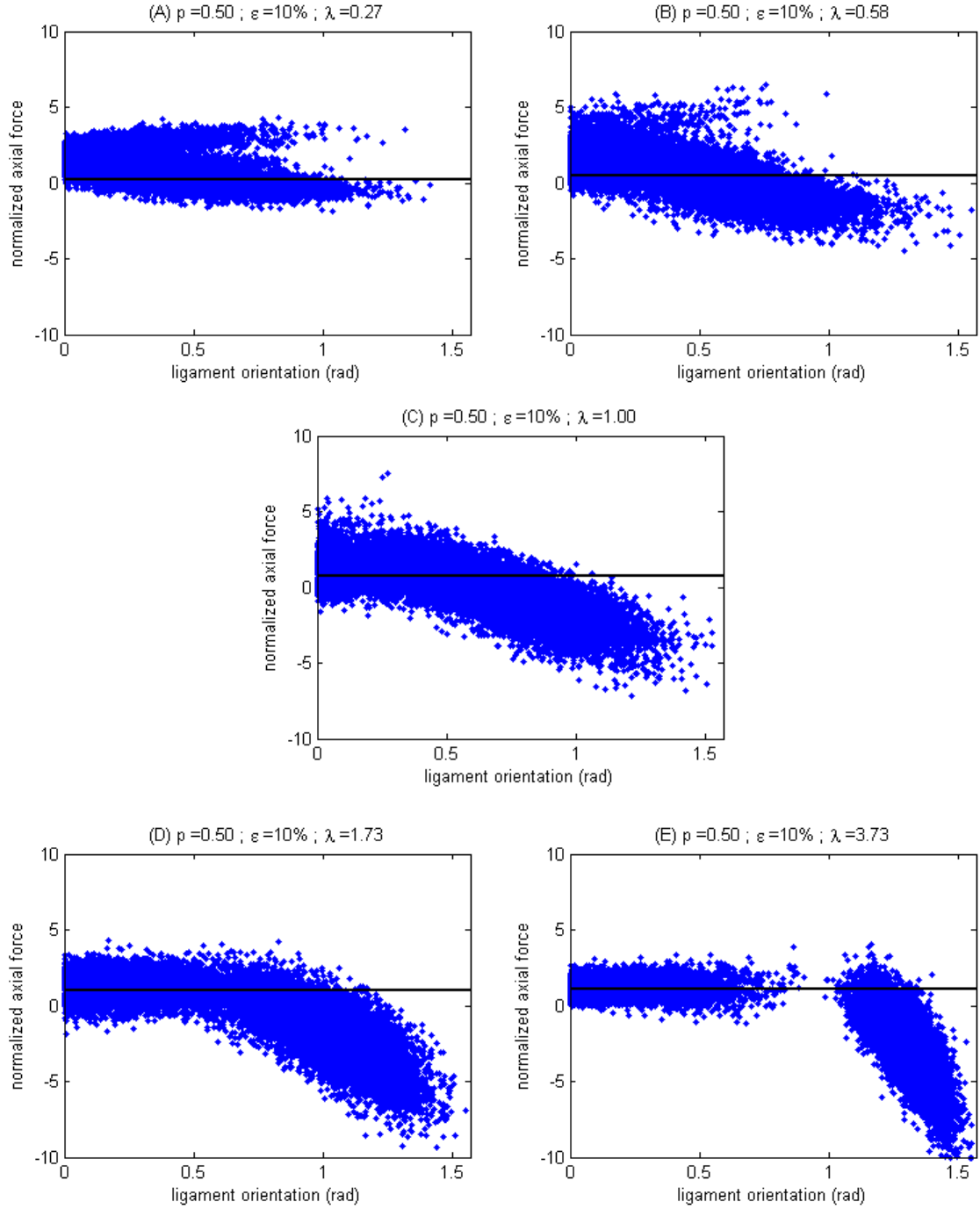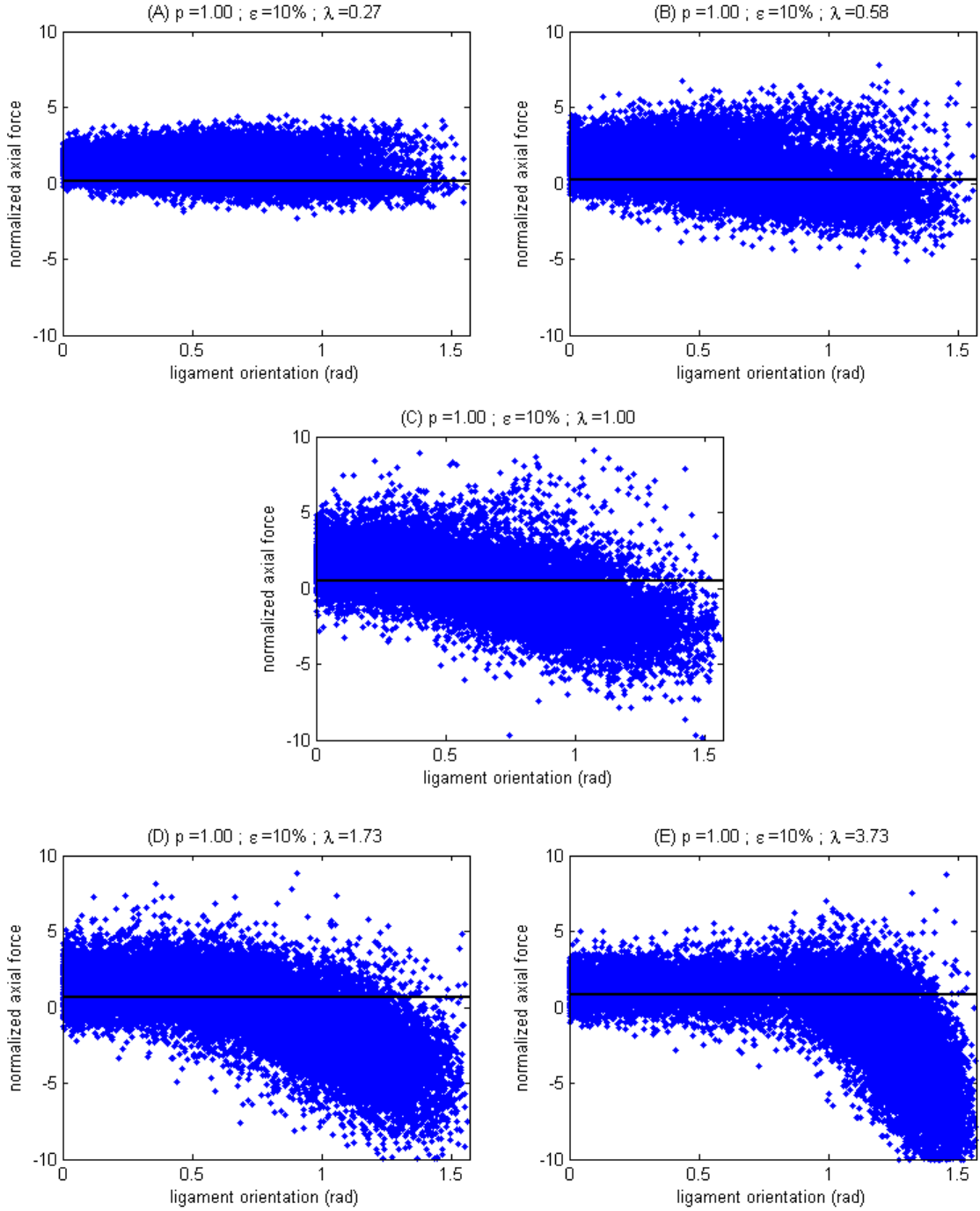**Figure 54: Axial force normalized by mean axial force in isotropic unperturbed network with respect to ligament orientation for perturbed network (p=1.00) under 10% applied strain with (A) λ=0.27 (B) λ=0.58 (C) λ=1.00 (D) λ=1.73 (E) λ=3.73**

It is observed in Figures 52, 53, and 54 that as the anisotropy ratio increases and

the cells are stretched in the rise direction (along the direction of loading as in Figures 48

of Section 6.3.2), the effect of ligament orientation on axial force becomes more pronounced. The opposite occurs when the anisotropy ratio decreases (cells stretched in a direction other than the rise direction). In these networks, the orientation of a ligament has diminishing effect on the magnitude of axial force. This is due to the nature of large axial force being experienced primarily by vertically oriented elements. As anisotropy ratio increases, the distribution of ligament orientation separates into two distinct regimes, vertical and horizontal. Because more vertically oriented ligaments will experience higher axial force and the majority of ligaments are oriented vertically in networks with higher anisotropy ratios, the relationship between orientation and axial force is heavily weighted in favor of higher (more vertical) orientations. Conversely, in networks with anisotropy ratio less than one, most ligaments are effectively horizontal and therefore the axial force is distributed among fewer ligaments (the vertical) and the relationship is stretched across a larger range of orientations. Any ligament that is not horizontal will experience axial force whereas in networks with large anisotropy ratios, axial force is primarily experienced by a small range of ligament orientations, though most of the ligaments in the network are within this range.

The effect of anisotropy on the relationship between orientation and axial force is due to the fact that as anisotropy increases, a greater percentage of the ligaments in the network will be oriented more severely along the axis of loading as shown in Table 18.

Table 18: Percentage of ligaments oriented at angle greater than or equal to $\pi/4$

Λ	$p = 0.10$	$p = 0.50$	$p = 1.00$
0.27	0	3.6	17.3
0.58	0	10.2	21.1
1.00	32.9	31.1	32.8
1.73	69.0	64.0	54.8
3.73	69.0	69.1	72.1

The increase in percentage of ligaments oriented more along the axis of loading is further illustrated in Figure 55, which show histograms of ligament orientation as anisotropy ratio increases.
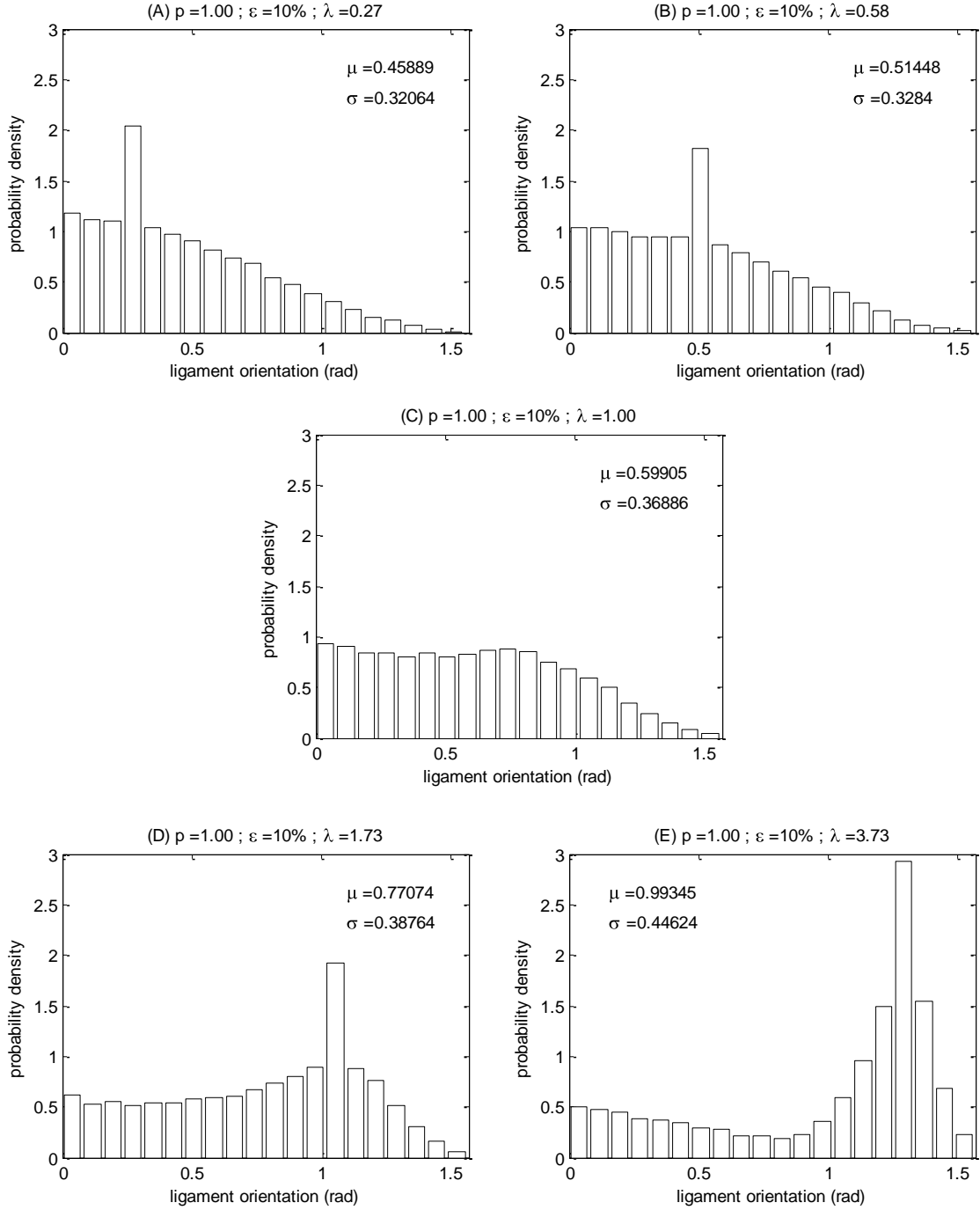
Figure 55: Histograms of ligament orientations in perturbed networks (p=1.00) with anisotropy ratios of (A) λ=0.27 (B) λ=0.58 (C) λ=1.00 (D) λ=1.73 (E) λ=3.73

The increase in mean orientation as anisotropy ratio increases is shown in Figure

56 for perturbation factors of 0.10, 0.50 and 1.00.
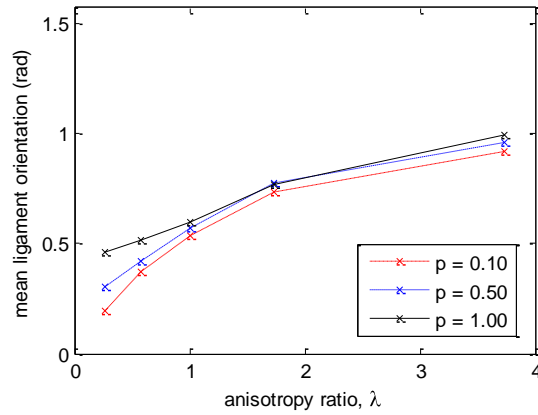
Figure 56: Plot of mean ligament orientations to illustrate shift in dominant ligament orientation as anisotropy changes in perturbed networks

As the dominant range of ligament orientation shifted increases (towards the axis of loading), the effect of orientation on the axial force, specifically the compressive axial force, becomes significantly more pronounced. This is illustrated in Figures 53, 54, and 55 in that as anisotropy increases above 1.00, the number of unique orientations of ligaments that experience large compressive axial force lessens. Because the range of orientations that experience compressive axial force is more concentrated, the effect of these orientations on the axial force is more pronounced. Conversely, for networks with anisotropy less than 1.00, the majority of ligaments are oriented perpendicular to the axis of loading and thus do not display any obvious relationship between orientation and axial force.

6.3.3. Distribution of stresses

As previously described, failure of aluminum foam occurs when individual ligaments fail by crushing or buckling in compression or fracture in tension. For this reason, it is useful to investigate the stresses that occur within the ligaments of a foam network in an attempt

to gain insight on the method of failure of the ligaments which would in turn cause failure of the global network. The combined axial and bending stresses, defined as

$$\sigma = \frac{P}{A} \pm \frac{Mc}{I},$$
(35)

were computed for each ligament in the network. In Equation (35), P is the axial force in the ligament, A is the cross-sectional area, M is the maximum moment, c is the distance to the centroid, and I is the second moment of inertia. Combined stresses are normalized using the same method as axial force normalization,

$$\sigma_{normalized} = \frac{\sigma - \mu_{unperturbed}}{\sigma_{unperturbed}},$$
(36)

where σ is the combined stress in the ligament, $\mu_{unperterbed}$ is the mean combined stress in ligaments of an unperturbed, isotropic network and $\sigma_{unperturbed}$ is the standard deviation of combined stress in an unperturbed, isotropic network. Histograms of normalized maximum compressive and tensile stresses for networks of different levels of perturbation are shown in Figure 57 and Figure 58.
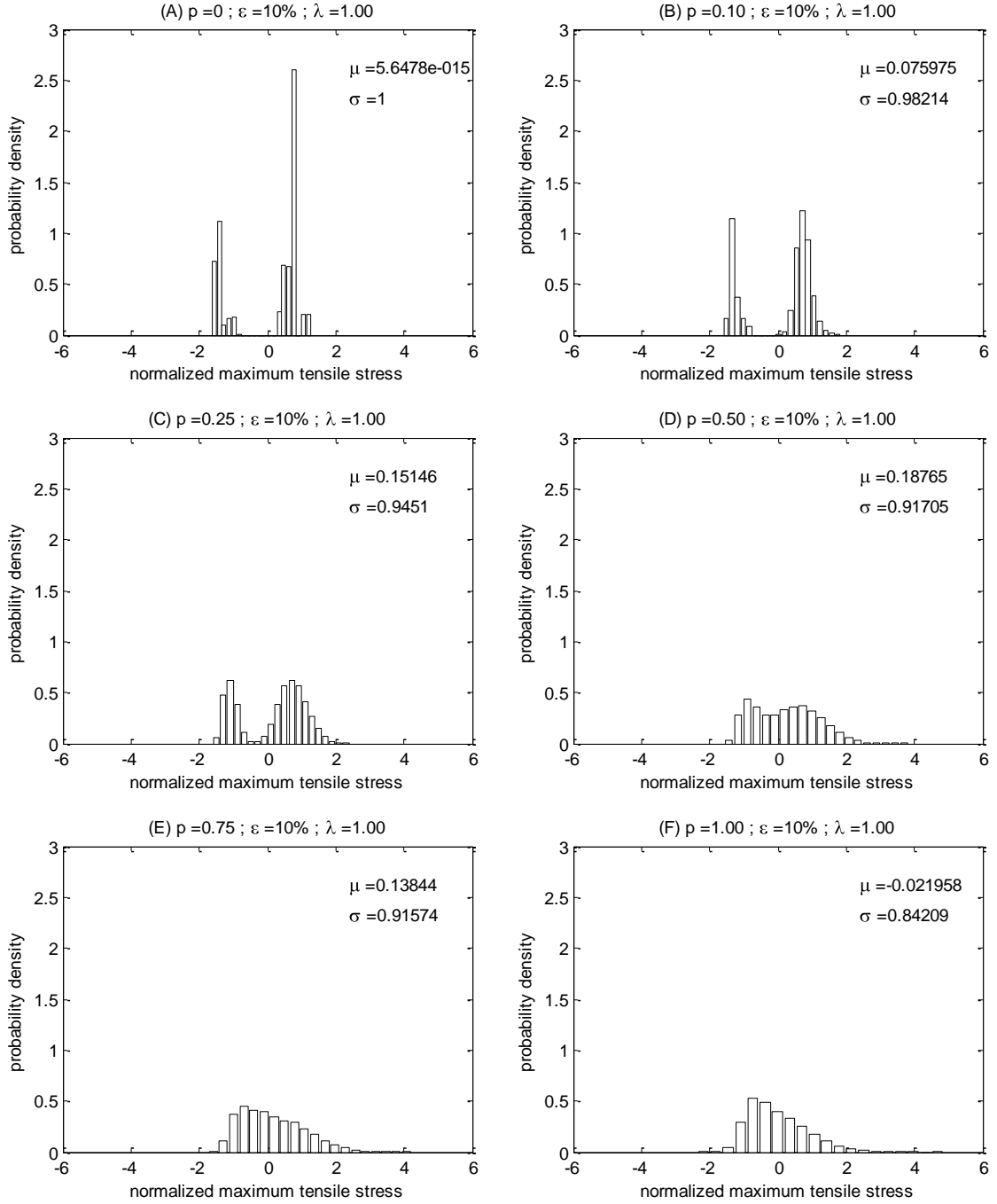
Figure 57: Histograms of normalized maximum tensile stress in ligaments of an isotropic foam network with 10% applied strain for (A) p=0 (B) p=0.10 (C) p=0.25 (D) p=0.50 (E) p=0.75 (F) p=1.00

113
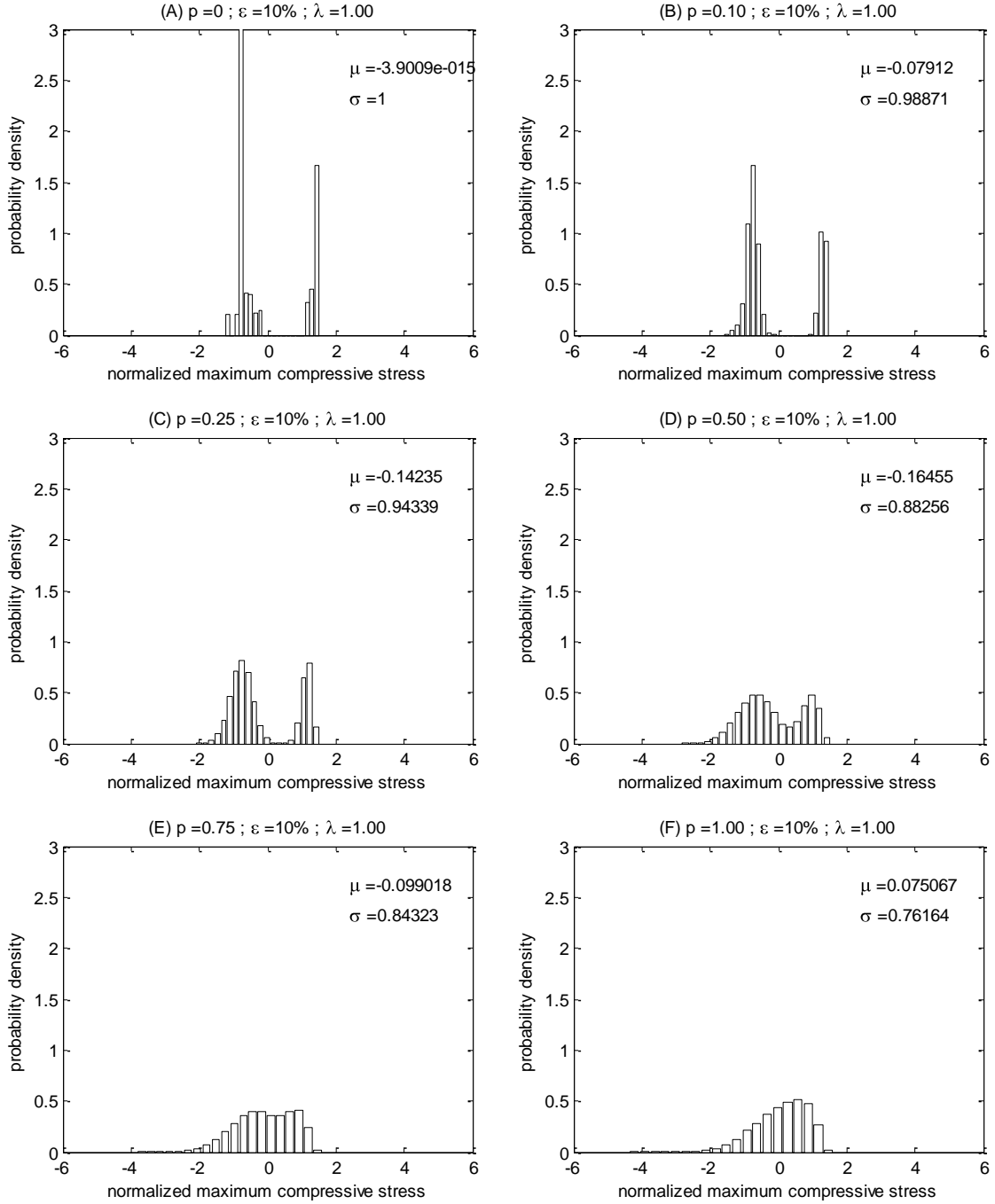
Figure 58: Histograms of normalized maximum compressive stress in ligaments of an isotropic foam network with 10% applied strain for (A) p=0 (B) p=0.10 (C) p=0.25 (D) p=0.50 (E) p=0.75 (F) p=1.00

To determine whether axial or bending stress had a greater impact on the combined stress in ligaments, the histograms for axial and bending stress can be

114

compared to those for the combined stresses to identify which has greater impact on the combined stress in a ligament.
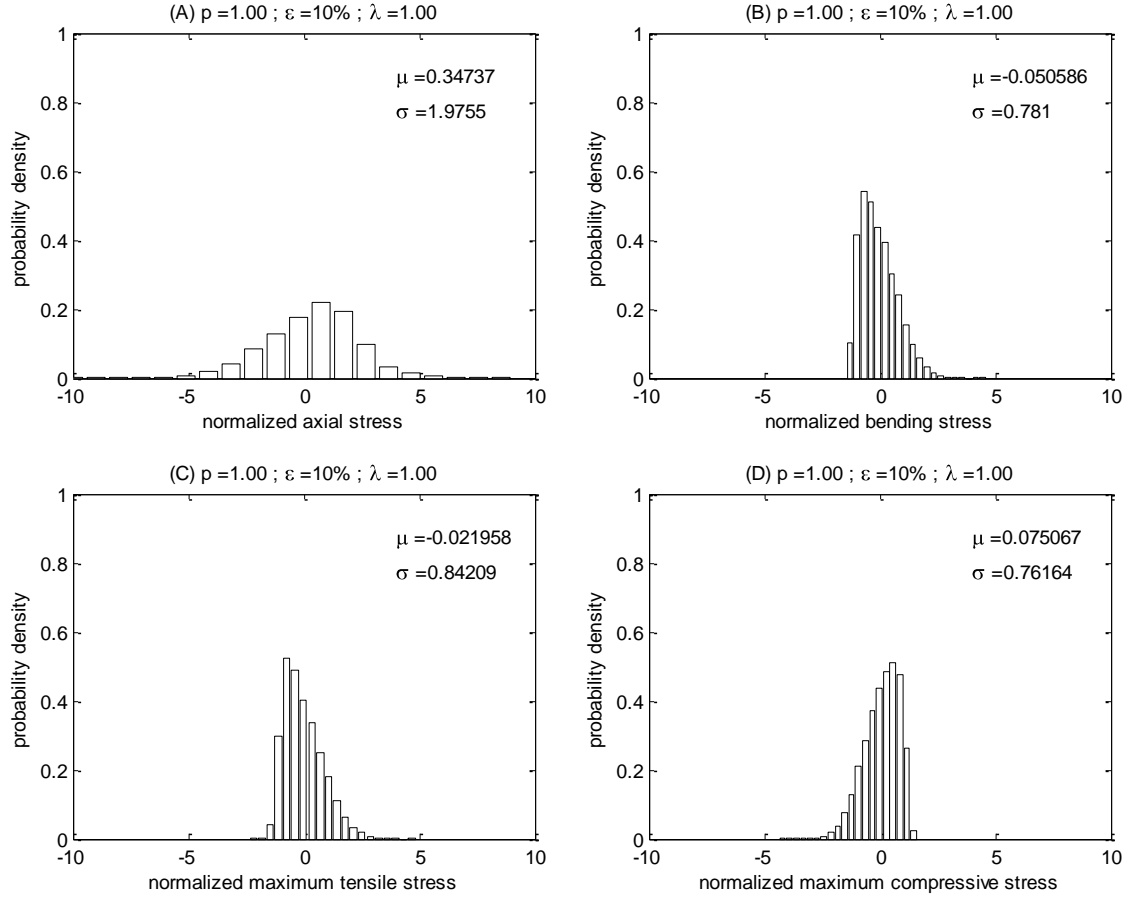
Figure 59: Histograms of isotropic foam network with p = 1.00 and 10% applied strain comparing (A) normalized axial stress (B) normalized bending stress (C) normalized maximum tensile stress (D) normalized maximum compressive stress

Table 19 shows the mean and standard deviation values for each type of stress to give a sense of the magnitude of each (Figure 59 provides normalized statistics which cannot be usefully compared to one another) and determine whether axial or bending stress has greater influence on the magnitude of the combined stress.

Table 19: Mean and standard deviation statistics for stresses in 10x10x10 isotropic network with p = 1.00 and 10% applied strain

		μ, Pa	σ, Pa
(A)	axial stress	-204.5	451.6
(B)	bending stress	3809.8	2047.6
(C)	maximum tensile stress	3605.3	2040.9
(D)	maximum compressive stress	-4014.3	2151.3

Table 19 clearly shows that the magnitude of combined stress, both tensile and compressive, is controlled by the magnitude of bending stress, whereas the axial stress has much smaller magnitude and has less influence on the combined stress.

Another method for comparing the histograms for axial and bending stresses to the histograms for the tensile and compressive stresses is with the measure of skewness. Skewness measures the asymmetry of the distributions and can be used to show which of the axial and bending stresses drives the shape of the combined stress distributions. The skewness statistics for these distributions are given in Table 20.

Table 20: Skewness statistics for distributions of stresses in 10x10x10 isotropic network with p = 1.00 and 10% applied strain

		Skewness, γ_1
(A)	axial stress	0.6816
(B)	bending stress	-0.6601
(C)	maximum tensile stress	-0.6689
(D)	maximum compressive stress	0.6518

In comparing the skewness of these distributions, it is seen that bending stress and maximum tensile stress both possess similar negative skewness, while axial stress and maximum compressive stress both have similar positive skewness. Though this would suggest the shape of the compressive stress distribution is driven by the distribution of

116

axial stress respectively throughout the network, the negative skewness of the compressive stress occurs due to the sign change of the bending stress from Equation (35). The bending stress is able to take either sign, while the axial stress cannot and the fact that bending stress skewness and maximum compressive stress skewness have similar magnitudes suggest that bending stress has a much larger influence on both the magnitude and distribution of total stress in ligaments of a cellular network than axial stress.

CHAPTER 7

CONCLUSION

The known characteristics of aluminum foam make it an attractive material for use in the field of structural engineering. The energy absorbing properties and high strength and stiffness to weight ratios of foam make it a potential option for use in building frame lateral bracing from which to absorb earthquake or wind forces and many other structural applications. In order for the material to fully translate into structural use, confidence in the material properties and an understanding of the behavior under typical loading scenarios must exist to avoid unexpected insufficiencies that could have catastrophic consequences.

Expressions defining the properties, specifically the elastic properties, of foam currently exist within the extensive research of Lorna Gibson and Michael Ashby on foam mechanics. However, the relationships developed are limited in terms of the parameters that are assumed to contribute to the elastic behavior of foam. In their expressions for the elastic properties of open cell foam, Gibson and Ashby consider primarily the bending mechanics of the cell ligaments, assuming that shear and axial contributions have negligible influence on the behavior. Furthermore, their definition of ligament geometry is limited to the use of solid, rectangular cross-sections, which are not necessary realistic representations of the microstructure of actual foam. To soften this assumption and apply the principles of not only bending, but also axial and shear deformations explicitly in determining the elastic properties, expressions were derived in terms of the axial and bending stiffness ratios. It was determined the axial stiffness of the

ligaments, in addition to the bending stiffness, has a significant effect on the properties and behavior of the network.

To further the understanding of the elastic properties and behavior of foam, tensile and compressive tests were performed on open cell samples provided by ERG Duocel. Compressive tests were used to measure the initial elastic modulus and yield strength and also analyze the behavior of the material it approached densification. Failure of foam in compression is governed by the buckling or yielding of individual ligaments. After an initial elastic regime, foams experienced a long collapse plateau as the material was crushed plastically due to the collapse of cells along a defined crushing band through the cross section. Once densification of the foam was complete, an abrupt increase in stiffness was observed as the foam adopted the properties of the base material. Measurements of the elastic modulus found that relative density had the most significant impact on the stiffness, as small changes in the relative density between samples resulted in substantial changes in the measured stiffnesses. The elastic modulus was found to be independent of porosity as both the 20 and 40 ppi samples tested produced results similar to predictions calculated based on the measured relative densities of the samples. Despite good agreement between predictions and measured values of the elastic modulus, especially for the 20 ppi samples, the large variations of relative density from sample to sample of the same porosity, especially in small volumes, make designing for stiffness a difficult proposition.

While failure of open cell foam in compression is characterized by ductile plastic collapse, behavior in tension is brittle and prone to sudden failure as individual fracture eventually tearing through the entire cross section. Failure is the propagation of a crack

119

across the cross section of the tested sample that initiates at a pre-existing defect or weak location within the microstructure. This failure mode is such that material with thicker ligaments will exhibit stronger, stiffer behavior in tension, as illustrated by the difference in results of different porosities. The elastic modulus of foam in tension is assumed to be equal to that in compression. However, while the mechanics of foam in compression are well understood, the discrepancy between tensile elastic modulus measurements and predictions suggest that more vigorous investigation into tensile foam mechanics is necessary. Furthermore, testing of foam in both tension and compression requires that the volume of the material is such that an adequate amount of cells exist in the cross section that behavior representative of larger samples is achieved. The tests performed produced results that were inconsistent in regards to elastic properties across tension and compression, where behavior is assumed to be identical in the elastic regime. This suggests that further testing is required to provide a more robust set of test results from which to draw conclusions. Should the inconsistency between tensile and compressive behavior persists for additional testing, the assumption that elastic behavior in both directions would need to be readdressed.

In order to usefully analyze results of cyclic testing of open cell foam, definitions of fatigue failure were necessary. Fatigue life results for tests over a range of applied strain amplitudes from 0.3 to 1.25% were defined by three distinct failure criteria: the increase of the H_C/H_T ratio (adopted from the Ingraham et al. fatigue tests on closed cell foam), the degradation of peak tensile strain and the degradation of peak tensile stress. The formation of a kink in the bottom half of the hysteresis loop identifying compaction

assisted crack propagation was investigated as a potential fourth definition of failure but results were inconsistent for the lower amplitude tests performed.

The behavior of foam in tension, and especially in compression, has been studied extensively to this point. The properties under cyclic loading, specifically for open cell foam, are much more limited. Fatigue behavior is essential to understand for the prospective structural use of foam. The fatigue tests performed sought to develop a preliminary analysis of the strain-life relationship of the material and provide direction for the continued study of the fatigue properties of open cell foam.

Like closed cell foam, open cell foam displays a Coffin-Manson relationship for applied strain and fatigue life. Failure is governed by the formation of tensile cracks resulting from the fracture of individual ligaments. After the initial crack forms, the foam is compacted plastically during the compressive cycle and in successive cycles the crack is forced to open further and the crack expands. It was determined that open cell foam has inherently longer fatigue life than closed cell material due to differences in microstructure of the two materials. Closed cell foam, at the same relative density, will have thinner cell walls than the ligaments in an open cell foam and thus promote fracture at earlier cycles and a shorter fatigue life. Differences in fatigue life for open cell foam of different porosities are also due to the intrinsic difference in ligament structure in that foams of different porosity, but similar density will possess different ligament geometry. Shorter, stockier ligaments that exist in 20 ppi foams allow the material to possess a longer fatigue life in general than 40 ppi material. The tests performed to date on open cell foam were characterized by high applied strain amplitude and low cycles to failure. The results from these tests can be used to develop initial knowledge about the fatigue failure of the

material with the intention of applying this to lower amplitude tests to determine if the behavior observed in low cycle tests is consistent at higher cycle tests.

Finite element modeling of foam was performed to analyze the parameters that affect both the elastic properties and the forces and stresses that develop in the ligaments, controlling failure of the material. Regular, order networks of periodically repeated Kelvin cells were created in ADINA and subjected to globally applied displacements. Simulations were performed on 10 by 10 by 10 cell networks with constant ligament length and diameter definitions to promote consistent relative density. It was determined that in addition to relative density, cell anisotropy has a significant effect on the elastic modulus of foam. As the cells of a network are stretched in the rise direction, a common occurrence during the manufacturing process of foam, the overall stiffness of the network in the rise direction is increased. While this result is consistent with previous research by Gibson and Ashby, the elastic modulus determined from finite element model simulations did not agree with the modulus measured from mechanical testing, even with realistic levels of anisotropy applied to the cells of the model. It was not until rigid end zones were applied over a percentage of each ligament length that the elastic modulus computed from the model results matched test results. These rigid end zones account for the thickening of material that exists in the ligaments of physical open cell foam. Models that incorporate accurate representations of not only relative density, but also cell isotropy and the rigidity at ligament joints, yielded results for the elastic modulus between 10 and 15% different from the testing results. While further optimization is possible through measurement of actual anisotropy and joint rigidity of foams, it was

concluded that the current regular models were adequate in determining properties and attention was turned to the effects of randomness on the model.

While irregular, randomly generated network models of foam would further increase the agreement with actual foam properties, these models were primarily used to assess the effects of ligament orientation on the forces and stresses that develop within the ligaments. Global failure of foam is governed by the fracture of ligaments in tension and by yielding or buckling in compression and for this reason, it is useful to investigate the magnitude of forces, both bending and axial, that develop within ligaments for different levels of randomness and anisotropy in networks. It was determined that ligaments oriented more closely along the axis of loading experience axial force of larger magnitude, a result that is exaggerated at more severe orientations as the anisotropy of the cells increases (i.e. cells are stretched in the rise direction). Maximum compressive and tensile stresses developed in ligaments were also computed and it was concluded that bending stress has a larger influence on the magnitude of combined than axial stress due to the ability of both positive and negative bending to occur in ligaments while the sign of axial force in the majority of ligaments in the network is dependent on the globally applied loading. The results of random network simulations provided insight into the effects of microstructural variability on the development of forces within the ligaments. Random network simulation of foam behavior can be used in further research endeavors to predict the percentage of ligaments that experience critical loads under applied loading conditions. If accurate predictions for the locations of the maximum forces and stresses within a network could be achieved, steps could be taken towards determining optimal uses of foam that best take advantage of the material properties.

The potential for use of aluminum foam in structural applications is high. It has been demonstrated that the material possesses many favorable qualities that would prove advantageous in structural uses ranging from filtration to bracing to insulation. The high strength and stiffness to weight ratios make it ideal for situations where such properties are desirable, but weight is of chief concern, such as in the core of a sandwich beam or as fill within a steel tube in compression. In order for foam to be utilized in a structural capacity, the material properties must be realized with a high level of confidence. This project has studied the behavior of foam under compressive, tensile and fatigue loading conditions and provided sound basis for determining the potential for structural use. Furthermore, finite element models were shown to be able to accurately predict properties provided accurate representation of ligament geometry, cell shape, and relative density. Further investigation of computer modeling of foams could lead to advances in the prediction of failure for the material in fatigue, a necessary measure for structural applications. The overall steps taken by this project in understanding the behavior of aluminum foam make structural use a reasonable expectation for the future.

REFERENCES

1. ASTM International, 2003. "Test Methods for Tension Testing of Metallic Materials." Standard E8.

2. Gibson, L.J. and Ashby, M.F., 1997. *Cellular Solids: Structure and Properties*, 2nd ed. Cambridge University Press, Cambridge.

3. Gong, L., Kyriakides, S. and Jang, W.-Y., 2005. "Compressive response of open-cell foams. Part I. Morphology and elastic properties. *International Journal of Solids and Structures*, 42, 1381-1399.

4. Harte, A.-M., Fleck, N.A., and Ashby, M.F., 1999. "Fatigue failure of an open cell and a closed cell aluminum alloy foam." *Acta Materialia.*, 47(8), 2511-2524.

5. Ingraham, M.D., et al., 2008. "Low cycle fatigue of aluminum foam." *Material Science Engineering,* A, doi:10.1016/j.msea.2008.10.045.

6. Jang, W.-Y. and Kyriakides, S., 2009. "On the crushing of aluminum open-cell foams." *International Journal of Solids and Structures*, 46, 617-650.

7. Jang, W.Y., Kraynik, A.M., and Kyriakides, S., 2008. "On the microstructure of open-cell foam and its effect on elastic properties." *International Journal of Solids and Structures*, 45, 1845-1875.

8. Ramamurty, U. and Paul, A., 2004. "Variability in mechanical properties of a metal foam." *Acta Materialia*, 52, 869-876.

9. Roberts, A.P. and Garboczi, E.J., 2002. "Elastic properties of model random three-dimensional open-cell solids." *Journal of the Mechanics and Physics of Solids*, 50, 33-55.

10. Sugimura, Y., et al., 1999. "Compression fatigue of a cellular Al alloy." *Materials Science and Engineering*, A269, 38-48.

11. Ugural, Ansel C. and Fenster, Saul K, 2003. *Advanced Strength and Applied Elasticity*, 4th edition. Pearson Eduction Ltd., London.

12. Zettl, B., et al., 2000. "Fatigue properties of aluminum foams at high numbers of cycles." *Materials Science and Engineering*, A292, 1-7.